

Connectivity Analysis of Brain States and Applications in Brain-Computer Interfaces

THÈSE N° 6779 (2015)

PRÉSENTÉE LE 30 OCTOBRE 2015

À LA FACULTÉ DES SCIENCES ET TECHNIQUES DE L'INGÉNIEUR
CHAIRE FONDATION DEFITECH EN INTERFACE DE CERVEAU-MACHINE
PROGRAMME DOCTORAL EN BIOTECHNOLOGIE ET GÉNIE BIOLOGIQUE

ÉCOLE POLYTECHNIQUE FÉDÉRALE DE LAUSANNE

POUR L'OBTENTION DU GRADE DE DOCTEUR ÈS SCIENCES

PAR

Huaijian ZHANG

acceptée sur proposition du jury:

Prof. D. Pioletti, président du jury
Prof. J. D. R. Millán Ruiz, directeur de thèse
Prof. S.-W. Lee, rapporteur
Prof. F. Babiloni, rapporteur
Prof. D. Van De Ville, rapporteur



ÉCOLE POLYTECHNIQUE
FÉDÉRALE DE LAUSANNE

Suisse
2015

To my family ...

Acknowledgements

I will express my deepest gratitude to Prof. José Millán and Dr. Ricardo Chavarriaga. It has been more than a great pleasure to work and grow as a researcher under their guidance. Learning from them is the biggest treasure I have possessed ever, which are more than the knowledges in research, the ways of being a scientist, also a model of character to be built in my life. Without their grace, I could not have reached this stage.

A great thank goes to the Nissan team, particularly Lucian Gheorghe, made the Nissan project possible, also provides technical supports and ideas in car simulator and real car studies. Thanks to Michaël Themans (EPFL transportation center) and Jonathan Martin (Cantonal road service) for their supports in the real car study.

I am grateful to the members of my defense committee, Prof. Dominique Pioletti, Prof. Dimitri Van De Ville, Prof. Seung-Whan Lee, and Prof. Fabio Bailoni for taking their time to read and provide valuable comments on the thesis.

I must thank the members of CNBI, for their helps in research, and their presence in my life. I especially want to thank Dr. Eileen Lew, who helped me a lot from the beginning till even after her leaving, in both technical aspects and life in Lausanne. Big thank to Zahra Khalili, who is always patient and cooperative. It is also pleasure to collaborate with Dr. Inaki, Dr. Luca (Tonin), Dr. Marija and Dr. Andrea. Thanks to the early generation, Dr. Simis, Dr. Nicolas, Dr. Robert, Dr. Ganga, Dr. Tom, for providing advices in research and programming, to the median generation, Dr. Hesam, Sareh, Pierluca, Dr. Mohit, Dr. Maria Laura, Alberto and Marco, for their helps in experiments and proofreading, and also the young PhDs, Michael, Stephanie, Luca (Randazzo), Christoph and Tiffany for bringing active atmosphere to the lab. My sincere thank to all the subjects, mainly PhD and master students, for spending their time to participate my experiments in the past few years. The studies were validated and becoming solid because of your presence and highly quality brain signals.

I thank my friends in Switzerland, Xiaoshen, Yuan, Chongqi, Su, Xiuzhen, and Yun, for the good time shared together, also friends, Yi, Zhaoyin, Yuanfan, Tao, Pao, Niu, Zisa and Bao, for the supports and encouragements during my hard times.

Lastly, but the most important, I thank my parents, sisters, brothers in law, uncle, aunt and brother Ping. Thank you for bearing my absence for these years. Without your love, solid support, encouragement and patience it is impossible to pursue this challenging work.

Lausanne, 21 Aug 2015

H. Zhang

Abstract

Human brain is organized by a large number of functionally correlated but spatially distributed cortical neurons. Cognitive processes are usually associated with dynamic interactions among multiple brain regions. Therefore, the understanding of brain functions requires the investigation of the brain interaction patterns. This thesis contains two main aspects. The first aspect focuses on the neural basis for cognitive processes through the use of brain connectivity analysis. The second part targets on assessing brain connectivity patterns in realistic scenarios, e.g., in-car BCI and stroke patients.

In the first part, we explored the neural correlates of error-related brain activity. We recorded scalp electroencephalogram (EEG) from 15 healthy subjects while monitoring the movement of a cursor on a computer screen, yielding particular brain connectivity patterns after monitoring external errors. This supports the presence of common role of medial frontal cortex in coordinating cross-regional activity during brain error processes, independent of their causes, either self-generated or external events. This part also included the investigation of the connectivity during left/right hand motor imagery, including 9 healthy subjects, which demonstrated particular intrahemispheric and interhemispheric information flows in two motor imagery tasks, i.e., the μ rhythm is highly modulated in intrahemispheric, whereas β and γ are modulated in interhemispheric interactions. This part also explored the neural correlates of reaction time during driving. An experiment with 15 healthy subjects in car simulator was designed, in which they needed to perform lane change to avoid collision with obstacles. Significant neural modulations were found in ERP (event-related potential), PSD (power spectral density), and frontoparietal network, which seems to reflect the underlying information transfer from sensory representation in the parietal cortex to behavioral adjusting in the frontal cortex.

In the second part, we first explored the feasibility of using BCI as driving assistant system, in which visual stimuli were presented to evoke error/correct related potentials, and were classified to infer driver's preferred turning direction. The system was validated in a car simulator with 22 subjects, and 7 joined online tests. The system was also tested in real car, yielding similar brain patterns and comparable classification accuracy. The second part also carried out the brain connectivity analysis in stroke patients. We performed exploratory study to correlate the recovery effects of BCI therapy, through the quantification of connectivity between healthy and lesioned hemispheres. The results indicate the benefits of BCI therapy for stroke patients, i.e., brain connectivity are more similar as healthy patterns, increased (decreased) flow from the damaged (undamaged) to the undamaged (damaged) cortex.

Acknowledgements

Briefly, this thesis presents exploratory studies of brain connectivity analysis, investigating the neural basis of cognitive processes, and its contributions in the decoding phase. In particular, such analysis is not limited to laboratory researches, but also extended to clinical trials and driving scenarios, further supporting the findings observed in the ideal condition.

Key words: Brain computer interface, Brain connectivity, Error-related brain activity, Motor imagery, In-car BCI, Reaction time.

Résumé

Le cerveau humain s'organise autour d'un large nombre de neurones corticaux fonctionnellement corrélés mais spatialement distribués. Les processus cognitifs sont généralement réalisés grâce à des interactions dynamiques entre de multiples régions cérébrales. Cependant, la compréhension des fonctions cérébrales nécessite la compréhension des modèles d'interaction entre les régions cérébrales. Cette thèse contient deux parties. La première partie se concentre sur les bases neuronales impliquées dans les processus cognitifs grâce à l'analyse de la connectivité cérébrale. La seconde partie s'intéresse à l'évaluation de modèles de connectivité cérébrale lors de scénarios réalistes ex : en voiture ou encore avec des patients ayant subi un accident vasculaire cérébral AVC.

Dans la première partie, nous avons tout d'abord exploré les corrélats neuronaux lors de processus cérébraux de détection d'erreur, Nous avons enregistré l'électroencéphalogramme (EEG) de 15 sujets sains pendant qu'ils surveillaient le mouvement d'un curseur sur un écran d'ordinateur, produisant un modèle de connectivité cérébrale particulier lors de la vision d'erreurs. Ces résultats renforcent l'idée d'un rôle commun du cortex frontal médian dans la coordination de l'activité cérébrale inter régionale pendant le processus cérébrale de détection d'erreur.

Cette partie inclue également la recherche de connectivité pendant la réalisation d'imagerie motrice de la main gauche et droite. Pour cela 9 sujets sains ont été inclus, et nous avons pu démontrer un flux d'information spécifique intrahémisphérique et interhémisphérique dans les deux tâches d'imagerie motrice. En effet le rythme μ est très modulé pour les interactions intrahémisphériques alors que pour celles interhémisphériques ce sont les rythmes β et γ qui sont modifiés. Cette partie explore enfin les corrélats neuronaux des temps de réactions pendant la conduite. Une expérience sur 15 sujets sains dans un simulateur de voiture a été mise en place, pendant laquelle ils devaient changer de voie pour éviter les collisions avec des obstacles. Des changements neuronaux significatifs ont été trouvés dans les ERP (event-related potentials), PSD (power spectral density) et le réseau fronto-pariétal, qui semble refléter un transfert d'information sous-jacent de la représentation sensoriel dans le cortex pariétal vers le cortex frontal afin d'y ajuster le comportement.

Dans la seconde partie, nous avons tout d'abord vérifié la possibilité d'utiliser une interface cerveau ordinateur (BCI) comme assistance à la conduite. Des stimuli visuels ont été présentés pour évoquer des potentiels reliés à une réponse erronée/correcte, et ils ont été classés pour déduire la direction préférée du conducteur lors d'un changement de direction. Le système a été validé dans un simulateur de voiture avec 22 sujets et 7 ont continué avec les tests

Acknowledgements

online. Le système a également été testé avec une vraie voiture, le modèle d'activité cérébrale était similaire et la précision de la classification similaire. Cette seconde partie contient également des analyses de connectivité chez des patients ayant subi un accident vasculaire cérébral. Nous avons mise en place une étude préliminaire pour tenter de corrélérer l'effet de la récupération motrice après une thérapie avec un BCI avec la quantification de connectivité entre les hémisphères lésé et sain. Les résultats démontrent les bénéfices apportés par le BCI aux patients atteints d'un AVC, par exemple la connectivité cérébrale ressemble plus à un modèle d'activité cérébrale d'un sujet sain grâce à l'augmentation (diminution) du flux du cortex lésé (non lésé) vers le cortex non lésé (lésé).

En résumé cette thèse présente des études préliminaires d'analyses de connectivité cérébrale, d'investigation des bases neuronales des processus cognitif et sa contribution dans le décodage de phase. De plus de telles analyses ne sont pas limitées à la recherche en laboratoire mais peuvent également être étendues aux essais cliniques ainsi qu'à des scénarios de conduite.

Mots clefs : Interface cerveau ordinateur, Connectivité cérébrale, Processus cérébral de détection d'erreur, imagerie motrice, Interface cerveau ordinateur en voiture, Temps de réaction.

Contents

Acknowledgements	i
Abstract (English/Français)	iii
List of figures	xi
List of tables	xvii
1 Introduction	1
1.1 Brain computer interfaces	1
1.2 Brain connectivity	3
1.2.1 Brain connectivity	3
1.2.2 Brain connectivity analysis in BCI	5
1.3 Objectives	5
1.3.1 Exploring neural correlates using connectivity analysis	6
1.3.2 Classification based on brain connectivity features	7
1.3.3 Build in-car BCI	7
1.4 Thesis outline	8
2 State of the art	11
2.1 Computational methods for brain connectivity	11
2.1.1 Dynamic causal model	11
2.1.2 Multivariate auto-regressive models and Granger causality	12
2.1.3 Partial directed coherence	12
2.1.4 Directed transfer function	13
2.1.5 Adaptive MVAR model	13
2.1.6 Coherence measurements	14
2.1.7 Nonlinear methods	14
2.1.8 Characteristics of brain connectivity methods	15
2.2 Brain error processing	15
2.2.1 Brain source and signatures in time domain	15
2.2.2 Oscillatory and brain connectivity patterns	16
2.2.3 Applications in BCI	16
2.3 EEG-based in-car studies	17

Contents

2.3.1	Brain controlled vehicles	17
2.3.2	Fatigue and drowsiness detection	17
2.3.3	Detection of other cognitive states	18
3	Methods	19
3.1	EEG recordings	19
3.2	Preprocessing of EEG data	19
3.2.1	Spectral filter	19
3.2.2	Spatial filter	20
3.3	EEG data analysis	21
3.3.1	Data extraction	21
3.3.2	Feature selection	22
3.3.3	Gaussian classifier	24
3.3.4	Cross validation	25
3.3.5	Performance evaluation	25
3.4	Brain connectivity computation	26
3.4.1	Directed transfer function	26
3.4.2	Short time directed transfer function	28
3.4.3	Direct Short time directed transfer function	28
3.4.4	Parameter specification	29
3.5	Beamforming source localization	29
3.6	Statistical analysis	31
3.6.1	Chance level using random classifier	31
3.6.2	Permutation tests	31
4	Brain connectivity in motor imagery tasks	33
4.1	Introduction	33
4.2	Methods	34
4.2.1	Participants	34
4.2.2	Experimental protocol	34
4.2.3	Feature extraction and selection	35
4.2.4	Classification settings	35
4.3	Main results	36
4.3.1	Brain connectivity patterns	36
4.3.2	Analysis of connectivity features	38
4.3.3	Offline classification performance	38
4.3.4	Online classification performance	40
4.4	Discussion and future work	41
5	Brain connectivity for stroke studies	43
5.1	Introduction	43
5.2	Study 1: Brain connectivity of stroke patients (motor area) after motor imagery based BCI rehabilitation	43

5.2.1	Patients	43
5.2.2	Experimental protocol	44
5.2.3	Signal preprocessing and brain connectivity	45
5.2.4	Results and discussion	45
5.3	Study 2: Brain connectivity analysis for neglect patients	47
5.3.1	Patients	47
5.3.2	Experimental protocol	47
5.3.3	Signal acquisition and processing	49
5.3.4	Brain connectivity	49
5.3.5	Statistical test	50
5.3.6	Results and discussion	50
6	Brain Connectivity Patterns of Performance Monitoring at Average and Single-trial Levels	53
6.1	Introduction	53
6.2	Participants and experiment procedure	53
6.2.1	EEG recording and pre-processing	54
6.2.2	Multi-trial brain connectivity	55
6.2.3	Statistical analysis	56
6.2.4	Single trial connectivity and classification	57
6.3	Results	58
6.3.1	Event related potentials (ERP) and spectrogram	58
6.3.2	Information inflow and outflow	60
6.3.3	Multi-trial brain connectivity patterns	60
6.3.4	Single trial connectivity and classification	63
6.3.5	Methodological Considerations	65
6.4	Discussion and conclusion	67
7	EEG-based Decoding of Error-Related Brain Activity in a Real-World Driving Task	71
7.1	Introduction	71
7.2	Materials and Methods	72
7.2.1	Participants	72
7.2.2	Experimental settings in car simulator	72
7.2.3	Experimental settings in the real car	74
7.2.4	Data acquisition and pre-processing	75
7.2.5	Classification	75
7.3	Results	76
7.3.1	Event-related potentials	76
7.3.2	Offline classification results	79
7.3.3	Online classification	80
7.4	Discussions	82

Contents

8	Estimating Brain Connectivity Patterns of Monitoring Error during Driving	85
8.1	Introduction	85
8.2	Methods	86
8.2.1	Data preparation	86
8.2.2	Computation of brain connectivity	86
8.2.3	Classification settings	86
8.3	Results	87
8.3.1	Feature analysis	87
8.3.2	Classification performance	88
8.4	Conclusion	89
9	Analysis of Neural Activity Related to Lane Changing Reaction Time	91
9.1	Introduction	91
9.2	Experimental setting and specification of data analysis	92
9.2.1	Experimental protocols	92
9.2.2	Experimental setup	93
9.2.3	Specifications for signal processing and data analysis	93
9.2.3.1	Data recording and processing	93
9.2.3.2	Source analysis	94
9.2.3.3	Analysis of brain connectivity	94
9.3	Main results	95
9.3.1	Behavior analysis	95
9.3.2	Event-related potential	96
9.3.3	Power spectral density	97
9.3.4	Frontoparietal network	99
9.4	Discussion and conclusion	101
10	Conclusions and future directions	103
10.1	Summary	103
10.2	Future work	105
	Bibliography	128
	Curriculum Vitae	129

List of Figures

3.1	EEG caps. A. Layout of 16 channels EEG cap, gTec system. B. Layout of 64 channels EEG cap, Biosemi system.	20
3.2	Trial extraction for motor imagery. The subject starts motor imagery after 'Start'. Individual trials are represented by the short line between 'Start' and 'End' period.	22
3.3	Evaluation of classification performance in the space of receiver operating characteristic. The x axis indicates the false positive rate or (1 - Specificity), whereas the y axis indicates the true positive rate or Sensitivity. Perfect classification can be found at coordinate (0,1), whereas the random performance can be found at (1,1). For the ROC curves, the classification is perfect when the area under the curve (AUC) is 1, and is random when it is 0.5.	26
4.1	Experimental protocol of motor imagery. A. Offline protocol. Each trial includes fixation (1000 ms), cue (1000 ms) before the bar starts moving, and the bar moves with constant speed within 4 seconds. B. Online protocol. Each trial includes fixation and cue with the same timing as offline, and the bar moves until it reach one of the targets, either left or right side.	35
4.2	Left and right hemisphere for brain connectivity analysis	36
4.3	A: The modulation of DTF during left and right hand motor imagery. The values indicate the difference between left hand and right hand motor imagery. Each curve indicate the modulation between or within two hemispheres, e.g., Left->Right indicates the information flow from left hemisphere to right hemisphere. B and C: Average and variance of brain interaction patterns in A of two frequency ranges across subjects, and the statistical tests between brain interaction patterns. The values are the difference between two motor imagery tasks. Two frequency ranges are specified in this analysis, 10-14 Hz and 26-32 Hz, according to the differences in A.	37

List of Figures

4.4 Fisher score of single channel brain connectivity pattern. The values of the Fisher score is computed between two motor imagery classes, averaged in three frequency bands, 10-14 Hz, 18-26 Hz and 30-50 Hz. Results of two subjects are shown, in A and B respectively. These two subjects are further recorded in the online experiments. The connectivity patterns from channel j to channel i is indicated in the location (i, j) . The Fisher score of the connectivity pattern between each pair of electrodes is color coded (red indicates higher scores). Notice that subplots have different ranges. 39

4.5 The offline performance of classifying two motor imagery tasks with three types of features. Number of features increase from 1 to 50. The gray area indicate the feature with significant difference ($p < 0.05$) between PSD and BOTH. 39

5.1 A. Mean levels (\pm SD) of brain connectivity patterns between two hemispheres. Four causal brain interaction pairs in beta rhythm (25-40 Hz) are illustrated in each group (experimental and sham) for both before and after BCI therapy. Mean values and standard deviations are shown as bars. Wilcoxon rank sum tests are adopted and the p values are shown. B. Normalized SdDTF for each electrodes in the experimental condition. 46

5.2 Experimental paradigm of CVSA. Each trial started with a fixation period (3000 ms) where patients had to gaze at a cross, visible at the center of the screen. Then the cross was replaced by a cue (300 ms duration) indicating the to-be-attended location. The covert attention period lasted for 3000–4000 ms; afterwards, one of the two images was highlighted in red (target selection, 100 ms) as online feedback of the classification result. Immediately afterwards, the image started moving toward the center of the screen (target movement, 1000 ms) and it disappeared after 400 ms (target stop). Patients were required to press a button with their right hand as soon as they perceived the moving image. 48

5.3 Directed connectivity between regions of interest across the online sessions in the case of the left target condition. The figure shows the SdDTF values per run of each patient, for each online session. Mean and standard deviation are reported in black. P1: Green circle. P2: Red diamond. P3: Blue cross. Asterisks indicate significantly different pairs ($p < 0.05$) found by the Tukey’s range test. 51

6.1 Experimental protocol. 20 squares in light red are presented in a computer screen in front of the subject. The green square indicates the moving cursor and the red square represents the target. The green cursor moves to the target with 80% probability, i.e., correct trials (in the left column). The position of the moving cursor is randomly initialized after reaching the target (the target turned to light green) or continuing moving for more than 10 steps. The moving cursor stops on each position for 2000 ms. 55

6.2 A. Grand average of the event-related potential (ERP). The black lines indicate the error condition, the gray lines show the correct condition, and green areas show the periods with significant differences between error and correct. Origin of the time axis, 0 s, represents the onset of the visual stimuli (i.e. cursor movement). Four EEG channels in frontolateral (F3 and F4) and midline central (FCz and CPz) areas are illustrated. B. Topographies of the ERP difference (error - correct) at selected time points, -0.2 s, 0s, 0.24 s and 0.33 s. C. Differences of event related spectral perturbation of selected channels. The gray ($p < 0.05$) and black ($p < 0.01$) contours indicate the areas where significant differences between correct and error conditions were found. 59

6.3 Grand average of information inflow and outflow for all electrodes in theta band. Results were referenced by dividing the mean value of the pre-stimulus time window (-875 ms to -125 ms) and averaged for all subjects. Values equal to 1 denote no change from pre-stimulus levels. Greater values indicate an increase in inflow/outflow, while smaller values represents a decrease. Gray circles indicate $p < 0.002$, and the black markers denote statistical significance using Bonferroni correction. 60

6.4 Brain connectivity between frontocentral, frontolateral and centroparietal areas. 62

6.5 Single trial analysis of brain connectivity between F3, F4, FCz and CPz. 64

6.6 A. The difference (error - correct) of topographies in source level at 240 ms and 330 ms after visual stimuli, using beamforming of 41 ROIs under 41 central EEG electrodes. The values are thresholded at $-0.2 \mu V$ for the negative peak and $0.4 \mu V$ for the positive peak. B. Time-frequency spectrogram (error - correct) of four brain sources under electrodes F3, F4, FCz and CPz. C. Fisher score of brain connectivity patterns between four selected brain sources, in two frequency bands, 4-15 Hz and 20-30 Hz. The values of the Fisher score are represented by the color and the thickness of the arrows. Power spectrum density (error - correct) of the brain sources at 240 ms is indicated by the color. 66

7.1 Experimental settings and protocols. A. Setup of experiments in car simulator with EEG recording. B. Virtual environment as perceived by the driver in the car simulator. Directional signs (white panel with black arrow in the center) shows the direction of turning; while information from the driving assistant are shown over the dashboard (gray and green arrows). C. Timings for experimental protocol. A visual cue is shown to notify subjects that a new trial is starting, and the directional cue informs a possible turning direction to elicit error-related brain activity if conflicted with subject's preference, and the visual feedback indicates whether the system have detected error activity. The arrows disappear at 500 ms. D. Vehicle Infiniti FX30 used for the real car experiments. The inset shows the monitor displaying the experimental cues. E. The closed track used for the real car experiments. The red flag indicates the start point of the lap. . . 73

List of Figures

- 7.2 Grand average of ERP and PSD at FCz. EEG trials are epoched according to the directional cue (0 s), from -1 s (presence of the three gray arrows) to 1 s. A. ERP of the car simulator data. B. ERP of the real car data. Significant differences ($p < 0.01$) across time samples between error and correct trials are found by two-sample t -test for all trials, which are shown as green thick lines. The red triangles indicate the time points selected for the illustration of topography in Figure 7.3. C. PSD of the car simulator data. D. PSD of the real car data. PSD is computed in time window [200 400] ms. Statistical tests are performed by a two-sample t -test for all trials, and the significances ($p < 0.05$) are shown as the green area. 77
- 7.3 Topographic illustration of brain activity at time points of ERP peaks and $t = 0$ ms (onset of the directional cue). A. Car simulator dataset. B. Real car dataset. 41 central electrodes are shown in the figure, excluding the peripheral regions. . . 79
- 7.4 Offline classification performance of both car simulator ($N=22$) and real car data ($N=8$). A. Results in ROC space for the car simulator, i.e., quantified by false positive rate and true positive rate. Each curve shows results of one subject (10-fold cross validation) B. Results in ROC space for the real car. C and D. Median and 25th/75th percentiles of accuracy and area under the curve in car simulator and real car datasets. Black boxes show the results of using EEG signal, gray boxes show the results of using EOG signal, and the empty boxes indicate the chance levels. Asterisk indicates significant difference using t -test. 80
- 7.5 Performance of online experiments in the car simulator ($N=7$). A. Classification accuracies in the online runs (from 2 to 5), averaged across participants. Error bars represents the standard deviation. B. False positive and true positive rate of all online runs for. Each type of marker represents one specific subject and the face color (white to black) indicates the run order, i.e., lighter markers correspond to earlier runs than darker markers. 81
- 7.6 Online performance of real car experiments ($N=7$). A. Classification accuracy for each subject with different number of runs. Runs that did not deliver visual feedback was labeled as 'No Feedback'. B. False positive and true positive rate of all runs. Subjects are represented by marker types, and the color convention is the same as in A. The runs with feedback are indicated with filled markers. . . . 82
- 8.1 The distribution of the discrimination power of connectivity features for simulated driving. A. The distribution of the Fisher score in temporal domain. B. The distribution in the frequency domain, 1-30 Hz. The gray areas indicate the standard error across all subjects and the dark curves represent the grand average. 87
- 8.2 The distribution of the discrimination power of connectivity features for the real car experiments. A. The distribution of the Fisher score in the temporal domain. B. The distribution in the frequency domain, 1-30 Hz. The gray areas indicate the standard error across all subjects and the dark curves represent the grand average. 88

8.3	The discrimination power of connectivity patterns between 4-10 Hz, from 200 ms to 800 ms. A. Real car. B. Simulated driving. The information flow is from the vertical index to the horizontal index.	88
8.4	Classification performance of the datasets in the car simulator (N = 22) and the real car (N = 8). A. ROC curves for each subject using connectivity features (red trace) and combined features (black trace). The bar plots indicate the averaged and standard deviation of the AUC. B. The results of the dataset for real car. . .	89
9.1	Experimental protocol. A. Timing of the protocol. Subject drives straight in a two lane motor way. An obstacle will appear either in the same lane (rare condition, 20%) or the other lane (frequent condition, 80%). The subject need to change lane immediately if the obstacle is in the same lane to avoid collision. B. The screenshot of the 3D environment.	93
9.2	Analysis of lane changing behaviors in the rare condition (an obstacle appeared in front of the car, thus requiring a lane change).A. Steering curves are averaged across all subjects for each distance level between the car and the obstacles. Distances are represented by the gray scales of the curves. B. Histogram of the reaction time for all rare trials. Trial number was calculated from all subjects. C. Histogram of the reaction time for each subject for all rare trials. The curves are the fitted lognormal distribution.	95
9.3	Event-related potentials and their correlation with reaction time. A and C: Event-related potentials in FCz and CPz. Reaction time of a trial is color coded (the darker the faster), and the grand average is shown by the thick red curve. B and D: Correlation between reation time and the peak time. To compute the correlation, we chose an ERP peak before the steering reaction: First positive peak for FCz and first negative peak for CPz. E: Topography of ERP amplitude for all trials at 300 ms for lane change trials. F Topography of correlation coefficients. G. Topography of ERP amplitude for all trials at 300 ms for no lane change trials.	97
9.4	Analysis of power spectrum density. A and B. PSD of the electrode FCz and CPz in no lane change and lane change cases, respectively, and the topograpies of theta and beta power (200 ms to 400 ms). C: Linear fitting between the reaction time and the band power, theta (4-8 Hz) and beta bands (20-35 Hz), for electrodes FCz and CPz, and the topographies of correlation coefficients for theta power and beta power.	98
9.5	Analysis of frontoparietal network. A: Directional connectivity patterns between frontal and parietal regions in time-frequency domain. B: Linear fitting between reaction time and the averaged connectivity in theta and beta bands. C. Correlation analysis between the reaction time and the peak timing of directional connectivity pattern in theta and beta bands.	100

List of Tables

4.1	Online command delivery accuracy and command delivery speed for three subjects. Three types of features are evaluated, and each method with four different of feature number, 25, 50, 75 and 100.	40
5.1	Patients' characteristics	44
5.2	Information of the neglect patients	47
5.3	Region of interest and related electrodes defined for brain connectivity analysis	49

1 Introduction

1.1 Brain computer interfaces

Mind reading is always one of the most fascinating capabilities that human being would appreciate to have, not only appears in the ancient mythology and the recent urban tale, which is also the basis of realizing remote object moving with direct mental command even from the scientific point of view. For more than hundred years, many explorations and studies have attempted ways to record, understand and translate people's mind into a realistic implementation. The first obtained electrophysiological signal from the human brain was from the surface of the head, electroencephalogram (EEG), which was recorded by Hans Berger in 1924. Even though it was questioned and not fully understood in the beginning, the EEG signals had already been recognized by researches and had been widely used in different aspects of the scientific societies by 1938.

The modern concept and definition of Brain computer interface (BCI) comes from studies performed around 1970s with non-invasive EEG recordings (Vidal, 1973; Vidal, 1977), and the early studies of single neuron firing using the implanted electrodes in monkeys to control an artificial arm with neural activity (Fetz, 1969; Schmidt et al., 1978). The real-time control of external devices has been achieved more than ten years ago, benefiting from the developments of computer science and techniques for measuring the brain activity (Nicoletis, 2001; Serruya et al., 2002; Wolpaw et al., 2002; Millán, 2002; Taylor et al., 2002; Velliste et al., 2008; Galán et al., 2008; Do et al., 2013; Höhne et al., 2014). As how it is intuitively understood and practically implemented, a brain computer interface system allows us to control an external device or a computer using direct brain activity without any limb movement. This extends people's approach of communication, and is particularly helpful as direct control of wheelchair or prosthetic arm for limb impaired patients.

Due to the different signal acquisition techniques for recording brain signals, there are basically two categories of BCI, i.e., non-invasive and invasive systems (Millán and Carmena, 2010). Invasive systems require surgery to implant electrodes either penetrating into the cortex or to put electrodes under the skull to obtain single unit action potentials or local field potentials

Chapter 1. Introduction

(Nicolelis, 2001; Serruya et al., 2002; Carmena et al., 2003; Musallam et al., 2004; Leuthardt et al., 2004; Hochberg et al., 2006; Velliste et al., 2008; Ganguly and Carmena, 2009). The invasive techniques could provide clean brain activity (not being contaminated by muscular noise from the movements of the head/neck) with high spatial resolution, and possibly to answer the fundamental questions about how the brain modulates and adapts to environmental contexts and internal intentions, which could further contribute to the improvement of future BCI designs. Even though the chronic stability of the brain signal and the cortical condition could be more or less verified in these invasive systems (Nicolelis, 2003; Nicolelis et al., 2003; Lebedev and Nicolelis, 2006), it is still not acceptable for a healthy person to admit such an open skull operation to place implants under the skull for an on-developing technology. However, such risk might still be accepted by patients who have little or no reliable muscle movements, or for those who have already been implanted with electrodes for other medical purposes.

The non-invasive BCI systems do not require any surgery to place the electrodes, which are usually located on the surface of the scalp and use conductive gel to improve the conductivity between the skin and the sensor (Birbaumer et al., 1999; Wolpaw et al., 2002; Millán, 2002; Wolpaw and McFarland, 2004; Millán et al., 2004; Ferrez and Millán, 2008; Galán et al., 2008; Millán et al., 2009; Höhne et al., 2014). Even though it is still somewhat not fully comfortable to wear an EEG cap for a long period to perform BCI tasks, the risk and the side effects are trivial comparing with the surgery-based invasive BCI systems.

Although debates of choosing different brain sources for BCI systems exist for decades, either invasive or non-invasive, and even given the many pros of the invasive brain signals, it is a simple truth that the primary goal of translating human thoughts into executable commands is to improve the quality of life. Therefore, we believe that the non-invasive systems are more suitable for the current stage of BCI, which is also the focus of this thesis.

The most popular non-invasive brain computer interfaces use scalp EEG recordings, due to its high temporal resolution and simplicity in implementations compared to other non-invasive recording means, e.g., functional Magnetic Resonance Imaging (fMRI) (Weiskopf, 2012; Birbaumer and Cohen, 2007; Weiskopf, 2012), Near-Infrared Spectroscopy (NIRS) (Sitaram et al., 2007; Luu and Chau, 2009; Pfurtscheller et al., 2010) or Magnetoencephalography (MEG) (Weiskopf et al., 2004; Mellinger et al., 2007; Buch et al., 2008). Typically, two main categories could be found in EEG based BCI systems, one of which aims to recognize brain modulation patterns when people are given specific stimulus, and the other category uses voluntary performance of a given mental task that could be discriminated from other pre-defined tasks.

The first category is also called reactive BCI due to the fact that the associated brain patterns are the reactions to external stimuli, and the brain activities are normally phase-locked to the provided stimuli, e.g., P300 spellers (Farwell and Donchin, 1988; Donchin et al., 2000; Krusienski et al., 2008; Townsend et al., 2010), error-related BCI (Schalk et al., 2000; Ferrez and Millán, 2005; Buttfeld et al., 2006; Ferrez and Millán, 2008; Chavarriaga and Millán, 2010), and

visual potentials (Sutter, 1992; Middendorf et al., 2000; Müller-Putz et al., 2005; Müller-Putz and Pfurtscheller, 2008; Allison et al., 2008; Guo et al., 2008; Vialatte et al., 2010). On the other hand, the most popular active EEG BCI is based on motor imagery of limbs, i.e., hands or feet, generating spontaneous modulation of brain patterns during the imagination (McFarland et al., 2000; Pfurtscheller and Neuper, 2001; Pfurtscheller et al., 2006). This thesis will focus on the analysis of EEG based non-invasive BCI of both kinds, reactive and spontaneous, and also the implementations in realistic scenarios.

BCI systems have been mainly developed to restore control or communication functions for people with motor impairments, and to extend the interaction ability for healthy people. One of the possibilities to implement BCI in healthy people could be the driving assistant systems, for the purpose of reducing driving complexity or preventing traffic accidents. Researchers have explored BCIs to drive cars via mental commands (Göhring et al., 2013; Chang et al., 2010; Hood et al., 2012), Even though this attempt is limited by the current state of brain signal decoding accuracy. Alternatively, a BCI system could assist the detection of driver's cognitive states, e.g., mental fatigue (Lal and Craig, 2000; Eoh et al., 2005; Papadelis et al., 2009; Lin et al., 2010; Maglione et al., 2014), emotion state (Herbert et al., 2007; Katsis et al., 2008; Fan et al., 2010), behavior intention (Khaliliardali et al., 2012; Gheorghe et al., 2013a), or emergency braking (Haufe et al., 2011; Haufe et al., 2014; Kim et al., 2015), given that these processes are highly related with traffic accidents, e.g., drowsiness during driving (Idogawa, 1991; Horne and Reyner, 1995; Häkkinen and Summala, 2000; Philip, 2005), road rage (Hennessy and Wiesenthal, 1999; James, 2000; Galovski et al., 2006). BCI could also decode people's decision preference through the detection of error-related brain activity (Zhang et al., 2013), which can be used in intelligent vehicles, e.g., to automatically control the direction indicator, window open/close, or Windshield wiper. This thesis implements BCI systems in driving tasks.

1.2 Brain connectivity

1.2.1 Brain connectivity

Brain connectivity refers to a pattern of anatomical links (anatomical connectivity), of statistical dependencies (functional connectivity) or of causal interactions (effective connectivity) within a nervous system (Sporns, 2007). Before the development of brain connectivity, the mainstream of neuroscience was focusing on brain segregation, which suggests that a cortical group (clusters or modules) is specialized for some aspects of cognitive functions and it is anatomically segregated within the cortex, or functional localization, which implies that a function can be localized in a specific cortical area (Tononi et al., 1994; Rubinov and Sporns, 2010; Friston, 2011). Even though the studies of segregated brain activity have been dominating the brain mapping and neuroscience research for many decades, the rising trend of the publication number on brain connectivity is paramount during the last years, especially after 2000 (Friston, 2009).

Chapter 1. Introduction

Given that the human brain is organized in a large number of functionally specialized and spatially distributed cortical neurons, processing of cognitive functions and motor tasks are associated with multiple brain regions and correlated with dynamic interactions between these areas (Bressler, 1995; Varela et al., 2001; Gusnard and Raichle, 2001; Buzsáki and Draguhn, 2004; Mason et al., 2007; Bullmore and Sporns, 2009; Siegel et al., 2012). The exploration of the neural basis and mechanisms of specific cognitive process requires fundamental understanding of the functional interaction between brain regions. Accordingly, these information transfer patterns can be further exploited for the recognition of cognitive processes.

Brain connectivity is a tool to analyze interactions between distinct brain regions within the nervous system. It can be described at several levels, i.e., structural, functional, or effective. The structural connectivity describes networks of anatomical links, while functional connectivity denotes the statistical dependencies between remote regions. Finally, the effective connectivity is specified as causal/directional interaction between distinct areas (information flows) (Bullmore and Sporns, 2009).

The structural connectivity is usually referred to synaptic, axonal projections, or fiber pathways within certain groups of neurons. The long term connectivity is relatively not as stable as the short term one due to the morphological and neural plasticity. It could only be assessed by *in vivo* markers in invasive tracing studies with pre-defined brain locations (Sporns, 2007). The functional and effective connectivity are usually approached by mathematical computations, based on the results of correlation or covariance on multi-channel time series recorded at different locations. The effective connectivity further concerns the causality between these locations, or the directionality of the information transfers, which could be obtained by multivariate autoregressive models (Kamiński and Blinowska, 1991; Baccalá and Sameshima, 2001). Normally, the computation of effective connectivity requires high temporal resolution, since the directionality is usually determined by the temporal order of activation across different brain regions. The functional connectivity does not include the information of directionality, thus could be obtained through the computation of coherence or mutual information (Bendat and Piersol, 1980; Pfurtscheller and Andrew, 1999; Rissanen and Wax, 1987; Na et al., 2002).

Electrophysiological (EEG and MEG) and fMRI signals have been used to evaluate brain connectivity patterns. Electrophysiological techniques measure neuronal activity directly with high temporal resolution using a certain number of sensors, whereas fMRI records haemodynamics rather than neuronal activity, which has poor temporal resolution (0.001-0.5 Hz). On the other hand, fMRI has good spatial resolution (the voxels are in millimeter), whereas electrophysiological methods have lower spatial resolution (millimetres for MEG and centimetres for EEG) or less complete anatomical topology, which covers only some parts of the brain. Since the analysis of effective brain connectivity needs high temporal resolution, especially when oscillatory modulations (theta, alpha and beta bands) patterns are taken into account, the electrophysiological approaches appear to be more appropriate to be used to obtain such causal interactions. However, the spatial resolution is low and

only surface activity can be recorded by non-invasive electrophysiological recordings. Hence some source reconstruction methods can be adopted to estimate neuronal activity in task specific brain regions (Hipp et al., 2011), and effective connectivity are computed from the reconstructed source level cortical activities. This thesis focuses on analyzing effective brain connectivity through the recording of EEG signals from human subjects, exploring the task specific directional information flows to find intrinsic neural mechanisms.

1.2.2 Brain connectivity analysis in BCI

The BCI applications usually use the machine learning approaches to detect or discriminate brain patterns during specific cognitive processes. Even though the performance of BCI systems relay on the selection and performance of machine learning algorithms, the basis of BCI is in fact the understanding of the brain function and the findings from neuroscience studies, for instance, the implementation of motor imagery is built on the classification of the desynchronization patterns in sensorimotor regions, and the error monitoring based BCI systems depend on the detection of theta oscillatory activity originated in anterior cingulate cortex. As a tool of analyzing causal correlation between brain regions, the connectivity analysis leads to further understanding of the neural mechanisms, not only from the temporal causality but also the oscillatory influences in specific frequency bands. This provides extra evidences to interpret cognitive processes and show additional neural signatures apart from the results in brain areas separately.

The other concern of applying brain connectivity is to use these modulation patterns as input knowledge to recognize brain status. In this case, the connectivity patterns are exploited in classification models, assuming that these information is discriminative between different BCI tasks, or not identical between a specific task and the resting state. Such features have already been adopted in some BCI implementations as exploratory assessments. In general, the connectivity features are equivalent to other features, e.g., amplitudes of temporal signals or powers of spectral density. However, the computation of brain connectivity results in a large amount of features, i.e., square of the spectral features, which leads to a curse of dimensionality. Thus, a preliminary refining of these information is necessary before feeding them into classification models, which could be achieved either by supervised machine learning methods or constrained to those holding physiological meanings. In fact, some kernel methods can also project original data into specific hyperplanes that possibly reflect certain correlation between original. These information could also be exploited in classification models. However, these projections remain as a black box which could not successfully provide physiological interpretations of the features.

1.3 Objectives

This thesis contains two mains aspects. The first aspect focuses on the exploration of neural basis for different cognitive processes through the use of brain connectivity analysis and its

potential use in BCI applications. In this part, the oscillatory modulation patterns during motor imagery, error monitoring and emergent motor reaction will be analyzed. The second aspect aims at developing an in-car BCI system to improve the driving experience, which will be validated in both simulated and real driving environments. In this part, the cognition of monitoring error is adopted to estimate driver's intentional turning direction when vehicles are approaching intersections. The studies conducted in this thesis are based on EEG recordings.

1.3.1 Exploring neural correlates using connectivity analysis

Error processing

As an essential function of the human brain for behavior adjusting and learning (Holroyd and Coles, 2002; Taylor et al., 2007), error processing has been used in BCI systems to recognize the correctness of the feedback, either to correct the previous executed BCI commands or as pure monitoring of external stimuli (Schalk et al., 2000; Buttfeld et al., 2006; Ferrez and Millán, 2008; Chavarriaga and Millán, 2010). An electrophysiological signature of this process appears as an event-related potential over frontocentral areas elicited both in the case of self-generated errors –when subjects make wrong decisions in response to cues, e.g., in speed response tasks– as well as when they observe erroneous actions performed by external agents (van Schie et al., 2004; Milner et al., 2004).

Previous reports have shown the brain connectivity patterns of brain error processing, but they have limited their analysis to the responding error and do not report the evidences from the directionality and temporal evolution of the connectivity patterns (Kerns et al., 2004; Brown and Braver, 2005; Brázdil et al., 2007; Cavanagh et al., 2009; Brázdil et al., 2009). Therefore, the work in this thesis complements these studies by exploring directional information flow patterns during monitoring error and reports their dynamics in the temporal domain.

Reaction time

Reaction time measures how fast people can respond to the presentation of a sensory stimulus (Donders, 1969) and depends on both stimulus characteristics and people's mental states. These stimulus characteristics include stimulus modality, intensity and task urgency. The task urgency is correlated with the contextual environment that indicates, e.g., harmful situations. The translation between the stimulus task urgency and the motor reaction is modulated by afferent and cortical areas (Galton, 1890; Carlsen et al., 2004). Recent studies have shown the evidences of the correlation between brain activity and the reaction time, where frontal and parietal brain areas are associated with immediate response to urgent events (Kastner and Ungerleider, 2000). More particularly, the parietal region is believed to be activated earlier than frontal regions during stimulus driven behavior (Buschman and Miller, 2007).

However, the knowledge of these neural modulations during driving has not been revealed. This correlation information could possibly enable the prediction of reaction before the behavior onset, and could be potentially implemented in an intelligent car to improve the driving safety. So, this thesis explores this mechanism in simulated driving, evaluating the

reaction time in varied emergency levels and attempts to uncover the brain network patterns.

Motor imagery

As one of the most popular approaches for non-invasive BCI, motor imagery is based on the oscillatory desynchronization over the sensorimotor regions when people are imagining moving their limbs, i.e., hands or feet (McFarland et al., 2000; Pfurtscheller and Neuper, 2001; Pfurtscheller et al., 2006). The mechanisms of motor imagery have been probed for many decades and there are already some studies attempting to use brain connectivity to extract novel features for classification purposes (Wang et al., 2006; Grosse-Wentrup, 2008; Billinger et al., 2013).

However, the link between features used for BCI and the interpretation of the information flows is barely analyzed, thus this thesis will try to understand connectivity patterns between hemispheres during different types of motor imagery. This analysis will also be applied in the case of stroke patients, using motor imagery based BCI to improve motor function, in which the connectivity of two hemispheres will be computed and associated with the stroke recovery.

1.3.2 Classification based on brain connectivity features

The significance of including brain connectivity features in classification comes from the information it contains, which are independent and unique from the features extracted locally. Due to these attributes, it is not difficult to accept that the brain connectivity could improve the performance of discriminating different cognition states (Wang et al., 2006; Grosse-Wentrup, 2008; Billinger et al., 2013).

However, most of the recent studies only performed offline analysis of brain connectivity and did not evaluate their online implementation. This may be due to several reasons. First of all, the computational cost is much higher for obtaining the connectivity features than either temporal amplitude or band power. Secondly, the dimensionality of the connectivity results is the square of the original feature number, which requires further feature selection to refine the subset of features. Last but not least, the computation of connectivity requires significant amounts of data, which might not be trivial during online experiments. Therefore, this thesis will try to explore connectivity method for classification in online experiment, as well as to combine it with temporal feature and band power to improve the classification performance.

1.3.3 Build in-car BCI

In order to bring BCI outside of the lab and reach a large number of potential users, it will be ideal to build a system that can be utilized while performing daily tasks that normally require the use of hands and feet, e.g., for driving a car. In this case, the BCI system could bring an extra control channel without increasing the complexity of the original task, or replace an original physical button by pure mind command. Even though the BCI system could also be used to drive the car, e.g., deliver steer or brake commands to change lane or to stop the

Chapter 1. Introduction

vehicle. However, such application requires perfectly decoding of the human brain to avoid mis-control or safety problems, which could not be achieved by current BCI systems.

The study in this thesis will focus on an assistant function, e.g., decoding the preferred turning direction. The development of such BCI system is achieved by two steps. A first stage in laboratory settings using a car simulator was taken place to validate the feasibility of decoding brain signals during driving. A further step of real car experiments were performed to evaluate the system in a realistic environment, where the quality of the EEG signal is reduced due to the contaminations caused by the eyes/head moving and the vibrations of the vehicle. As an essential part of the study, the real car experiment is a significant step to move the BCI system from laboratory verification to the phase of real practice.

1.4 Thesis outline

This thesis is organized in four parts. The first part reviews the state-of-the-art of the related studies, mainly focusing on EEG based brain connectivity and current states of in-car BCI systems. This part will also include the main methods that are used in the studies, i.e., signal processing, data analysis and statistical tests. The second part of the thesis focuses on the brain connectivity study on motor imagery task and the real time motor imagery decoding based on connectivity features. It will also assess the use of connectivity in evaluating the recovery of stroke patients following BCI-based rehabilitation therapy. The third part includes the study on brain error processing and its application for in-car BCI in order to estimate mental preferences during driving. Both studies will adopt the analysis of cross-regional influences in order to understand the neural basis and as novel features for EEG pattern recognition. Additionally, this part includes the exploration of reaction time during emergent conditions in a driving task. The last part of the thesis will summarize and conclude the contributions of the studies and will foresee potential future works. A concise description of each chapter follows:

Chapter 2 describes the relevant state-of-the-art of our studies. This chapter will provide brief description of different methods for computing brain connectivity, and their pros and cons. Further overview will cover the recent studies of in-car BCI researches, assisting driving experience or improve safety through the detection of brain activity patterns from EEG recordings.

Chapter 3 elaborates the methods that will be used in the thesis. It starts from basic approaches of EEG related analysis, the recording system and the signal preprocessing methods. It also describes the machine learning algorithms to classify and recognize the EEG patterns. In our study, inverse solutions from scalp EEG to brain sources is used to extract activity in certain brain regions, thus the source localization methods will be described. The detail of the brain connectivity computation and the selection of parameters are specified in the chapter as well. The final part of this chapter will cover the statistical tests that are used in the thesis.

Chapter 4 reports the inter- and intra-hemisphere interaction patterns during motor imagery and the connectivity features in classification tasks. This study includes both offline and online studies. The offline analysis covers the statistical tests of the modulation patterns and the assessment of appropriate number of features. The details of online computation of brain connectivity is described as well. The decoding performance between connectivity features and the traditional power spectral density are compared in both online and offline data.

Chapter 5 implements brain connectivity in dataset of stroke patients. Two studies are included in this chapter, the first of which investigates motor imagery based BCI therapy for chronic stroke survivors, and the second one explores the benefits of covert attention based BCI for spatial neglect stroke patients. In both studies the modulation of connectivity patterns between healthy and lesioned cortices are evaluated.

Chapter 6 explores the neural basis of monitoring error based on the analysis of oscillatory directional information flows, mainly in theta and beta bands. This study aims to find the fundamental evidences to verify whether monitoring error has similar neural basis as self-responding error. The brain connectivity analysis is applied in both subject level and single trial level. The single trial connectivity pattern is further used as input features for the recognition of error perception. In addition, the results are consistent with the information transfer modulation at the source level, based on the beamforming source reconstruction.

Chapter 7 aims to develop an in-car BCI to estimate the turning direction when the vehicle is approaching intersections, using error related brain activity. The concept of this implementation is based on the fact that an error related brain activity, deflection of medial frontal theta, can be detected when a visual stimulus is conflicted with people's expectation. This chapter will validate the study in both simulated driving and real car experiments. The real car test is performed in a closed circuit and also uses visual stimuli to evoke error potentials. The protocol is also tested in real time classification, which further confirms the feasibility of decoding brain activity during driving.

Chapter 8 is an extension of Chapter 7 and is based on the findings in Chapter 6. In this chapter, we use the data recorded in Chapter 7 and analyze the feasibility of adopting connectivity features as classifier inputs in driving data, where we select specific brain regions according to the results in Chapter 7. The comparison between the traditional and connectivity features are compared, as well as the combination of both. This study justify the possibility of applying connectivity in real world EEG data, which is more noisy than those recorded in laboratory environment.

Chapter 9 targets on finding neural signature of reaction time in an emergency situation during driving, i.e., change lane to avoid collision with a suddenly appearing obstacle in front of the vehicle. The correlation between the reaction and the neural activities are analyzed, including peak timing of event-related potential, power spectrum density, and brain connectivity patterns. This study provides evidences linking human behavior and brain modulations, particularly in frontal and parietal regions and their interactions, which could possibly be

Chapter 1. Introduction

implemented in future application for behavior prediction during driving to improve safety.

Chapter 10 summarizes the contributions of the studies, particularly the two main lines of the thesis, brain connectivity analysis (chapter 4, 5, 6, 8 and 9) and in-car applications (chapter 7, 8 and 9). This chapter also outlooks the future study that could be achieved in both short time and the long term duration.

2 State of the art

2.1 Computational methods for brain connectivity

This section will provide a review of the studies on brain connectivity, particularly those recent publications measuring functional and effective connectivity with EEG. In the past decades, various methods have been developed to estimate the brain connectivity, and a lot of efforts have been contributed to improve the robustness and stationarity. In general, there are many ways to classify them. For instance, they can be considered as two categories depending on whether the prior information of the model is given, i.e., model based and data driven methods. Typically, dynamic causal model is a model based method and most of the others are building brain connectivity structure based on collected data, e.g., directed transfer function and coherence. Also, these methods could be classified as either linear or nonlinear. Most of the methods we introduced here are linear except phase and information theory related measures. Depending on whether the method could reflect direction of the connectivity, these methods could also be separated as functional or effective methods, e.g., coherence, phase and information theory based methods are non-directional, whereas others are directional.

2.1.1 Dynamic causal model

In case of the underlying model structure is already known, presumably based on other neuroscience evidences or plausible hypotheses, dynamic causal models (DCM) is developed based on the assumption that the response of a neural system is driven by the changes in inputs (Friston et al., 2003; Penny et al., 2004; David et al., 2006; Stephan et al., 2007; Stephan et al., 2010), and it could be modeled by a network of interactive sources, either neural mass (Jansen and Rit, 1995; Moran et al., 2007) or conductance based models (Morris and Lecar, 1981). The DCM treats the brain as a deterministic nonlinear dynamic system and estimate the connectivity by perturbing the system and measuring the response (Friston et al., 2003).

This method is valuable when preexistent knowledge have been well-defined to reveal the as-

sociated brain regions and advisable connections. However, the current state of neuroscience studies usually lack the detailed knowledge on anatomical connectivity in the human brain, causing a large number of possible combinations of parameters in DCM, which might be a disadvantage of this method. In this case, people should choose the most probable model structure to reduce the uncertainty. This method has been implemented for fMRI studies (Stephan et al., 2007; Kiebel et al., 2007; Stephan et al., 2008; Marreiros et al., 2008), as well as studies with EEG and MEG (David and Friston, 2003; David et al., 2005; David et al., 2006; Kiebel et al., 2006; Kiebel et al., 2007; Moran et al., 2007; Moran et al., 2008; Chen et al., 2008; Daunizeau et al., 2009; Moran et al., 2009; Marreiros et al., 2009; Penny et al., 2009).

2.1.2 Multivariate auto-regressive models and Granger causality

In contrast to model-based methods, a more general case of estimating brain connectivity is to use a model which does not require any prior knowledge or underlying hypothesis which limits the structure of the network. Without such concerns, a data driven model is an ideal for the estimation, where the network structure and weights are learned empirically from the data. In the analysis of time series, we could define the causality depending on the prediction capability of one variable for another. In this case, if one channel of brain signal could be predicted by the past information of the second one, one could define it as directional influence from the second channel to the first channel.

Granger causality is one of the algorithms with such definition (Granger, 1969), which is actually a prototype of many algorithms used for the computation of effective brain connectivity. The algorithm was extended from two variables to multiple variables using a vector input (Geweke, 1984; Hosoya, 2001). It has been applied in frequency domain (Geweke, 1982), given the concept of parametric estimation of power spectrum density. The parameters could be estimated through many ways, for instance, Yule-Walker equations (Yule, 1927; Walker, 1931), after which the spectral information can be obtained by the Fourier transform of the coefficients of the multivariate auto-regressive model (MVAR).

2.1.3 Partial directed coherence

Partial directed coherence (PDC) is one of the methods that is based on the multivariate autoregressive model and aims to estimate the effective brain connectivity between multiple brain regions (Baccalá and Sameshima, 2001; Astolfi et al., 2006). The computation of PDC follows the procedure of MVAR model, and it is defined as the Fourier transform of the coefficient matrices of MVAR model. This method is an extension of the traditional concept of partial coherence with the measurement of directionality of the information flows (Schelter et al., 2006; Wehling et al., 2007), as the coefficient matrices are not symmetric. Comparing with other methods for effective connectivity, e.g., directed transfer function, it emphasizes on the sinks of the information flows, or the information outflows (normalized based on the outflows) from predefined brain regions (Baccalá and Sameshima, 2001). The other

2.1. Computational methods for brain connectivity

choice of normalization for PDC based on information inflows has also been defined since the information sinks are not always the most focused (Baccald and de Medicina, 2007). Recent implementations of PDC could be found in fMRI and EEG studies (Sato et al., 2009; Sun et al., 2009; Biazoli Jr et al., 2013; Omidvarnia et al., 2014).

2.1.4 Directed transfer function

As another algorithm based on MVAR model, directed transfer function (DTF) is also achieved after obtaining the coefficient matrices of MVAR model (Kamiński and Blinowska, 1991; Franaszczuk et al., 1994; Kamiński et al., 1997; Kamiński et al., 2001; Astolfi et al., 2004; Astolfi et al., 2005; Babiloni et al., 2005). It is defined based on the system transfer function, as the normalized square of the system transfer function in the frequency domain, rather than coefficient matrices comparing with partial directed coherence (Kamiński and Blinowska, 1991; Baccalá and Sameshima, 2001). Non-normalized DTF has also been defined to represent the coupling strength among brain regions (Kamiński et al., 2001). Similarly, this method is also able to measure the brain connectivity in frequency domain or information flows in specific oscillatory brain rhythms. Directionality of the causal influences are defined in this method as well, given that the system transfer function is not symmetric.

The DTF is normalized to the information inflows of specified brain areas, which is not identical to the partial directed coherence. Furthermore, this method shows the cascaded connectivity, not only the direct flows. Therefore, it has been combined with partial coherence to consider only the direct propagations, which is named as direct Directed Transfer Function (dDTF) (Korzeniewska et al., 2003). Due to the stationarity of the brain signals, the evaluation of the evolution of brain connectivity (time-varying DTF) could be obtained through the using of sliding windows in the phase of estimating MVAR coefficients (Ginter et al., 2001; Kuś et al., 2005; Kuś et al., 2008; Blinowska et al., 2010), which is called as short-time DTF (SDTF). This time-varying form of MVAR is not unique for DTF, which could also be applied for partial directed coherence. A further extension of DTF is to present the time-varying direct DTF, which was reported in an ECoG study (Korzeniewska et al., 2008).

As the MVAR model that has been defined, DTF and PDC methods show causal influence only when there is a phase difference among channels, meaning that the value is not significantly different from zero if there is no phase difference between signals. Therefore DTF and PDC are immune from volume conduction, since volume conduction is a zero phase propagation with no phases difference between channels (Blinowska, 2011).

2.1.5 Adaptive MVAR model

Another alternative approach to estimate MVAR coefficients is using Kalman filter, in which the coefficients are concerned as the hidden state, which updates for each time step, and the recorded signals are considered as the observations of the model (Miller and Cohen, 2001;

Hesse et al., 2003; Pereda et al., 2005; Astolfi et al., 2008). This model provides a way to estimate the coefficients adaptively for each time sample, comparing with the sliding window in the method of SDTF. The coefficients are updated according to the ratio between error covariance from the measurement and from the prior estimation. People may comment on the computation time of this method and concern it as a serious drawback (Blinowska, 2011). Nevertheless, if the adaptation of each step could be finished within the time of signal acquisition, this method could be working perfectly for real-time implementations. This method is designed to find adaptive MVAR coefficients, thus it is available for both DTF and partial directed coherence (de Vico Fallani et al., 2008).

2.1.6 Coherence measurements

Coherence, or magnitude squared coherence, is a concept in the frequency domain, derived by Fourier transform of cross correlation between variables according to Wiener–Khinchin theorem, which allows the quantification of correlation between brain region in different frequency bands (Pfurtscheller and Andrew, 1999). Since no directionality is defined, this method is a measurement of functional connectivity, which is sensitive to both change in power and phase synchrony (Bendat and Piersol, 1980). Similar to the MVAR model, coherence requires the assumption of stationarity of the signal. Nevertheless, a sliding window could be adopted to assess the evolution of coherence over time. The other variations of coherence, wavelet coherence and significant wavelet coherence, are also capable to calculate time varying coherence in particular frequencies (Lachaux et al., 2002; Sakkalis et al., 2006). Furthermore, these methods could be applied only in pairwise fashion, thus the computational cost is heavy and the cascading or indirect interaction patterns could not be distinguished.

2.1.7 Nonlinear methods

Phase-related measurement

Phase synchronization is another alternative method to measure brain connectivity, which is popular in recent neuroscience studies due to the fact that phase synchronization has specific interpretations in neural systems, particularly as an adjustment of oscillatory rhythms from different sources (Lorenz, 1963; Pikovsky, 1984; Pecora and Carroll, 1990; Lachaux et al., 1999). This concept was developed based on the assumption that neural signals have nonlinear characteristics and could be concerned as chaotic oscillators (Pikovsky et al., 2002). The phase value of brain signals, which could be obtained either by Hilbert transform or wavelet transform, are further exploited as phase locked value and generalized synchronization (Arnhold et al., 1999; Mormann et al., 2000; Pereda et al., 2005; Sakkalis et al., 2009). The phase locked value has also been implemented in the discrimination tasks in BCI systems as an application of brain connectivity patterns (Gysels and Celka, 2004; Gysels et al., 2005; Wang et al., 2006; Brunner et al., 2006; Gysels et al., 2007; Krusienski et al., 2012). Even though this method could neither theoretically nor practically outperform linear algorithms (MVAR and coherence), it provides complementary information and extra evidences that are not

feasible by linear methods (Sakkalis et al., 2009).

Information theory

The other nonlinear methods for brain connectivity is based on information theory. Basically, these methods are similar as coherence, but the criteria of defining the connectivity is changed. Here, the connectivity is defined as the mutual dependence between two signals, which can be obtained by the quantification of information gain of one signal when another is given, or the degree of predictability of each as a function of another (Jeong et al., 2001; Na et al., 2002; Rissanen and Wax, 1987; Grosse-Wentrup, 2008).

2.1.8 Characteristics of brain connectivity methods

Even though in the beginning of this section the difference has been made between data driven and model based methods, the border between these two is actually becoming vague. In particular, it is the fact that we also need to specify the regions of interest even using data driven methods, given that more data is required with more parameters in the model, thus the number of the brain sites should be limited. Therefore, the prior knowledge of the involved brain sites is important for these methods to select specific regions of interest to reduce the computational cost and improve the reliability of the results. On the other hand, the complete knowledge of brain structure has not been built yet, which prevents the perfection of model based brain connectivity analysis.

The property of linearity is also a crucial concern of these methods since the brain is a chaotic system and highly nonlinear, which seems like the nonlinear methods should outperform the linear ones. However, before we could perfectly build an interpretable nonlinear model to find all the hidden regulations, the nonlinear tools still could not replace linear approaches, since they are more robust and generalized even though they might have been oversimplified. This thesis mainly applies the MVAR based methods, DTF and its variations, to explore the neural basis for brain error processing and find novel features for classification in BCI tasks.

2.2 Brain error processing

2.2.1 Brain source and signatures in time domain

Brain error procession is an essential function of the human brain for behavior adjusting and learning (Holroyd and Coles, 2002; Taylor et al., 2007). The medial frontal cortex (MFC), and more specifically the anterior cingulate cortex (ACC) has been suggested as the putative locus of these mechanisms (Milner et al., 2004; de Bruijn et al., 2009; Shane et al., 2008). Activity in this area has been reported to be sensitive to expectation mismatch, error of motor commission, and erroneous feedback, reflecting both endogenous and exogenous performance-relevant information (Cavanagh et al., 2012).

The electrophysiological signature of the error processing appears as an event-related potential

(ERP) over frontocentral areas elicited by both self-generated and external errors (Cavanagh et al., 2012; Ullsperger et al., 2014). In the former case, the ERP shows an early negative deflection, termed as error-related negativity (ERN), appearing no later than 120 ms after the erroneous motor response (Gehring et al., 1993). Monitoring of external events elicits a similar modulation around 250 ms after stimuli (feedback-related negativity, FRN). Despite the timing difference, the negativities in both conditions precede a frontocentral positive deflection, followed by a sustained positivity over parietal areas (Ullsperger et al., 2014). Furthermore, source analysis of scalp ERP signals suggests that the brain systems associated with the monitoring of self-generated errors are also activated in the process of monitoring external errors (van Schie et al., 2004).

2.2.2 Oscillatory and brain connectivity patterns

EEG activity after self-generated errors exhibits response-locked theta band modulations at ACC (Luu et al., 2000; Trujillo and Allen, 2007; Cavanagh et al., 2012). This region is believed to coordinate local and distant functional brain connectivity with other cortices during the process of monitoring error events (Luu et al., 2000; Ullsperger and von Cramon, 2001; Brown and Braver, 2005). In particular, there exists strong evidence of causal influences from ACC to lateral prefrontal cortex (LPFC) via increased theta activity (Luks et al., 2002; Brázdil et al., 2007; Cavanagh et al., 2009; Brázdil et al., 2009). Further studies in goal-directed behavior suggests that the ACC detects conflicting or unmatched information and notifies LPFC and other related cortices as part of a monitoring system (Carter et al., 2000; Luks et al., 2002; Kerns et al., 2004). Moreover, both scalp EEG and magnetencephalography (MEG) studies have shown increased amplitude of theta interactions (Cavanagh et al., 2009; Brázdil et al., 2009), as well as beta rhythm suppression after the monitoring of erroneous responses (Cohen et al., 2008; Koelewijn et al., 2008; Mazaheri et al., 2009). These studies provide a consistent depiction of the connectivity patterns related to the monitoring of self-generated errors. In this thesis, we will analyze the brain connectivity patterns generated by the process of monitoring external errors.

2.2.3 Applications in BCI

Furthermore, the error-related potentials have been used in BCI implementations, detecting error activity while human subjects either controlling moving objects (Parra et al., 2003; Ferrez and Millán, 2008) or monitoring a moving cursor (Chavarriaga and Millán, 2010), to correct user's erroneous decision (Parra et al., 2003), improve the information transfer rate of BCI system (Ferrez and Millán, 2008), or detect subject's intentional preferred target (Chavarriaga and Millán, 2010; Zhang et al., 2012). This thesis exploits the the monitoring error in a in-car BCI application, attempting to decode driver's turning direction when the vehicle is approach an intersection.

2.3 EEG-based in-car studies

Recently, many systems have been developed to record brain signals during vehicle driving, typically scalp EEG. The objectives of such systems include driving the car using brain signal directly, assessment of driving safety through the detection of drowsiness and fatigue condition, recognition of cognitive states during driving, e.g., workload, stress and emotion, and improve the driving experience as an assistant system. Most of these studies are still in the stage of laboratory tests based on simulated driving in virtual environments.

2.3.1 Brain controlled vehicles

As an essential concern of brain computer interface is to find a bypass approach to control devices through direct mental commands, there are studies that already tested the BCI control of vehicles. Semi-autonomous driving has been implemented by classifying motor imagery tasks, using Epoc EEG cap from Emotive, and a vehicle with variety of sensors which could be controlled by wire signals (Göhring et al., 2013). In this case, the study is based on real car experiments. The other study exploited SSVEPbased BCI for the decision of control commands, e.g., steering and acceleration, represented by whether the user directs visual attention to one of the frequency-modulated lights (Chang et al., 2010; Hood et al., 2012). Even though the study by Göhring has already been implemented in real car experiments, given the fact that it is hardly to achieve very high accuracy in BCI tasks, these studies are still far from daily use concerning the safety of either the BCI controlled vehicle and other automobiles in the road.

2.3.2 Fatigue and drowsiness detection

Another EEG based application during driving is to detect driver's mental fatigue and drowsiness, which are related with reduced efficiency, decreased alertness and a disinclination for efforts (Grandjean, 1979; Grandjean, 1989). Such depress in mental states is a serious problem in driving tasks and is believed to be a direct or contributing cause of road-related accidents (Kecklund and Akerstedt, 1993; Horne and Reyner, 1995; Häkkinen and Summala, 2000; Connor et al., 2001; Philip, 2005), causing 40% of all vehicle accidents (Idogawa, 1991). The effects of mental fatigue during driving could be addressed by real car driving or simulated driving with the involvement of secondary tasks, e.g., listening to the radio, answering mobile phone or reading information in the GPS device, or a long term driving period.

Recent studies have revealed the crucial role of EEG oscillations after mental fatigue of drowsiness, particularly theta, alpha and beta bands (Torsvall and Akerstedt, 1987; Hirvonen et al., 1997; Lal and Craig, 2000; Lal and Craig, 2002; Eoh et al., 2005; Lin et al., 2005; Papadelis et al., 2006; Papadelis et al., 2007; Papadelis et al., 2009; Lin et al., 2010; Maglione et al., 2014). Apart from EEG modulations, other physiological signatures have also been adopted to detect fatigue and drowsiness during driving, i.e., decreased heart rate and EOG activity (Lal and Craig, 2001; Tsuchida et al., 2009; Hu and Zheng, 2009).

2.3.3 Detection of other cognitive states

Other cognitive states have also been considered in EEG studies during driving, in particular, mental workload, emotion and behavior intention. As it is defined, mental workload relates to an individual's limited mental capacity required by the demand of the ongoing task, which is affected by task complexity, experience, skill level and the individual differences (O'Donnell and Eggemeier, 1986), and these factors may lead to imperfect perception and inadequate attention, which have been explored using physiological signals during driving (Kramer, 1990; De Waard and Brookhuis, 1991; Lenné et al., 1997; Brookhuis and de Waard, 2010).

Emotion is also an important aspect towards driving behavior. Especially the inability to manage one's emotion while driving is often harmful to the public and is another major causes for accidents, particularly anger, which impairs normal thinking and judgment thus altered and misinterpretation of events (Hennessy and Wiesenthal, 1999; Rathbone and Huckabee, 1999; James, 2000; Lupton, 2002; Galovski et al., 2006). The current state of emotion detection is mostly based on facial expression and behavioral features, however, several studies have also attempted with brain signals (Herbert et al., 2007; Katsis et al., 2008; Fan et al., 2010).

The detection of driver's intention of action has been assessed as well, through the use of EEG signals, which might be valuable when combined with environmental context, e.g., whether the driver has the intention of braking the car in front of red light or when pedestrian is approaching (Khaliliardali et al., 2012), or in the situation of emergency braking (Haufe et al., 2011; Haufe et al., 2014; Kim et al., 2015).

Even though most of these studies are correlated with the safety issues during driving, e.g., fatigue, mental workload, emotion and behavior prediction, the EEG system could also be performed as an assistance during driving, which monitors the mental states of the driver and interacts with the intelligent car to decide providing certain amount of assistance. This thesis will explore another type of application during driving, which attempts to find the mental preference during driving using EEG signals (Zhang et al., 2013).

3 Methods

This chapter covers the general methods used in this thesis, i.e., EEG recording modalities, signal processing methods and data analysis approaches. Classification and feature selection methods are described as they are implemented in all the chapters except the last one. We also include the detail of the computation steps for estimating brain connectivity method, applied in chapter 3, 4 and 6. Source localization methods are used in chapters 3, 5 and 6. Methods for statistical tests are also described in this chapter, mainly about the choices of multiple tests correction. Readers familiar with them can skip this chapter.

3.1 EEG recordings

Two different EEG recording system were used: 64 channels (Biosemi system, Active Two, The Netherlands); 16 channels (gTec system) EEG cap. Electrodes are placed according to the extended 10/20 system. The layouts of the 64 and 16 channels EEG caps are illustrated in Figure 3.1. The layout with 64 electrodes covers the whole scalp, and the 16 layout is a subset of electrodes covering the sensorimotor area with the same density.

3.2 Preprocessing of EEG data

3.2.1 Spectral filter

To extract specific frequency bands associated with human cognition, we restricted the analysis to particular frequency ranges, such as NAME. For this purpose, spectral filtering is applied as one step of pre-processing before extracting task related epochs. Spectral filtering is computed through the convolution between the designed filter and the signal in the temporal domain. The Fourier transform of the filter indicates its frequency attributes.

The design of spectral filter is according to its magnitude and phase responses. The requirements of the designs vary according to different tasks and the objectives of analysis. For instance, classification of error-related brain activity uses cut off between 1 and 10 Hz, whereas

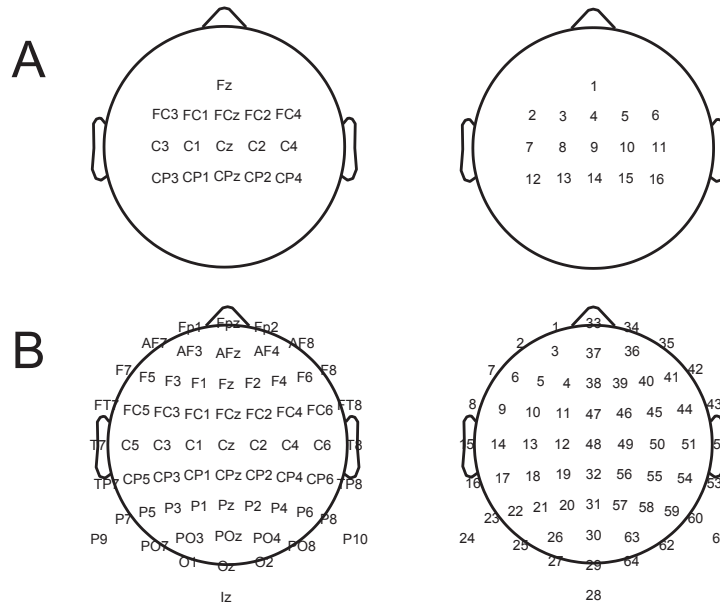


Figure 3.1: EEG caps. A. Layout of 16 channels EEG cap, gTec system. B. Layout of 64 channels EEG cap, Biosemi system.

for the brain connectivity analysis we applied broad filtering between 1 to 50 Hz, since most discriminative information in temporal waves is in the theta (4-8 Hz) band but the connectivity patterns in beta and gamma band may also be modulated. In this thesis, most studies use the Butterworth filter with the order set to 4.

The filter design is also altered in online experiments due to the fact that only previous and current time samples can be accessed. In this thesis, non-causal filtering is applied for offline analysis to explore the modulation patterns with zero phase delay by filtering the data for both directions. However, this is not feasible in real time analysis, given that the backward filtering is not possible, thus causal filtering is applied. To keep the preprocessing consistent for model training and real time classification, we use causal filtering during model training as well. In this thesis, for each task and analysis, we specify the type and the parameters of the spectral filtering.

3.2.2 Spatial filter

The purpose of using spatial filtering is to refine or extract specific spatial patterns from the given electrode layout information. By computing a weighted average across all electrodes for each location, this technique leads to either smoother or more localized brain activity. The spatial filter can be applied in real time analysis since no extra temporal information is involved.

Common average reference (CAR) is adopted in this thesis for most of the analysis, used to

re-reference the EEG data to the averaged activity across channels (McFarland et al., 1997). The removed common activity is not related to specific cognitive process or not informative to particular classification problem. The computation of CAR is applied for each time sample $S_i(t) = S_i(t) - \text{mean}(S_1(t) \dots S_N(t))$, where $S_i(t)$ indicates the EEG activity at time t and channel i , and N is the total number of the EEG channels. Here, the weights for all electrodes are the same ($1/N$), so the removed term could be reused for all electrodes. In this thesis, CAR was applied in the data preprocessing, unless otherwise stated (e.g. another type of spatial filter is used or no spatial filter is applied).

Another type of spatial filter applied in this thesis is cortical source density (CSD), which is estimated by the second spatial derivative of the potential between electrodes, thus giving prominence to local activity and attenuating common distal activity which is usually considered as volume conduction (Kayser and Tenke, 2006). In this thesis, the CSD is applied as a preparation for brain connectivity estimation to reduce the effect of volume conduction, which sustains the evolution of relative spatial patterns rather than the proportionally changed brain activities across areas, preventing the effect of common activities.

Beamforming is another type of spatial filter that is used in the thesis, which estimates brain activity in source level through weighted average of scalp electrodes. The concept of beamforming is also related to source activity estimation, and is therefore further described in Section 3.5.

3.3 EEG data analysis

3.3.1 Data extraction

This section describes the EEG data preparation for classification, as well as the trial extraction, which depend on the task under study, e.g., stimulus-driven time-locked brain activity or continuous voluntary cognition.

For stimulus-driven tasks, specific types of cognitive process are evoked, and the brain response is time-locked to the onset of the stimulus. The EEG data is extracted according to the timing of the external stimuli. In this thesis, we normally use a hardware trigger (parallel port) to synchronize the task events and EEG data, thus the timing information of the tasks is available in both offline and online experiments. In this case, for each stimulus one trial can be generated, and the dimension for each trial is $N * L$, where N channels and L time samples are included. L is related to the sampling rate of the data. In our analysis, data are extracted from one second before (-1 s) to one second after (1 s) the stimulus onset (0 s), whereas the task relevant features are between 0 s and 1 s.

When brain activity is associated with voluntary movement intention, e.g., motor imagery, the input for the classifier is not necessarily time-locked to external events. In the particular case of motor imagery, subjects are imaging hand moving until the probability of one class

reaches the threshold, where the length of the motor imagery period is not fixed. In this case, we apply classification continuously on 1-second windows of EEG data overlapping by 15/16 s, and update the output of the classifier (probabilities of classes) with the same rate, as shown in Figure 3.2. The dimension of the data for each trial is $N * L$, where L is fixed to 1 s (time window).

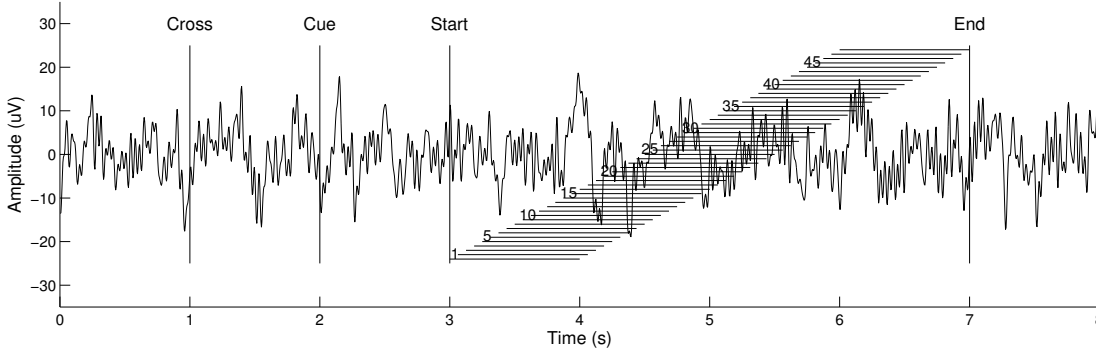


Figure 3.2: Trial extraction for motor imagery. The subject starts motor imagery after 'Start'. Individual trials are represented by the short line between 'Start' and 'End' period.

3.3.2 Feature selection

The extracted EEG trials still contains relatively large amount of data. In 1 s EEG data $64 * 512 = 32768$ (64 EEG channels with sampling rate at 512 Hz) samples are included. In the case of stimulus driven event, all these samples are possible to be used as classification features. However, not all these features are informative to discriminate tasks, and some of them are redundant to each other. Furthermore, performing classification with all the available features likely suffers from the problem of biased variance, given the low number of trials available in BCI tasks, compared to the high number of features. For instance, in linear discriminant analysis, $K(K - 1)/2$ variables (536854528 in the previous example of 32768 features) need to be estimated in the covariance matrix in case all features are included, which is actually not feasible with only hundreds (or even less) trials. Hence, selecting the most informative features is necessary for classification.

Fisher score is a commonly used feature selection method, for its simplicity and effectiveness. It is defined as the ratio of discrimination and total scatter. The Fisher score of the i^{th} feature between class c_1 and c_2 can be computed using Equation 3.1. The numerator in the equation is the distance between the centers of two classes, indicating the discrimination between them, whereas the denominator calculates the summation of variance, representing the total scatter within each class. The larger the Fisher score the more likely this feature is discriminative for the two classes, thus this value can be used as a criterion for feature selection. As a filter method, the Fisher score does not reveal the correlation among features, so it can not get rid of redundant features. One should notice that, some individual features may have low Fisher score, but the combination of features could perform well separation between classes, which

could not be found by Fisher score. Even though disadvantages exist, it is still a very efficient and reliable method with little computational costs.

$$Fs = \frac{(\bar{x}_{i,c_1} - \bar{x}_{i,c_2})^2}{s_{i,c_1}^2 + s_{i,c_2}^2} \quad (3.1)$$

An alternative feature selection usually compared with Fisher score in this thesis is mutual information, which measures how much the uncertainty of one variable can be reduced given the knowledge of another. The formal definition can be found in Equation 3.2, where X and Y are two random variables, and $I(X; Y)$ indicates the mutual information between them. $p(x)$ and $p(y)$ are the marginal distributions of X and Y , and the joint distribution is represented by $p(x, y)$. The mutual information is a non-negative value, and the higher the value, the higher the correlation between the two variables. This measurement can be used for feature selection, through calculating the mutual information between class labels and feature values in the training data, weighting the importance of each feature. A further implementation of mutual information estimates the similarity across features and reduce the redundancy among features.

$$I(X; Y) = \sum_{x \in X} \sum_{y \in Y} p(x, y) \log \frac{p(x, y)}{p(x)p(y)} \quad (3.2)$$

Pearson's correlation coefficient is also applied and compared with Fisher score and mutual information in this thesis. It measures the linear correlation between two random variables. The definition can be found in Equation 3.3, where the correlation coefficient between variables X and Y are calculated as the ratio between the covariance and the product of standard deviations. The range of correlation coefficient is between -1 and 1. In case the two variables are completely correlated, the covariance equals to the variance of each variable, with which the correlation coefficient is found to be 1. The zero value occurs when no correlation could be found between two variables. The value is below zero when the sign of two variable are opposite, which usually happens when phase delay exists between variables. Normally, the absolute value of correlation coefficient between class labels and feature values is used to indicate the importance of a feature. Similar to mutual information, this measure could also estimate the correlation among features, thus possibly be implemented to remove redundant features.

$$r = \frac{\sum_{i=1}^n (x_i - \bar{x})(y_i - \bar{y})}{\sqrt{\sum_{i=1}^n (x_i - \bar{x})^2} \sqrt{\sum_{i=1}^n (y_i - \bar{y})^2}} \quad (3.3)$$

3.3.3 Gaussian classifier

Classification is a task to assign an input data to one of the classes defined in the trained model. A practical example in BCI is to classify whether the subject is performing on left or right hand motor imagery. In this example, the classification result is binary, either left or right. Even though the realistic tasks are probably more than two options, the classification in this thesis mainly focuses on two-class problems. Gaussian classifiers are applied in most of the cases.

A Gaussian classifier defines a normal distributed class conditional probability, $p(x|y = c)$, and combines it with a class prior $p(c)$ to compute the class posterior using Bayes's theorem, as described in Equation 3.4. A unknown sample is assigned to the class with larger posterior probability. The form of class conditional probability can be defined as $p(x|y = c_i) = G(x, \mu_i, \sigma_i) = 1/\sqrt{2\pi\sigma_i^2} e^{-(x-\mu_i)/2\sigma_i^2}$.

$$p(y = c|x) = \frac{p(x|y = c)p(y = c)}{\sum_{i=1:2} p(c_i)p(x|c_i)} \quad (3.4)$$

The decision of classification can be formulated as an optimization problem in Equation 3.5. The border of separating two classes can be estimated as the equal probability between two classes, which is determined by the parameters (mean value and standard deviation) of two Gaussian functions, also adjusted by the prior probabilities.

$$\begin{aligned} i &= \arg \max_i \{ \log p(x|y = c_i) + \log p(y = c_i) \} \\ &= \arg \max_i \left\{ \log \left\{ \frac{1}{\sqrt{2\pi\sigma_i^2}} e^{-\frac{(x-\mu_i)^2}{2\sigma_i^2}} \right\} + \log p(y = c_i) \right\} \\ &= \arg \max_i \left\{ -\frac{1}{2} \log(2\pi\sigma_i^2) - \frac{(x-\mu_i)^2}{2\sigma_i^2} + \log p(y = c_i) \right\} \end{aligned} \quad (3.5)$$

However, a real classification problem rarely contains only one variable, thus the class conditional distribution is multivariate Gaussian, $p(x|y = c_i) = (2\pi)^{-\frac{p}{2}} |\Sigma_i|^{-\frac{1}{2}} e^{-\frac{1}{2}(x-\mu_i)^T (\Sigma_i)^{-1} (x-\mu_i)}$, where p indicates the dimension of the variables and Σ_i represents the covariance matrix across them in class i . Accordingly, the optimization in Equation 3.5 becomes multivariate, as shown in Equation 3.6. Similarly, the separating border is determined by the shape of the Gaussian functions and further adjusted by the prior probabilities. Linear border could be found if the covariance matrices between two classes are assumed to be the same (linear discriminant analysis, LDA), whereas quadratic border results if covariance matrices are arbitrary

(Quadratic discriminant analysis, QDA).

$$\begin{aligned}
 i &= \arg \max_i \{ \log p(x|y = c_i) + \log p(y = c_i) \} \\
 &= \arg \max_i \left\{ \log \left\{ \frac{1}{(2\pi)^{p/2} |\Sigma_i|^{1/2}} e^{-\frac{1}{2}(x-\mu_i)^T (\Sigma_i)^{-1} (x-\mu_i)} \right\} + \log p(y = c_i) \right\} \\
 &= \arg \max_i \left\{ -\frac{1}{2} \log |\Sigma_i| - \frac{1}{2} (x-\mu_i)^T \Sigma_i^{-1} (x-\mu_i) + \log p(y = c_i) \right\}
 \end{aligned} \tag{3.6}$$

3.3.4 Cross validation

Classification is performed in both offline and online frameworks. M -fold cross validation is applied in the offline analysis for the purpose of keeping the testing data blind from the model training. This method is useful when the dataset does not contain too many samples, which occurs very often in BCI experiments. In this thesis, the number of folds (M) is normally set to 10. If the sample size is relatively small, we increase the number of folds to include more data for classifier training. If not specified, we partition the dataset in a random order, obtaining each fold uniformly distributed in the dataset. In some cases, the temporal information of the trials are critical, so we keep the trials with the original temporal order. For online classification, the model is usually trained based on all available data obtained before. Some performance relevant parameters, e.g., feature number, are specified using cross validation in the training phase.

3.3.5 Performance evaluation

As the classification model results in discrete outputs, i.e., class labels, we use the classification accuracy as an intuitive evaluation of the performance, $A = \frac{n}{N}$, where n is the number of correctly classified samples (true positives plus true negatives) and N indicates the total number of samples in the dataset. This measurement tells the percentage of samples that are correctly classified, no matter which class the sample belongs to. The theoretical chance level of a binary classification problem is 0.5, however, offline analysis using cross validation usually get higher chance level (details in (Müller-Putz et al., 2008)). In this thesis, we compute the chance level as an average value of 1000 random classifier created by randomly shuffling the class labels in the training set.

Even though using accuracy as performance evaluation is straightforward and intuitive, the method actually does not include the information of what type of errors has been made, false positive or false negative. Particularly, for the classification of unbalanced dataset, i.e., number of samples in one class is larger than in the other, the accuracy could not tell whether the performance is really above chance level. For instance, a complete biased classifier could provide 90% accuracy if the ratio of sample size between two classes is 9:1. Therefore, we also use the information in confusion matrix as another measure for performance evaluation,

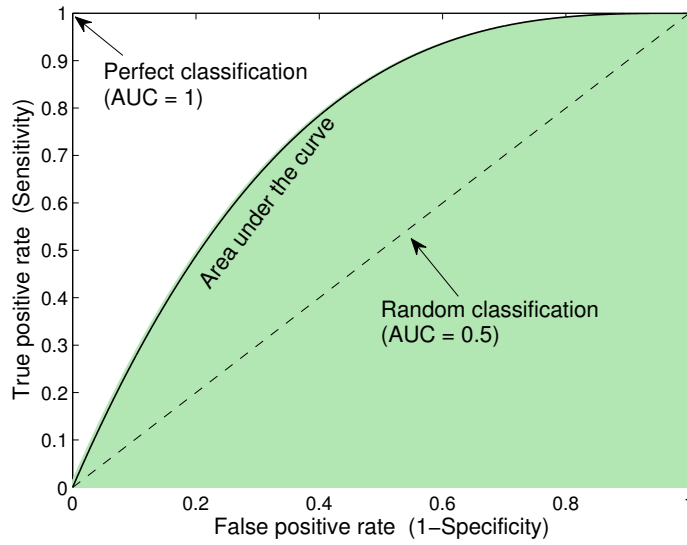


Figure 3.3: Evaluation of classification performance in the space of receiver operating characteristic. The x axis indicates the false positive rate or (1 - Specificity), whereas the y axis indicates the true positive rate or Sensitivity. Perfect classification can be found at coordinate (0,1), whereas the random performance can be found at (1,1). For the ROC curves, the classification is perfect when the area under the curve (AUC) is 1, and is random when it is 0.5.

which provides detailed results for binary classification problem, i.e., false positive, false negative, true positive and true negative. The indicator in the receiver operating characteristic (ROC) space, true positive rate against false positive rate, area under the curve (AUC), is used as an alternative metric to the accuracy, whose theoretical chance level is 0.5 even when the data are unbalanced. Practically, the chance level is also recomputed by a random classifier (see Figure 3.3).

3.4 Brain connectivity computation

3.4.1 Directed transfer function

In this thesis, the method used for the computation of brain connectivity is directed transfer function (DTF), which is based on the estimation of multivariate autoregressive model (MVAR), and is an extension of Granger causality to multiple variables (Kamiński and Blinowska, 1991). The basic idea of this method is to evaluate whether the past states of one variable contributes to the prediction of the current state of another variable. If the contribution is non-trivial, there is a causal influence from the first variable to the predicted variable.

Defining $X_t = [x_{1,t}, x_{2,t}, \dots, x_{k,t}]^T$ to be a vectors of an EEG sample including k channels at time point t (superscript T denotes matrix transposition), the MVAR model can be represented as in Equation 3.7 and its matrix form is as in Equation 3.8. E_t is a vector of zero-mean white noise with size $1 \times k$, and A_i is the $k \times k$ coefficient matrix with $A_0 = -I$ (I is the identity matrix).

3.4. Brain connectivity computation

Here, p is the model order, indicating how many previous samples are used to estimate the current state.

$$\begin{bmatrix} x_{1,t} \\ x_{2,t} \\ \vdots \\ x_{k,t} \end{bmatrix} = \begin{bmatrix} a_{1,1}x_{1,t-1} & \cdots & a_{1,p}x_{1,t-p} & \cdots & a_{1,(k-1)p+1}x_{k,1} & \cdots & a_{1,kp}x_{k,t-p} \\ sa_{2,1}x_{1,t-1} & \cdots & a_{2,p}x_{1,t-p} & \cdots & a_{2,(k-1)p+1}x_{k,1} & \cdots & a_{2,kp}x_{k,t-p} \\ \vdots & \ddots & \vdots & \ddots & \vdots & \ddots & \vdots \\ a_{k,1}x_{1,t-1} & \cdots & a_{k,p}x_{1,t-p} & \cdots & a_{k,(k-1)p+1}x_{k,1} & \cdots & a_{k,kp}x_{k,t-p} \end{bmatrix} + \begin{bmatrix} e_{1,t} \\ e_{2,t} \\ \vdots \\ e_{k,t} \end{bmatrix} \quad (3.7)$$

$$X_t = \sum_{i=1}^p A(i)X_{t-i} + E_t \Rightarrow \sum_{i=0}^p A(i)X_{t-i} = E_t \quad (3.8)$$

The estimation of the coefficient matrix $A(i)$ in Equation 3.8 could be achieved using Yule-Walker method (Stoica and Moses, 1997). The details of the solving the problem will not be described here, as it is not the scope of this thesis. We used the Matlab package *arfit* (Schneider and Neumaier, 2001) to compute the coefficient matrices. Using Fourier transform, we can analyze the system transfer function in frequency domain, as shown in Equation 3.9.

$$E^{\mathcal{F}} = A^{\mathcal{F}} X^{\mathcal{F}} \Rightarrow X^{\mathcal{F}} = H^{\mathcal{F}} E^{\mathcal{F}}, \quad (3.9)$$

where $H^{\mathcal{F}} = (A^{\mathcal{F}})^{-1}$, and $A^{\mathcal{F}}$ is the Fourier transform of the coefficient matrix A , $A^{\mathcal{F}}(f) = -\sum_{i=0}^p A_i e^{-j2\pi f i}$, where j is the imaginary unit.

The non-normalized DTF $\theta_{ij}^2(f)$ is defined by the system transfer matrix $H^{\mathcal{F}}$. The Equation 3.10 represents the information transfer from channel j to i at f Hz (Kamiński and Blinowska, 1991).

$$\theta_{ij}^2(f) = |H_{ij}^{\mathcal{F}}(f)|^2 \quad (3.10)$$

The normalized DTF is defined as Equation in 3.11, which is the ratio of causal influence from channel j to i with respect to the influences from all the other channels to the i^{th} channel.

The value of normalized DTF ranges between 0 and 1.

$$\gamma_{ij}^2(f) = \frac{|H_{ij}^{\mathcal{F}}(f)|^2}{\sum_{m=1}^k |H_{im}^{\mathcal{F}}(f)|} \quad (3.11)$$

In the MVAR model, the power spectral matrix can be estimated by $S^{\mathcal{F}} = H^{\mathcal{F}} V H^{\mathcal{F}*}$, where the asterisk represents the transposition and complex conjugation and V is the covariance of the noise term $E^{\mathcal{F}}$. The diagonal elements of $S^{\mathcal{F}}$ represent the power spectral densities of individual channels, while the coherence between channels is indicated by the off-diagonal elements.

3.4.2 Short time directed transfer function

Some of the analysis in this thesis focus on the evolution of information flows over time, so a sliding window is adopted to estimate the DTF continuously. To this end, we apply the multi-trial analysis assuming that the EEG signal is quasi stationary over the time domain, and estimate the coefficient matrix by averaging the covariance matrix across multiple trials (Kamiński et al., 2001). This preserves the reliability of the parameter estimation even when short windows are selected (having a smaller number of data samples) or a larger number of channels are taken into considerations (i.e., increasing number of parameters).

3.4.3 Direct Short time directed transfer function

Additionally, partial coherence can be used as a factor to avoid indirect cascaded influences in the network, i.e., influences between two channels are mediated by a third channel. The short time direct DTF (SdDTF) (Korzeniewska et al., 2008) is thus defined as:

$$\zeta_{ij}^{\mathcal{F}}(f) = \frac{|H_{ij}^{\mathcal{F}}(f)||\chi_{ij}^{\mathcal{F}}(f)|}{\sqrt{\sum_f \sum_{ij} |H_{ij}^{\mathcal{F}}(f)|^2 |\chi_{ij}^{\mathcal{F}}(f)|^2}} \quad (3.12)$$

where $\chi_{ij}^{\mathcal{F}}(f)$ indicates the partial coherence (elements of the inverse of spectral matrix, $H^{\mathcal{F}} V H^{\mathcal{F}*}$). The denominator in the equation is a normalization term across channels and frequencies, thus the SdDTF values ranges between 0 to 1. The asymmetry of the matrix reflects the directionality of the cross-channel influences. One should notice that the SdDTF reflects the phase difference between channels, thus the elements of the matrix are non-zero only when there is phase difference between them.

Before computing MVAR model, we need to normalize the data within each sliding window

(subtracting the mean and dividing the standard deviation within the window) for each channel to meet the zero mean requirement of the MVAR model (Kamiński and Blinowska, 1991). For the analysis of short time DTF, data in each sliding window was also normalized across trials for each time sample to avoid spurious connectivity (Korzeniewska et al., 2008; Oya et al., 2007).

3.4.4 Parameter specification

To find reliable MVAR coefficients, the order needs to meet the inequality: $K(p+1)/(N_s n_t) < 0.1$, where K is the number of selected channels, p is the order of the MVAR model, N_s represents the length of the sliding window, and n_t denotes the number of the trials. It indicates that less data and more parameters require lower order values. In our analysis, the order of the model was determined by Schwarz's Bayesian Criterion and the logarithm of Akaike's final prediction error using arfit (Schneider and Neumaier, 2001). Small variations might be resulted in the order number of different sliding window. We keep the model order consistent throughout analysis, as an averaged order of a testing trial.

3.5 Beamforming source localization

As described before, beamforming is indeed a spatial filter, extracting EEG sources originating within pre-defined regions by weighted average of the scalp EEG channels. This method assumes that only variance changes provide information about specific source activity. Accordingly, the criterion to build such spatial filter is to solve the optimization problem of maximizing the ratio of variances of EEG sources originating inside and outside the ROI (Grosse-Wentrup et al., 2009). The beamforming can be described as Equation in 3.13, where $X(t)$ is the signal from scalp EEG channels and $y(t)$ indicates the derived activity in source level, and ω represents the beamforming spatial filter.

$$y(t) = \omega^{*T} X(t) \quad (3.13)$$

The optimization of ω can be found in Equation 3.14, where ROI_{in} and $ROI_{out} \in \mathbb{R}^{M \times M}$ indicate the spatial covariance matrices of the signals originating inside and outside the ROI, and M indicates the number of included scalp electrodes. The weights ω are estimated separately for different ROIs.

$$\omega^* = \arg \max_{\omega \in \mathbb{R}^M} \left\{ \frac{\omega^T ROI_{in} \omega}{\omega^T ROI_{out} \omega} \right\} \quad (3.14)$$

The estimation of spatial covariance matrices can be obtained by interpreting scalp EEG as a combination of projected activity from brain sources, in Equation 3.15, where V is the volume of the brain, P indicates the dipole moment at position r' , and L represents the projection of a source from r' to the scalp location r . As ordinary summation, we could split the brain regions into inside and outside the predefined ROI.

$$\begin{aligned}
 x(t) &= \int_V L(r, r') P(r', t) dV(r') \\
 &= \int_{ROI_{in}} L(r, r') P(r', t) dV(r') + \int_{ROI_{out}} L(r, r') P(r', t) dV(r') \\
 &= x_{ROI_{in}}(t) + x_{ROI_{out}}(t)
 \end{aligned} \tag{3.15}$$

The approximation of $x_{ROI_{in}}$ can be found in Equation 3.16, where J indicates the number of brain sources included, α is a constant value. $\mathcal{L} \in \mathbb{R}^{1 \times 3J}$ indicates the projection from the J sources (three dimensional, x , y and z) to the scalp location of $x(t)$, $p(t) \in \mathbb{R}^{3J}$ represents the dipole moments of the J sources, and \mathcal{R}_p is accordingly the source covariance matrix of the J sources. After obtaining the spatial covariance matrices, the optimization problem in Equation 3.14 could be solved as a generalized eigenvalue problem 3.17, where $R_{ROI} = R_{ROI_{in}} + R_{ROI_{out}}$, and eigenvector has the largest eigenvalue constitutes the desired beamforming filter.

$$\begin{aligned}
 x_{ROI}(t) &= \alpha \sum_{j=1}^J L(r, r'_j) P(r'_j, t) = \alpha \mathcal{L} p(t) \\
 R_{ROI_{in}} &= \alpha^2 \mathcal{L} \mathcal{R}_p \mathcal{L}^T
 \end{aligned} \tag{3.16}$$

$$\mathcal{L} \mathcal{R}_p \mathcal{L}^T \omega = \lambda R_{ROI} \omega \tag{3.17}$$

To estimate brain activity in source level, we need to provide a leadfield matrix to describe geometric and conductive properties of the head. In this thesis, a template of lead field matrix includes 3013 sources is adopted to construct the source activity for all subjects. The beamformer (spatial filter) is estimated for each subject respectively, i.e., using their own data to estimate the spatial covariance matrices. For most of the cases in this thesis, the beamforming is performed as a step to extract source activity before the analysis brain connectivity, thus evaluating causal influence in source level. In case the tasks have two or more than two conditions, to avoid spurious effects when conditions are compared, we averaged the spatial covariance matrices for all conditions (Hipp et al., 2011), then obtain a common weighting values (ω) for all the conditions.

3.6 Statistical analysis

Statistical test is a central step to find substantial and reliable results in our studies, which allows us to generalize observation from a sample study to population conclusions. The choice of the statistical test depends on the problem and also on the distribution of the data, thus it is described in each analysis separately. Here we introduce the general approach applied to obtain the chance level of classification performance, as well as the permutation test to control family wise error rate in multiple tests.

3.6.1 Chance level using random classifier

As mentioned in 3.3.5, to evaluate whether the classification performance is above chance level, we build random classifier using randomly shuffled training labels. In this case, the training data of each class contains mixed samples from both classes of the original dataset, which supposedly conserve the same mean and the variances for two classes. Performing this in M-fold cross validation, the position and the shape of the Gaussian functions are permuted across folds, which assign samples to classes randomly comparing with the original Gaussian functions.

Since the analysis is done in M-fold cross validation, we use Student's t -test (one sample, paired) with the null hypothesis that the difference between two groups are normal distributed with zero mean and unknown variance. A rejection to this hypothesis indicates that the classification performance is significantly higher than the chance level. The other way is to repeat the random classification for a large number of times (at least 1000), and obtain the range of 95% percentile of the random classifiers. In case the result of the original classifier is outside (higher) of this interval, we could conclude that its performance is significantly higher than the chance level.

3.6.2 Permutation tests

When multiple statistical tests are carried out simultaneously, the risk of making Type I error (false significance) is greater than when a single test is performed. The more tests we perform, the greater the likelihood of getting false positives under the null hypothesis. In this thesis, we adopted two ways to control such family-wise error rate: Bonferroni correction and permutation test.

For k independent tests, the Bonferroni correction replaces the original significance level $\alpha = 0.05$ by an adjusted level $\alpha' = \alpha/k$. The results of the test is decided to be significant according to the new threshold of significant level. The Bonferroni correction is efficient and simply to apply, however it is generally too conservative and usually leads to too many Type II error, or rejecting too few individual hypothesis. Furthermore, the results of the tests depend on the size of the tests. For example, the significance of the difference between two types

Chapter 3. Methods

of time series, e.g., two conditions of ERP, are related to the sampling rate and length of the signal.

The method of permutation test uses randomization of the samples in two groups, e.g., exchanged samples in t -test, to generate reference distribution of the statics. The actual value of the test static is compared to the generated distribution. Similar to any other statistical test, the decision is made based on how extreme the actual static is compared to the typical values in the generated distribution under the null hypothesis, e.g., the difference between two groups is a random sample from a normal distribution with zero mean. The precision of the permutation test is inverse of the number of the randomization, thus a large number of repetitions is required. Even though the more permutation the better results, the computational cost is another concern. Therefore in our analysis, we typically use 1000 permutations as a trade-off between the precision and the running time.

4 Brain connectivity in motor imagery tasks

4.1 Introduction

Motor imagery is a typical sort of BCI system to send mental command by imagining the movement of limbs (Wolpaw et al., 2002; Ramoser et al., 2000), which does not require actual motor performing and involves similar brain regions as the real movement (Decety, 1996). Therefore, it is an ideal BCI system for those who have lost physical motor function but still keep the moving intention in the cortex, and the task is more natural as compared with stimulus-driven BCI systems, i.e., subjects attempt imagining the movement they would like to perform and the system translates the cortical activity to certain types of control commands to the external devices.

The modulation of brain activity during motor imagery has been known as event-related desynchronization (ERD) and event-related synchronization (ERS). The ERD is usually related to the suppression of the band power at μ and β rhythms over sensorimotor cortex (Pfurtscheller and Da Silva, 1999). Different cortical correlates relating to motor imagery of different limbs was reported, particularly the spatial distributions of ERS and ERD is different (Decety et al., 1994; Neuper et al., 2005). Thus the spatio-spectral EEG brain modulations could be discriminated and implemented as the control commands for BCI systems (Pfurtscheller et al., 2006).

Currently, most motor imagery based BCI systems use power spectral density (PSD) or common spatial filter to find discriminative features between tasks (Zhang et al., 2014). Some studies have already attempted to explore the feasibility of using the brain connectivity patterns between EEG channels as the classification features, e.g., phase difference and directed transfer function (DTF) (Wang et al., 2006; Grosse-Wentrup, 2008; Billinger et al., 2013). The objective of the present study is to use the brain connectivity features to decode motor imagery tasks, as well as the exploration of the fundamental understanding of the brain connectivity patterns during different types of motor imagery, i.e., left hand versus right hand. The modulation of brain connectivity will be computed either between left and right hemisphere, or within one of them, to evaluate the interhemispheric and intrahemispheric interaction patterns. We compare the features extracted by connectivity with the PSD features, and we will also attempt

to use the combination of both types of features. An offline dataset including nine subject will be analyzed in the first phase, and a further online test of three subjects is performed to probe the feasibility of computing brain connectivity and performing classification in real time. Some of the results in this chapter has been previously published in (Zhang et al., 2014).

4.2 Methods

4.2.1 Participants

Nine able-bodied students, six males with age 28.8 ± 3.58 , participated the offline experiments. All participants had normal or corrected-to-normal vision, and no known neurological or psychiatric disease were reported. Three of the nine participants performed the online test.

4.2.2 Experimental protocol

In this study, we focus on a two-class motor imagery task, left hand versus right hand (Leeb et al., 2013). Subjects are instructed to move a horizontal bar by imaging the movement of their hands. For the offline experiments, each subject performs two runs comprising 30 trials motor imagery for each class. Before each trial, a visual cue is presented to show the target, either left or right side, and the feedback bar (white bar) starts moving in one second, as shown in Figure 4.1.A. During offline trials the bar moves to the target continuously with constant speed for 4 seconds. The order of the targets (left and right targets) in each run is randomized.

During online experiments, the location of the white bar is updated according to the posterior probability of the classifier. We integrate the posterior probability as $p'_t = p_t * r + p'_{t-1} * (1 - r)$ in order to smooth the moving of the feedback bar. The integration rate, r , is normally set to 0.02, with the assumption that the brain activity is not always reliable and the system trust more on the accumulated probability rather than the output of single time window. The time window is 1/16 s. The classification and the integration of p'_t is performed for each 1/16 s. The trial ends when the white bar reaches one of the sides (left or right), i.e., the integrated posterior probability reaches the pre-defined threshold, which is usually set to 0.7-0.85 depending on the performance and preference of each subject. Each subject performed 12 runs of online test, and each run has different classifier according to feature type.

EEG signals are recorded using a 16-channel g.USBamp amplifier (g.tec medical engineering, Schiedelberg) with the sampling rate at 512 Hz. The signal is band-pass filtered between 0.1 Hz and 100 Hz and notch filtered at 50 Hz. The 16 EEG channels are over the sensorimotor cortex. The montage of EEG channels are shown in Figure 3.1.

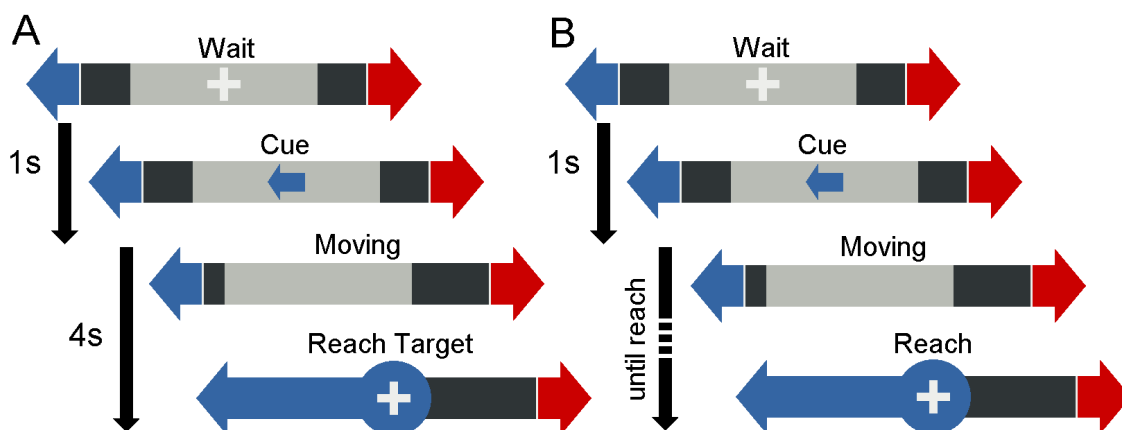


Figure 4.1: Experimental protocol of motor imagery. A. Offline protocol. Each trial includes fixation (1000 ms), cue (1000 ms) before the bar starts moving, and the bar moves with constant speed within 4 seconds. B. Online protocol. Each trial includes fixation and cue with the same timing as offline, and the bar moves until it reach one of the targets, either left or right side.

4.2.3 Feature extraction and selection

To compare the performance between two types of features, PSD and DTF, we compute those features 16 times per second, which is the rate as we update the posterior probability. PSD of each channel is computed using the Welch method for the past one second, with the window (Hanning) size 500 ms and overlapping 50%. Afterwards, we collect PSD features between 2-50 Hz with the step size 2 Hz. The computation of DTF is performed within the same period and with the same rate, by estimating the coefficients of MVAR model based on Yule-Walker equation (the details can be found in the chapter 3.4.1), which includes all 16 EEG channels, and the order of MVAR model is 8. The system transfer matrix in frequency domain is obtained by applying fast Fourier transform on the MVAR coefficients, as the so-called non-normalized directed transfer function (Kamiński and Blinowska, 1991). The step size of DTF is also set to 2 Hz, resulting DTF as a three dimensional matrix $16 \times 16 \times 25$ (channel \times channel \times frequency) for each time step of $1/16$ s, whereas the size of PSD output is 16×25 . We took logarithm of both PSD and DTF before feeding to classifiers.

4.2.4 Classification settings

We compare the classification performance with three types of features: (1) PSD features; (2) DTF features; (3) Combination of both PSD and DTF features. We compute the Fisher score on the offline dataset to select the most informative features, defined by $Fs = (m_1 - m_2)^2 / (s_1^2 + s_2^2)$, where m_k and s_k^2 represent the mean and variance of the samples from class k . The combined features use the features that are selected in PSD and DTF separately. The number of features was the same for each type (50% of them were PSDs, and the remaining DTFs). Linear discriminant analysis (LDA) is used for classification (left vs right motor imagery), assuming

Gaussian distribution of the data samples in each class. The classification performance is evaluated by a 10-fold cross validation and the area under the curve (AUC) of the testing sets.

The classifier for online experiments is trained based on the offline data collected before. We tested the performance of each feature type with different feature numbers: 25, 50, 75 and 100. The command delivery accuracy and the command delivery speed are used to evaluate the performance.

4.3 Main results

4.3.1 Brain connectivity patterns

We compute the interactions *between* and *within* hemisphere to explore the modulation patterns during motor imagery tasks. The left hemisphere is defined as the channels FC3, FC1, C3, C1, CP3 and CP1, whereas the right hemisphere corresponds FC2, FC4, C2, C4, CP2 and CP4. For instance, the brain interaction level from left to right hemisphere is defined as the mean value of DTF from the channels in the left hemisphere to the channels in the right, as shown in Figure 4.2.

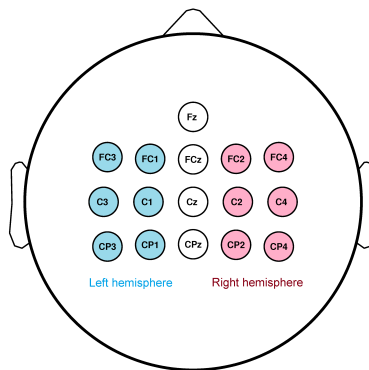


Figure 4.2: Left and right hemisphere for brain connectivity analysis

Figure 4.3.A shows the difference of DTF between left and right hand motor imagery ($DTF_{left} - DTF_{right}$) for four brain interaction patterns: left to right hemisphere, within left hemisphere, right to left hemisphere and within right hemisphere. The curves illustrate the mean values of all subjects. As shown in the figure, the connectivity levels within hemispheres are highly modulated in the mu rhythm (blue and red curves), around 10-14 Hz, indicating evident disassociation between the two motor imagery tasks. In particular, the connectivity within left hemisphere is much higher in the condition of left hand motor imagery, c.f., the positive peak in red curve, and vice versa (negative peak in the blue curve). This might be due to the fact that the contralateral mu rhythm is much more desynchronized than is the ipsilateral one, which causes the lower interaction level in the left hemisphere when people are perform right hand motor imagery. The modulation of intrahemispheric connectivity disappear in the high frequency bands, 35-50 Hz. The green and black curves represent the interhemispheric

connectivity patterns, which are almost zero in the low frequency bands, indicating no difference between the two motor imagery tasks. The differences are noticeable in high frequency bands, particularly 26-32 Hz, in which the information flow from left to right hemisphere is higher when subjects are performing left hand motor imagery (green curve), and vice versa (dark curve).

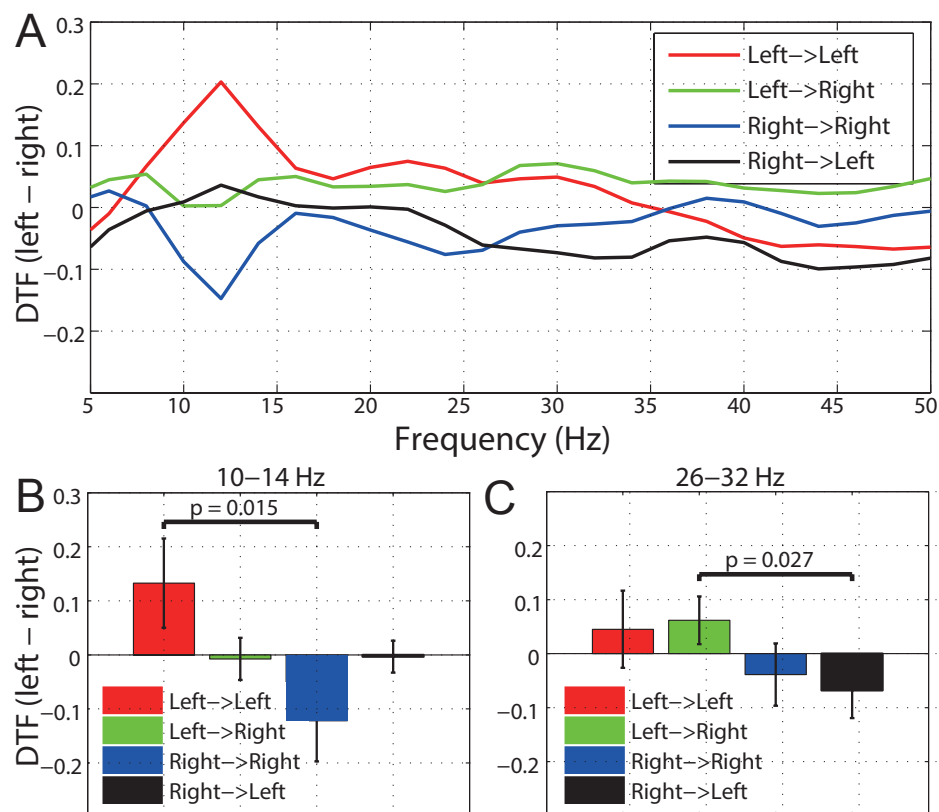


Figure 4.3: A: The modulation of DTF during left and right hand motor imagery. The values indicate the difference between left hand and right hand motor imagery. Each curve indicate the modulation between or within two hemispheres, e.g., Left->Right indicates the information flow from left hemisphere to right hemisphere. B and C: Average and variance of brain interaction patterns in A of two frequency ranges across subjects, and the statistical tests between brain interaction patterns. The values are the difference between two motor imagery tasks. Two frequency ranges are specified in this analysis, 10-14 Hz and 26-32 Hz, according to the differences in A.

Figure 4.3.B and C represent the mean value of the curve in Figure 4.3.A for two selected frequency subbands, 10-14 Hz and 26-32 Hz. Significant differences (Wilcoxon signed-rank test) could be found between within left and within right hemisphere interactions in the mu band ($p = 0.015$). The values of interhemispheric interactions does not show difference, i.e., both values (Left -> Right and Right -> Left) are close to zero. The modulation in high frequency

band is not as high as the low band, and there is no significance between two within hemisphere interactions ($p > 0.05$). The connectivity from left to right hemisphere is increased, whereas the pattern from right to left regions is decreased. It is significant between two interhemispheric interactions ($p = 0.027$). These results indicate that the interhemispheric, or distant, brain interactions are more modulated in high frequency bands than local connections, and motor related brain signals are originated from the contralateral brain regions.

4.3.2 Analysis of connectivity features

For classification we used the connectivity patterns between EEG channels, not averaged between two hemispheres, in order to keep the detail of discriminative patterns in channel level. For illustration, we show results of two subjects (according to online performance) in three frequency bands, 10-14 Hz, 18-26 Hz and 30-50 Hz, in Figure 4.4. The discrimination power is quantified using the Fisher score. In general, the two subjects have different patterns, i.e., the most discriminative features are not identical and the first subject (Figure 4.4.A) has higher discrimination power than the second one (Figure 4.4.B) according to the scale of the color bars.

The most discriminative feature (excluding the midline electrodes, Fz, FCz, Cz and CPz, which are not included in the previous analysis between hemispheres) in band 10-14 Hz for the first subject is from C3 to CP3, which is within the left hemisphere, and is from CP3 to C4 and CP4 for the band 30-50 Hz, which are from the left to the right hemisphere. For the second subject, the connectivity from CP4 to FC4 and C1 to CP3/CP1 are the most informative in the low band except midline channels, which are all within hemispheres. For the high frequency range, 30-50 Hz, the channel FC3 is the most active for information output. The information flow from FC3 to C2 and C4 are the most informative, as well as from C3 to FC2, C2 and CP2. These patterns are from left hemisphere to the right side of the brain. The patterns of the single channel Fisher score observed in this section are consistent with the analysis using combination of electrodes in two hemispheres, indicating that the low frequency ranges are more related to the local interactions, whereas the high frequency band is associated with the distant brain connectivity.

4.3.3 Offline classification performance

10-fold cross validation was used to evaluate the offline training performance. We tested the effect of feature quantity by varying the number of selected features. For each feature number we used, the features with highest Fisher scores are selected. The combined feature (BOTH) has the same number of features as the other two methods, e.g., when the feature number is 20, 10 of them are from PSD and the other 10 from DTE, so the combined method only performs classification when the feature number is even, e.g. 2, 4, and etc. Results of each subject were averaged for all testing folds. The classification is performed in sample level rather than command deliveries, thus the classification performance is not that high.

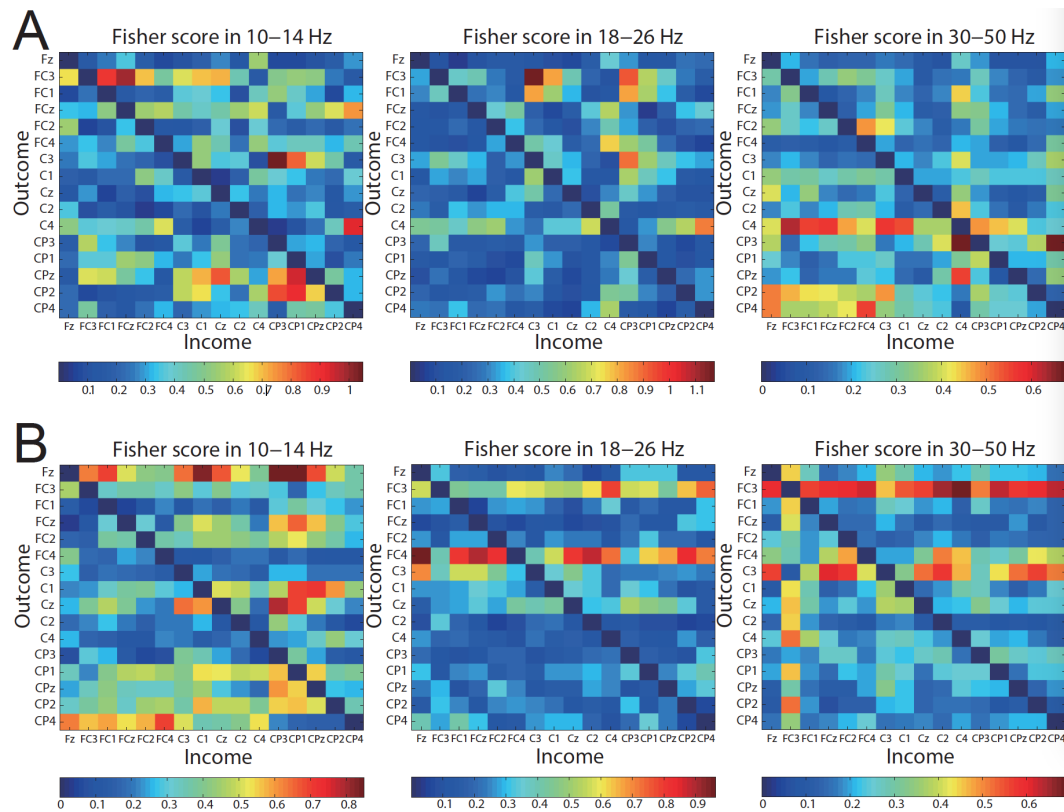


Figure 4.4: Fisher score of single channel brain connectivity pattern. The values of the Fisher score is computed between two motor imagery classes, averaged in three frequency bands, 10-14 Hz, 18-26 Hz and 30-50 Hz. Results of two subjects are shown, in A and B respectively. These two subjects are further recorded in the online experiments. The connectivity patterns from channel j to channel i is indicated in the location (i, j) . The Fisher score of the connectivity pattern between each pair of electrodes is color coded (red indicates higher scores). Notice that subplots have different ranges.

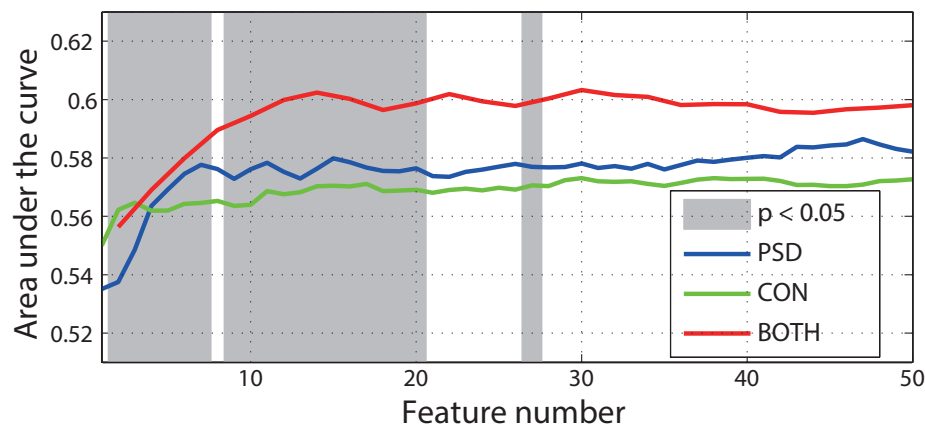


Figure 4.5: The offline performance of classifying two motor imagery tasks with three types of features. Number of features increase from 1 to 50. The gray area indicate the feature with significant difference ($p < 0.05$) between PSD and BOTH.

Chapter 4. Brain connectivity in motor imagery tasks

As shown in Figure 4.5, rapid increase of AUC can be observed when the feature number is very low, i.e., below 10 feature, after which performance stabilizes. In the average level across all subjects, the PSD features show higher AUC than the DTF method. The combined feature set (BOTH) yields the highest performance among them. The statistical test indicates that the BOTH method has significantly higher AUC than PSD when the feature number is from 1 to 20, except using 8 features, suggesting that the DTF method can provide extra discriminant information for classifying left and right hand motor imagery.

4.3.4 Online classification performance

As preliminary tests, three subjects performed online motor imagery. The performance is evaluated by command delivery accuracy ($\frac{\text{Correct command number}}{\text{Total command number}}$) and command delivery speed (second). In general, one of the subject has much better motor imagery performance than the other two, Table 4.1, who had extensive experience of motor imagery based BCI. For this subject, the command delivery accuracy of all feature numbers using DTF (97.50%) and BOTH (92.50%) is higher than the PSD (87.25%) feature. The command delivery time is shorter in PSD (3.02 s) than using DTF (5.65 s), and there is no significant difference between PSD and BOTH (3.07 s).

For subjects 2 and 3, who were naive BCI users, the DTF method has lower accuracy (57.25% and 44.33%) than PSD (60.75% and 59.25%), which is probably close to the random level in subject 3. The highest accuracy of these two subjects was obtained using combined features (BOTH), 60.75% and 61.50%. The command delivery time is longer when we use DTF (10.56 s and 9.70 s) in these two subjects, and the command delivery speed between PSD (7.02 s and 5.55 s) and BOTH (6.27 s and 5.20 s) are not significantly different.

Type	PSD				DTF				BOTH			
Number	25	50	75	100	25	50	75	100	25	50	75	100
Command Delivery Accuracy (Correct commands/Total commands)												
Subject 1	0.93	0.83	0.83	0.90	1.00	1.00	0.90	1.00	1.00	0.97	0.83	0.90
Subject 2	0.53	0.60	0.67	0.63	0.53	0.69	0.50	0.57	0.53	0.73	0.60	0.60
Subject 3	0.70	0.60	0.60	0.47	0.43	-	0.43	0.47	0.53	0.73	0.60	0.57
Command Delivery Speed (Unit: second)												
Subject 1	3.2	3.3	2.5	3.1	8.5	4.6	3.7	5.8	3.0	3.4	2.9	3.0
Subject 2	8.64	5.72	7.65	6.06	11.37	3.57	14.52	12.77	7.05	6.10	5.90	6.02
Subject 3	5.81	5.83	5.47	5.10	10.30	-	8.71	10.08	5.44	5.68	5.03	4.63

Table 4.1: Online command delivery accuracy and command delivery speed for three subjects. Three types of features are evaluated, and each method with four different of feature number, 25, 50, 75 and 100.

4.4 Discussion and future work

Even though some recent studies have already reported brain connectivity modulations for motor imagery, most of them are either restricted to multi-trial analysis with the scope of revealing cortical patterns (Kuś et al., 2005; Stavrinou et al., 2007), or focus on boosting classification performance (Wang et al., 2006; Billinger et al., 2013). The study in this thesis provides evidences for both sides, exploring the cortical modulation pattern of brain connectivity when human subjects are performing left hand versus right hand motor imagery, and attempt to probe the feasibility of adopting connectivity information to discriminate these tasks. The results of offline experiments with nine subjects demonstrate that the modulations of intra-hemispheric and interhemispheric information flows are not identical during left and right hand motor imageries. Particularly, the μ rhythm is highly modulated in intrahemispheric brain interactions, whereas the high frequency bands are more related with distant interhemispheric brain interactions. Furthermore, classification results of single samples (62.5 ms time window) suggest that the DTF features bring additional informative features for the classification between two tasks. The pilot study of online BCI operation with three subjects further indicates the feasibility of improving BCI accuracy when adopting connectivity features.

In our analysis, we used all the available channels during recording to compute the MVAR model and thus the DTF values. This may generate a huge output for each time window, however, this enables us to analyze the patterns across different areas, i.e., between and within hemispheres. The other reason to keep all the channels is due to the fact that the pattern might be varied across subject at the single channel level, for instance the results in Figure 4.4.A and 4.4.B are not identical at the channel level, but they are consistent with the grand average picture. The analysis based on hemispheres is consistent with the theory that the desynchronization at one side of sensorimotor cortex is associated to the limb movement of the other side, which could also be reflected in Figure 4.3.A and B, where the left hand motor imagery has more desynchronization in the right hemisphere at μ band, $DTF_{left\ hand} - DTF_{right\ hand} > 0$.

One should notice that an essential issue of implementing DTF method in real time analysis is the computational cost, since heavy computation is required to obtain the coefficient matrix of the MVAR model (Daly et al., 2012), for our case $16 \times 16 \times 8$ (8 is the order of MVAR model, determined by AIC criteria) parameters are estimated using 1 second EEG data, and the computation should be shorter than 1/16 second, given that we update the DTF values with 16 Hz to operate the BCI. Both higher order or more number of EEG channels will increase the number of parameters, thus requiring more computational cost. In our experiment, it took around 0.01 s to do the computation of DTF, shorter than 1/16 s. The PSD computation in our analysis uses the Welch's method with 1000 ms data and 50% overlapping. The fast Fourier transform (FFT) is actually applied using a 500 ms sliding window, and the PSD is obtained by averaging the results of FFT through three windows. This strategy can also be adopted in our computation of DTF, i.e., averaging MVAR coefficients in a sliding window within past 1 s EEG signal using certain overlap, as the Hanning window in Welch's method, to obtain more stable

results, particularly when high number of channels are involved.

Concerning future studies, an extended subject pool should be explored, as neither the offline nor the online study did include enough subjects to draw solid conclusions. For the online implementation, we could attempt to apply dynamic updating of MVAR coefficients rather than re-compute it for each time window, which is helpful to decrease the computation cost (Arnold et al., 1998), i.e., updates of the MVAR coefficients are considered as linear state equation and the measurements are the EEG samples in a Kalman filter. Further experiments could be performed based on this method, and be compared with the sliding window based DTF computation (Miller and Cohen, 2001; Hesse et al., 2003; Pereda et al., 2005; Astolfi et al., 2008).

5 Brain connectivity for stroke studies

5.1 Introduction

This chapter covers two works in collaboration with other researchers in the lab. The contributions reported in this thesis focus mainly on the brain connectivity analysis for stroke patients. Detailed descriptions of the approaches used for BCI-supported rehabilitation therapy and the functional outcomes are reported elsewhere (Tonin, 2014; Biasiucci, 2014). The first study explores the BCI-controlled neuromuscular electrical stimulation (NMES) therapy in chronic stroke survivors (motor area). The stimulation was triggered by decoding motor imagery patterns. In this study, 15 stroke patients received either BCI-NMES therapy or sham-NMES (random stimulation at similar rates and timing as BCI group). The brain connectivity is calculated and considered as a quantification measurement to evaluate eventual neuroplasticity effects. The second study considers another type of stroke patients, with symptom of Spatial Neglect Syndrome (visual area), aiming to show the effects of a covert attention based BCI system in rebalancing cortical activity. Three spatial neglect patients participated the study, and the brain connectivity values are adopted to evaluate the evolution of the brain network patterns with and within two hemispheres.

5.2 Study 1: Brain connectivity of stroke patients (motor area) after motor imagery based BCI rehabilitation

5.2.1 Patients

Chronic patients were recruited in this study to ensure that the effects are only induced by the rehabilitation therapy, excluding any effect due to spontaneous recovery (Dobkin, 2009). All patients were in their plateau phase of recovery. They received conventional physical therapy—sessions of 45 min comprising mobilization and activities of daily living—in addition to BCI-NMES or sham-NMES in order to filter out potential effects due to non-use and atrophy. Patients were ineligible if they presented any concomitant neurological pathology.

Chapter 5. Brain connectivity for stroke studies

Table 5.1 provide information about the patients. Both groups of patients had lesions at cortical and/or subcortical areas in the right and left hemispheres. The institutional ethical committees approved the study protocol and each participant gave written informed consent prior to their eligibility assessment. Participants were enrolled sequentially and randomly assigned to either receive conventional therapy added on BCI-NMES or sham-NMES therapy. The experiments were done in SUVACare rehab clinic Sion and University Hospital of Geneva, Switzerland.

Table 5.1: Patients' characteristics

patient	gender	age	lesion site	lesion side	stroke time
BCI-NMES group					
E1	M	64	subcortical	right	10 months
E2	M	71	cortical	right	14 months
E3	M	49	subcortical	right	10 months
E4	F	50	cortical	right	19 months
E5	F	49	cortical & subcortical	left	13 months
E6	F	67	subcortical	left	176 months
E7	F	41	subcortical	left	39 months
E8	M	48	cortical & subcortical	right	14 months
Sham-NMES group					
C1	M	40	cortical & subcortical	right	18 months
C2	M	58	cortical & subcortical (multiple embolization)	right	23 months
C3	M	75	subcortical	left	15 months
C4	M	53	subcortical	left	21 months
C5	M	65	subcortical	left	38 months
C6	M	57	cortical & subcortical	left	62 months
C7	F	62	cortical & subcortical	left	121 months

5.2.2 Experimental protocol

For the BCI-NMES therapy, the BCI classifier was individually trained to differentiate brain activity corresponding to either movement attempt or resting. For this purpose, each patient carried out a calibration session using a commercial EEG amplifier (g.tec medical engineering, Schiedelberg), recording at a sampling frequency of 512 Hz with 16 active surface electrodes placed on Fz, FC3, FC1, FCz, FC2, FC4, C3, C1, Cz, C2, C4, CP3, CP1, CPz, CP2 and CP4 of the 10/20 system (reference: right mastoid; ground: AFz), Figure 3.1. This session was not included in the therapy time.

During the training session, patients were asked to attempt opening the affected hand or to rest, in random order. A trial (movement attempt or rest) started with a "Preparation" cue (a cross in the middle of the screen) during 3 s, then a "Start" cue appeared for 1 s indicating the kind of trial, followed by 4 s of movement attempt or resting, and finished with the appearance of the "Stop" cue during 2 s. Inter-trial intervals lasted from 3 to 4.5 s.

5.2. Study 1: Brain connectivity of stroke patients (motor area) after motor imagery based BCI rehabilitation

Both groups (BCI- and sham-NMES) received therapy two times per week for a period of 5 weeks (10 sessions in total). Each session lasted approximately 60 min, including preparation and device setup time. We used the same 16-channel EEG system as for the calibration session.

All patients recorded a pre- and a post-treatment high-density EEG session where they performed 45 attempts of affected hand opening or resting, in random order, using the same protocol as for the calibration session. 64 EEG channels covering the whole scalp were recorded with a Biosemi ActiveTwo system at a sampling frequency of 2048 Hz.

In order to analyze and illustrate data in a uniform manner across patients, EEG channels were flipped for patients with a lesion in the right hemisphere so as to show the lesion over the left hemisphere for all subjects —i.e., electrode C3* covers the lesional hemisphere and electrode C4* the unaffected hemisphere.

5.2.3 Signal preprocessing and brain connectivity

Data was bandpass filtered using a 4th order causal Butterworth filter between 1 and 40 Hz and used to compute brain connectivity through the short-time direct directed transfer function (SdDTF) (Korzeniewska et al., 2008), 3.4.3. For each recording session (pre- or post-treatment, with high-density recording), all movement attempt and rest trials were used to compute the SdDTF between all pairs of electrodes in the two motor areas above for the BCI-NMES and sham-NMES groups. SdDTF results were referenced to the baseline level, estimated from 4 s to 1 s before the “Start” cue onset, and averaged in the time window [0 2.5] s after “Start” for different frequency bands. SdDTF was calculated with a sliding window of 500 ms overlapping 450 ms in order to obtain smooth modulations. Then, the relative measure of connectivity between two electrodes is defined as Equation 5.1.

$$\eta_{Rel}^{ij} = \eta_{Motor}^{ij} - \eta_{Rest}^{ij} \quad (5.1)$$

where η_{Motor}^{ij} is the average SdDTF of that electrode pair during motor attempts, and η_{Rest}^{ij} is its average SdDTF during resting. Finally, the SdDTF values of between/within hemispheres, $\langle \eta_{Rel} \rangle$, are the averages of η_{Rel}^{ij} values of all corresponding electrode pairs.

5.2.4 Results and discussion

Fugl-Meyer assessment for the upper extremity (FMA-UE), exhibited an improvement for BCI-NMES patients. Medical Research Council (MRC) score, strength of the target muscle extensor digitorum communis, showed a significant *session* × *group* interaction favoring the BCI-NMES group ($F(1,13)=6.26, p<0.03$). European stroke scale (ESS) score increased for six of the eight BCI-NMES patients (75%), whereas three sham-NMES patients (43%) also improved.

Chapter 5. Brain connectivity for stroke studies

The details of these results can be found in the PhD thesis of Dr. Biasiucci (Biasiucci, 2014).

Inter-hemisphere and intra-hemisphere brain connectivity patterns are shown in Figure 5.1.A. The normalized SdDTF values are close to zero for most of the situations. The connectivity from right (lesioned) hemisphere to both right and left hemispheres after BCI in the experimental group is lower than before BCI therapy. In this analysis, each subject may have different patterns, caused by different lesioned brain areas or varied recovery progressed. So, we performed the statistical tests using subsets of electrodes (not the single-electrode), which yields more generalized patterns between left and right hemispheres.

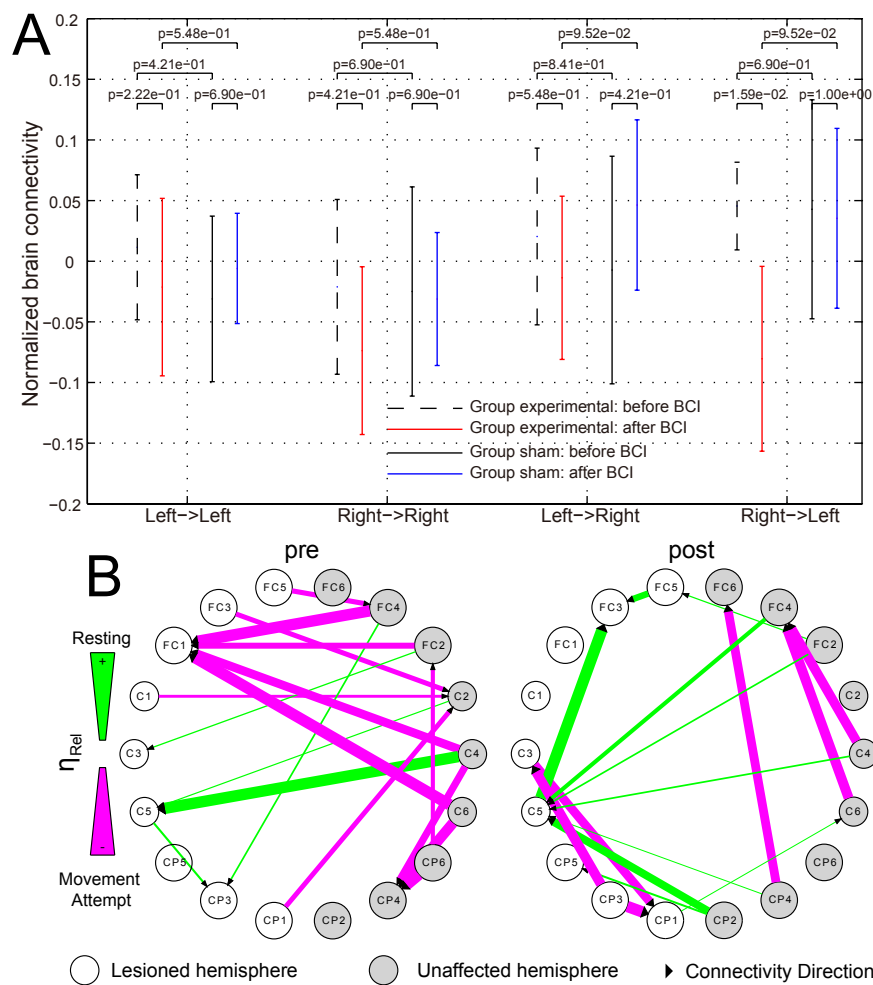


Figure 5.1: A. Mean levels (\pm SD) of brain connectivity patterns between two hemispheres. Four causal brain interaction pairs in beta rhythm (25-40 Hz) are illustrated in each group (experimental and sham) for both before and after BCI therapy. Mean values and standard deviations are shown as bars. Wilcoxon rank sum tests are adopted and the p values are shown. B. Normalized SdDTF for each electrodes in the experimental condition.

5.3. Study 2: Brain connectivity analysis for neglect patients

In particular, the ratio information flow from right hemisphere to the left hemisphere is significant between before and after BCI therapy, using Wilcoxon rank sum tests, and it is the only significant modulation in the results. This indicates significant reduction in directed connectivity during movement attempts from the unaffected to the lesioned hemisphere in the BCI-NMES group, but not in the sham-NMES group ($p > 0.05$). Further information for the Experimental group could be found in Figure 5.1.B, where in the condition of post BCI therapy the movement attempt (purple) has lower connectivity level from unaffected hemisphere to the lesioned hemisphere, and the decrease of the connectivity is mainly contributed by the electrodes in frontal and central regions, FC4, FC2, C4 and C6.

5.3 Study 2: Brain connectivity analysis for neglect patients

5.3.1 Patients

Three stroke neglect patients with unilateral right-hemisphere damage participated in the study. Informed consent was provided by all the participants, which was tested in accordance with the ethical standards of the institutional research committee and with the 1964 Helsinki declaration and its later amendments or comparable ethical standards. General cognitive impairment was excluded by a screening test, i.e., the Mini Mental State Examination test, MMSE (Wilke et al., 2008). The detailed information for patients can be found in Table 5.2. The experiments were performed at the IRCCS San Camillo Hospital Foundation, Lido-Venice, Italy.

Table 5.2: Information of the neglect patients

Patient	P1	P2	P3
Lesion site	F-P, insula	capsulo-thalamic, insula	FTP
Time from lesion (months)	4	8	13
Gender	M	F	F
Age (years)	61	57	46

5.3.2 Experimental protocol

All patients performed a voluntary task of visuo-spatial attention shifting by covertly focusing their attention at specific locations on the computer screen (CVSA) (Tonin et al., 2013). The paradigm is a modified version of the Posner's spatial cuing task (Posner, 1980).

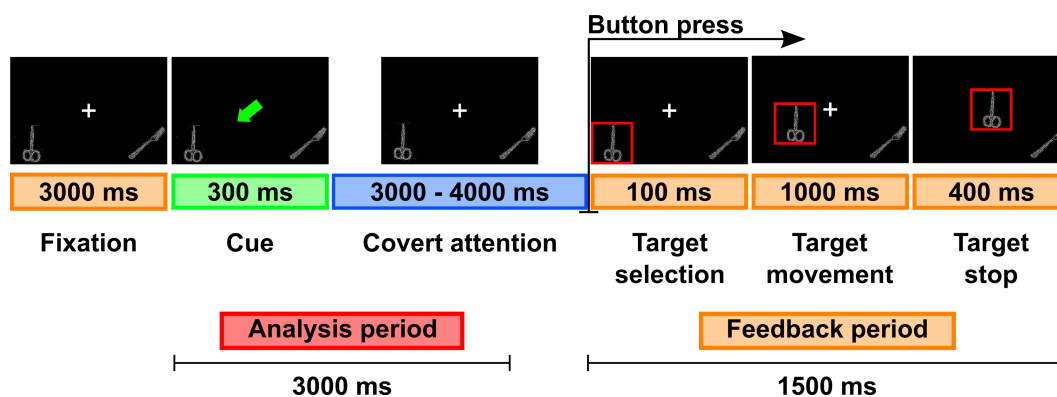


Figure 5.2: Experimental paradigm of CVSA. Each trial started with a fixation period (3000 ms) where patients had to gaze at a cross, visible at the center of the screen. Then the cross was replaced by a cue (300 ms duration) indicating the to-be-attended location. The covert attention period lasted for 3000–4000 ms; afterwards, one of the two images was highlighted in red (target selection, 100 ms) as online feedback of the classification result. Immediately afterwards, the image started moving toward the center of the screen (target movement, 1000 ms) and it disappeared after 400 ms (target stop). Patients were required to press a button with their right hand as soon as they perceived the moving image.

A white fixation cross (size 3.12°) was shown to indicate the beginning of each trial, with two images of real objects (distance 12° from the middle, size 4.8°), Figure 5.2. The fixation period lasted 3000 ms, after which the cross was replaced by a directional cue, pointing to one of the objects (as target), which lasted for 300 ms. After showing the directional cue, the patients were instructed to shift their attention to the target covertly (with their eyes still looking at the location of cross). The duration of covert attention was between 3000 ms and 4000 ms, which is randomized for each trial to avoid task-dependent adaptation. Afterwards, the target was outlined in red (100 ms) and started moving toward the center of the screen, which took 1000 ms. Once the target was in the center of the screen, it stopped moving. The inter-trial interval was 400 ms. The images were randomly selected from a dataset of nineteen real objects, e.g., spoon, scissors, watch, etc. In addition, patients were required to press a button with their right hand as soon as they detected the image was highlighted by the red-colored outline. A fixed time limit for the behavioral response (i.e., the RT) was set at 4500 ms after the target was selected. Button presses occurring before the target selection or after the settled time limit were interpreted as missed and were not considered in the analyses.

Each patient performed six sessions within two consecutive weeks. The first phase of the experiments was the calibration of the BCI system, i.e., train a classifier for recognizing where the patient was covertly focusing on. In this phase, the patients performed a three class CVSA task, or three attention locations i.e., bottom left (neglected side), bottom right, and center of the screen. A positive feedback was delivered to the patients, i.e., selection of the correct target image. The EEG data from first 3000 ms of the covert attention period were used to train the classifier for each patient. In the online phase, patients were asked to focus their attention

5.3. Study 2: Brain connectivity analysis for neglect patients

only at two locations, i.e., bottom left and center of the screen, given that the center of the screen can be considered as the "antagonist" class with respect to the neglected class. The using of the center class could avoid that the classifier was only based on brain activity from the ipsilesional hemisphere (right hemisphere) (Gainotti et al., 1991). In the online phase, the image selected at the end of the trial was based on the classification output, as a real-time feedback to the patient.

5.3.3 Signal acquisition and processing

EEG signals were acquired with an active 64-channel Biosemi ActiveTwo system (Amsterdam, Netherlands) at 2048 Hz, with the spatial locations following extended international 10-20 system. Eye movements were simultaneously recorded by means of three electrodes: two placed sideways to the eyes, and one at the gabella. The EEG signal was low pass filtered (Butterworth filter) with cutoff frequency at 200 Hz and then downsampled to 512 Hz.

5.3.4 Brain connectivity

For the online sessions we filtered the raw EEG signals with a 4th order non-causal Butterworth filter in the frequency band [4 20] Hz. Afterwards, we extracted the trials around the appearance of the symbolic cue, [-1000, 3250] ms, where the 0 ms represents the cue onset. Trials belonging to each condition, target at left and target at center, were analyzed separately.

The brain connectivity patterns were estimated for each run and each patient by means of the short-time direct directed transfer function (SdDTF) (Korzeniewska et al., 2003). In this study, we computed the SdDTF using a sliding window of 500 ms with an overlapping of 450 ms between windows. SdDTF was calculated for 17 EEG channels (P1, P2, P3, P4, P5, P6, P7, P8, Pz, O1, O2, Oz, PO3, PO4, PO7, PO8 and POz) covering the parietal and occipital regions. After the computation of SdDTF, we defined four regions of interest (ROIs) for further analysis of the interaction patterns: left and right occipital; left and right parietal (see Table 5.3).

Table 5.3: Region of interest and related electrodes defined for brain connectivity analysis

Regions of interest	Related electrodes
Left occipital	O1, PO3 and PO7
Right occipital	O2, PO4 and PO8
Left parietal	P1, P3, P5 and P7
Right parietal	P2, P4, P6 and P8

The information flow between regions was obtained by averaging the SdDTF values from all electrodes in the outflow region to the inflow region. For instance, the information flow from left occipital to right parietal is the average of all pairs from (O1, PO3, PO7) to (P2, P4, P6, P8). The SdDTF values in the covert attention period [250, 3000] ms were referenced to the baseline

connectivity level in order to remove the common brain interaction level in each run. The baseline window was defined as [-750, -250] ms.

5.3.5 Statistical test

For each condition (left and center), we assessed the statistical significance of the brain connectivity modulation in both temporal evolution and across patients. Two-way analysis of variance (ANOVA) was applied with this purpose, in which data was regrouped by two factors, sessions and subjects. In addition, post-hoc tests (Turkey's HSD test, Matlab function `multcompare`) were implemented to obtain specifications for significant information flows.

5.3.6 Results and discussion

The comparison across time (calibration or online sessions) and CVSA tasks (left neglected side of space or center of the screen) showed the effect of the BCI-based paradigm. Patient P1 did not exhibit any change in RTs for the left CVSA task between calibration and online sessions (0.51 ± 0.13 vs. 0.51 ± 0.28), but had a slightly increment for the middle CVSA task (0.45 ± 0.11 , vs. 0.56 ± 0.24 , $p < .05$ with Bonferroni correction). Conversely, both patients P2 and P3 reacted faster during the online sessions for the two CVSA tasks: P2 1.22 ± 0.27 vs. 1.10 ± 0.27 , left task and 0.71 ± 0.18 vs. 0.68 ± 0.10 , middle task; P3 0.57 ± 0.19 vs. 0.44 ± 0.11 , left task and 0.63 ± 0.13 vs. 0.45 ± 0.08 , middle task. Importantly, all decrements in RTs were statistically significant ($p < .05$, Bonferroni correction).

Statistical significance of brain connectivity flows was tested by a two-way ANOVA for both conditions (left-sided and central targets) and with respect to two factors: patients and sessions. Analysis was performed for each pair of RoIs. No statistical significance was found for the first factor (patients) in any pair of RoIs, nor in any experimental condition. Interestingly, analysis on the second factor (sessions) shows a statistical significance variation of connectivity across online sessions in the case of left target condition and, in particular, for inter-hemispheric RoIs (see Figure 5.3): from the right occipital region to the left occipital region ($F = 6.51$, $p < 0.002$) and from the right occipital region to the left parietal region ($F = 3.83$, $p = 0.02$). Asterisks indicate significantly different pairs ($p < 0.05$) found by the Tukey's range test. The results are coherent with the analysis on the evolution of the hemispheric activation presented in the previous section (i.e., observed during BCI-supported motor rehab) and suggest a progressive higher involvement of the affected hemisphere during the online sessions.

One of the major hypotheses is that the patients have an imbalance between the two cerebral hemispheres (Heilman and Van Den Abell, 1980; Kinsbourne, 1993), leading to hypoexploration of the neglected (left) space because of hyperattention toward the ipsilesional (right) space. This study shows how EEG based BCI can quantify the changes in the brain connectivity between the damaged and undamaged hemispheres when patients orient voluntarily their

5.3. Study 2: Brain connectivity analysis for neglect patients

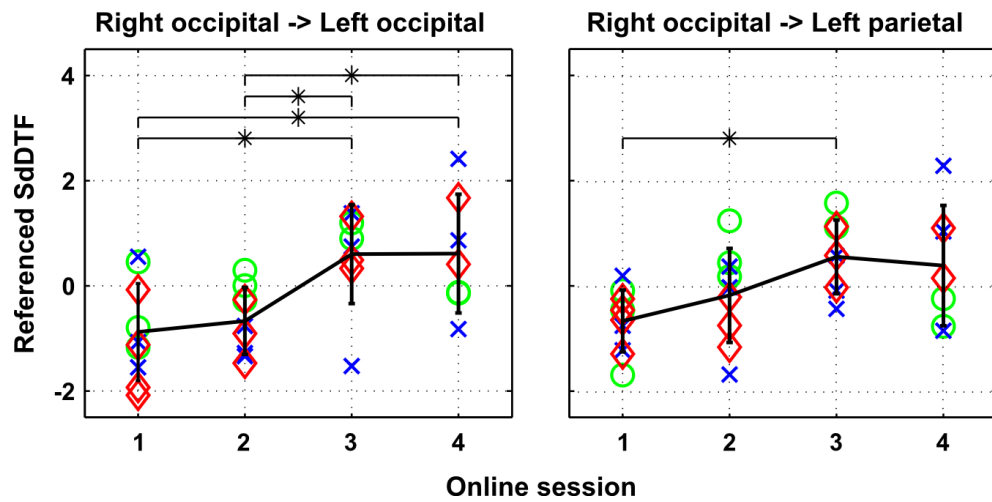


Figure 5.3: Directed connectivity between regions of interest across the online sessions in the case of the left target condition. The figure shows the SdDTF values per run of each patient, for each online session. Mean and standard deviation are reported in black. P1: Green circle. P2: Red diamond. P3: Blue cross. Asterisks indicate significantly different pairs ($p < 0.05$) found by the Tukey's range test.

attention toward the neglected side. The results of this study indicate that the CVSA-based BCI approach seems to yield faster reaction to the visual stimuli for stroke patients, and positive modulation in brain connectivity, i.e., flows from the damaged (right) occipital cortex towards the undamaged (left) occipital and parietal areas increased significantly during the online sessions for all patients, particularly between the first and the third sessions.

6 Brain Connectivity Patterns of Performance Monitoring at Average and Single-trial Levels

6.1 Introduction

Specific brain modulations can be observed when people perceive erroneous events, i.e., phase-locked event-related potential and specific interaction among distant brain regions, which are particularly related with ACC and theta oscillation (Holroyd and Coles, 2002; Luks et al., 2002; Brázdil et al., 2007; Taylor et al., 2007; Cavanagh et al., 2009; Brázdil et al., 2009). The erroneous events can be self-generated errors, or external events that conflict with people's expectation. Recently, electrophysiological and neuroimaging studies have provided evidences that the monitoring erroneous events are independent of the source of errors, i.e., having common neural mechanisms (Milner et al., 2004; de Bruijn et al., 2009; Shane et al., 2008). Previous works have described modulations of theta activity in the medial frontal cortex elicited by both self-generated errors or erroneous feedback. In turn, similar patterns have recently been reported to appear after the observation of external errors.

In this chapter, we report cross-regional interactions after the observation of errors at both average and single-trial level. We recorded scalp electroencephalography (EEG) signals from 15 subjects while they monitoring the movement of a cursor in a computer screen. Particularly, the event-related potential elicited by the visual stimuli will be analyzed, as well as the oscillatory information flows. Moreover, we analyze the cross-regional interaction in a trial-by-trial basis. These trial-specific patterns are further exploited for the recognition of erroneous events. In addition, we also consider the brain connectivity in source level, using beamforming as preprocessing to obtain source activity. The results in this chapter has been previously published in (Zhang et al., 2015).

6.2 Participants and experiment procedure

Fifteen subjects (4 females, mean age 27.13 ± 2.59) participated in the experiments. All subjects had normal or corrected-to-normal vision, and did not report any known neurological or psychiatric disease. Subjects were asked to monitor whether a cursor on a computer screen

Chapter 6. Brain Connectivity Patterns of Performance Monitoring at Average and Single-trial Levels

moved towards a given target.

This protocol has been previously shown to elicit error-related potentials in the frame of brain-machine interfacing (Chavarriaga and Millán, 2010; Iturrate et al., 2014). Subjects seated in front of a computer screen located at 50 cm from their eyes. During the experiment 20 light red squares were shown along a horizontal line in the center of the screen. At the beginning, one of the squares either at the left- or the right-most position turns red to indicate the target position (preferred direction), and one of the other squares turns green and becomes the moving cursor. The initial cursor position was chosen randomly, but at least two steps away from the target. At each trial, the cursor square moved one position either left or right, with 80% probability of approaching the target, and remained at its new position for 2000 ms before moving again. A correct trial is defined when the cursor moves towards the target, whereas trials where it moved in the opposite direction are labeled as error trials. The cursor and the target were relocated at random positions when the cursor reached the target or if 10 steps were performed without reaching it. During the experiments, subjects were requested to minimize eye blinking and movements. Each trial corresponds to a single cursor movement, and recordings yielded about 400 correct and 100 error trials for each subject. For all the subjects, the target was reached 94.27 ± 33.24 (mean \pm standard deviation) times on average, whereas it was not reached in 6.60 ± 4.95 occasions. Since the location of the target was randomized, the moving directions of cursor (left or right) for both conditions were balanced and uncorrelated to the trial type (i.e., correct or error). Moreover, previous studies using this protocol have shown that ERPs are not correlated to the target position or to eye movements (Ferrez and Millán, 2008; Chavarriaga and Millán, 2010).

6.2.1 EEG recording and pre-processing

Scalp EEG was recorded using 64 electrodes (Biosemi Active Two, The Netherlands) with an extended 10-20 system montage at a sampling rate of 2048 Hz. The EEG signals were downsampled to 512 Hz. We filtered the EEG data in the frequency band [1, 50] Hz with a 4th order non-causal Butterworth filter. Afterwards, EEG data were epoched into trials, corresponding to cursor movements either correct or erroneous. Each trial lasted 2 s, from 1 s before the onset of the action to 1 s after.

Before estimating the connectivity patterns, we computed current source density (CSD) from the EEG signal to reduce the effect of volume conduction (Kayser and Tenke, 2006). This avoids spurious bi-directional brain connectivity patterns (Kayser and Tenke, 2006). CSDs are estimated by the second spatial derivative of the potential between electrodes, thus giving prominence to local activity and attenuating common distal activity which is usually considered as volume conduction (Kayser and Tenke, 2006).

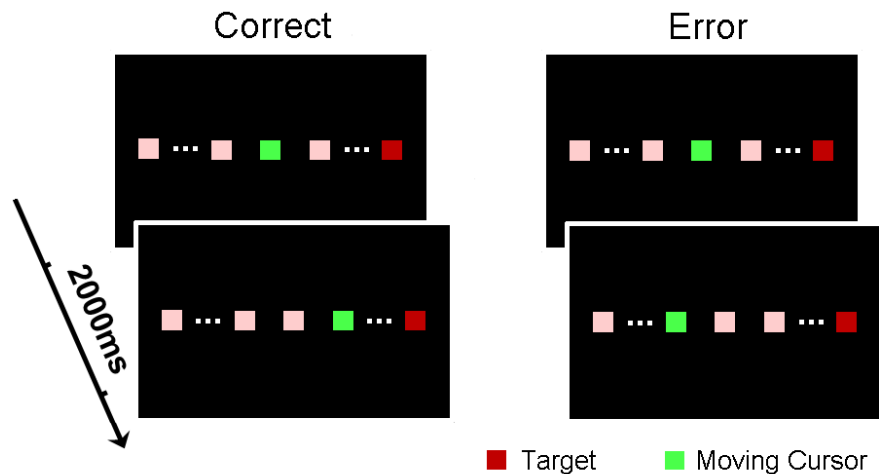


Figure 6.1: Experimental protocol. 20 squares in light red are presented in a computer screen in front of the subject. The green square indicates the moving cursor and the red square represents the target. The green cursor moves to the target with 80% probability, i.e., correct trials (in the left column). The position of the moving cursor is randomly initialized after reaching the target (the target turned to light green) or continuing moving for more than 10 steps. The moving cursor stops on each position for 2000 ms.

6.2.2 Multi-trial brain connectivity

The brain connectivity patterns were computed both at the subject level and single trial level. At the subject level, we explored the dynamics of the modulation with high temporal resolution between broad brain regions using multiple trials to increase the reliability of the estimated patterns. When analyzing the single trial connectivity, we assessed the feasibility of estimating discriminant connectivity patterns between a subset of channels selected from the results at the subject level.

The multi-trial connectivity between CSDs was computed using SdDTF (Korzeniewska et al., 2008). We estimate connectivity patterns within sliding windows of 250 ms with 90% overlapping. 41 CSDs were considered for the analysis, excluding the most peripheral electrodes, i.e., AF3, F1, F3, F5, FC5, FC3, FC1, C1, C3, C5, CP5, CP3, CP1, P1, P3, P5, PO3, POz, Pz, CPz, AF4, AFz, Fz, F2, F4, F6, FC6, FC4, FC2, FCz, Cz, C2, C4, C6, CP6, CP4, CP2, P2, P4, P6 and PO4. We used the same number of trials (100) for both correct and error conditions, as otherwise the order of the autoregressive model of the two conditions may be different. The 100 error/correct trials used in the analysis are uniformly distributed across the duration of the experiments. Before computing the MVAR model, we normalized the data within each sliding window (subtracting the mean and dividing the standard deviation within the window) for each CSD before computing the SdDTF to meet the zero mean requirement of the MVAR model (Kamiński and Blinowska, 1991). After that, data in each sliding window was also normalized across trials for each time sample to avoid spurious connectivity (Korzeniewska et al., 2008; Oya et al., 2007). The order of the model was determined by Schwarz's Bayesian Information

Chapter 6. Brain Connectivity Patterns of Performance Monitoring at Average and Single-trial Levels

Criterion (BIC) and the logarithm of Akaike's final prediction error using arfit (Schneider and Neumaier, 2001). Despite small variations, this resulted in a minimal order of about 10 for most sliding windows. We therefore fixed the model order to this value for both error and correct conditions on all subjects, so as to keep the same size of the coefficient matrices.

We identify brain regions that exhibit high levels of interaction by estimating the total information inflow and outflow at each location. The information inflow (outflow) at one point was defined as the sum of resulted SdDTF values from (to) all the other channels, or the total received (sent) information amount. For a given channel i and frequency f , we compute these values as $inflow = \sum_j \zeta_{ij}^F(f)$ ($outflow = \sum_j \zeta_{ji}^F(f)$). Given the prominent role of the theta oscillations in monitoring processes (Holroyd and Coles, 2002; Taylor et al., 2007; Cavanagh et al., 2012), we estimated the inflow and outflow of theta band in the error condition to determine the most active brain regions for the statistical analysis. Furthermore, this information was also used to select the subset of channels on which the single-trial analysis is performed (see below).

6.2.3 Statistical analysis

In the multi-trial level, we analyzed the statistical significance among the regions of interest, i.e., the subsets of electrodes selected according to the results of the inflow/outflow analysis. We computed the SdDTF between -875 ms and 875 ms (window size of 250 ms) from 1 Hz to 50 Hz. When reporting our results sliding windows are referred to by the time of its center point. The SdDTF values were divided by the average of the pre-stimulus activity (-875 ms to -125 ms) with the purpose of canceling out the variations across subjects. To assess the role of different frequency ranges, we analyzed the statistical significance in four bands following their common definitions, i.e., theta (4-8 Hz), alpha (8-13 Hz), beta (13-30 Hz) and gamma (30-50 Hz). Seven time windows were specified, including the baseline activity (-875 ms to -125 ms, whose value is 1 after normalization) and six windows at the moment of and after stimulus presentation (i.e., -100 to 100 ms, 0 to 200 ms, 100 to 300 ms, 200 to 400 ms, 300 to 500 ms and 400 to 600 ms), in order to verify the temporal evolution of significant brain connectivity modulations caused by the monitoring processes. After obtaining the average value of SdDTF in these time-frequency blocks (baseline/monitoring phases and four frequency ranges), we used Wilcoxon signed rank test to assess the significance of the null hypothesis that there was no difference in connectivity patterns between baseline and each monitoring time window. The type I error of these multiple tests was corrected by permutation tests, in which we randomly shuffled the baseline window (-875 ms to -125 ms) and the other 6 time windows for 1000 times, and obtained the corrected p value as the percentage of those permutations having lower p value than the original test.

6.2.4 Single trial connectivity and classification

We further assessed the information conveyed by the connectivity patterns by evaluating whether such information can be used to discriminate between error and correct conditions in single trials. In this analysis, we preprocessed the data with a 4th order causal Butterworth filter after downsampling to 512 Hz, as the single trial analysis will be further implemented in a real-time framework. To estimate connectivity on a single trial basis, we restricted the analysis to a smaller number of channels and a longer time window since fewer data samples were available. In this case, the size of the time window used was 400 ms with an overlap of 360 ms. Four EEG electrodes located at the center of frontolateral, frontocentral and centroparietal regions, i.e., F3, F4, FCz and CPz, were included in the MVAR computation. These regions showed high levels of information inflow/outflow as reported in the results section. The order of the MVAR model was set to 5 for all subjects, satisfying the same criteria used for the multi-trial case. We used the non-normalized DTF (i.e., θ_{ij}^2) as features for classification without considering the indirect effects due to the fact that less electrodes were included which are less likely to produce critical cascading indirect effects. Moreover, the computational cost is highly reduced as it is not necessary to compute the inverse of the spectral matrix. As in the multi-trial analysis, brain connectivity values were divided by the pre-stimulus level (-800 ms to -200 ms). Then, statistically significant differences between baseline (-800 ms to -200 ms) and post-stimulus connectivity (200 ms to 400 ms) were assessed using the Wilcoxon signed rank test. Notice that, compared to the multi-trial analysis, different time periods had to be defined for the analysis since longer time windows were used for computing the DTF values.

Moreover, we compared the classification accuracy (error vs. correct) based on the connectivity patterns to the use of standard temporal features. To verify whether connectivity features provide extra information with respect to the temporal features we also assessed classification accuracy using both types of features combined. Linear discriminant analysis (LDA) was used to classify correct and error trials. Three sets of features were compared: (1) Temporal features, corresponding to the most common approach used for classification of these type of signals for brain-computer interfacing (Chavarriaga et al., 2014); (2) Brain connectivity features (θ_{ij}^2); (3) Combination of temporal and connectivity features. Temporal features were extracted from the same 4 electrodes utilized in the single trial connectivity analysis, between 200 ms and 700 ms after the stimulus onset. This yielded a total number of 52 (13 time samples \times 4 channels) features. In the second case, for each trial we extracted features between [1-30] Hz in the same time range as above. Since this results in more than 10^4 features, we selected for classification the 50 highest ranked features according to their Fisher score. This score indicates the discrimination capability of each feature and is defined as $fs = |m_1 - m_2| / (s_1^2 + s_2^2)$, where m_k and s_k^2 are the mean value and the variance of class k , respectively. In the third case, both temporal and connectivity features were used (selected separately) and then fed into the classifier. We report the classification performance as the area under the specificity-sensitivity curve (AUC) computed using 10-fold cross-validation. To verify whether the classification performance was significantly better than chance level, we used a permutation test, through training classifiers using randomly shuffled labels. The

Chapter 6. Brain Connectivity Patterns of Performance Monitoring at Average and Single-trial Levels

procedure of generating random classifier was repeated for 1000 times, and for each of them we obtained its testing performance. The upper 95% percentile of the testing performance distribution was obtained and compared to the results of the original classifier. This assesses how likely it is to obtain the classification performance by chance alone.

6.3 Results

6.3.1 Event related potentials (ERP) and spectrogram

On average, we obtained 121.33 ± 15.43 (mean \pm standard deviation) error trials and 441.33 ± 12.71 correct trials per subject. Figure 7.2.A shows the grand average ERP of correct and error trials of four electrodes (F3, F4, FCz and CPz). For visualization, we filtered the raw EEG data between [1-10] Hz after using common average reference across all 64 channels. Significant differences between two conditions are shown as green areas in the figure (t-test, Bonferroni correction).

ERPs in FCz and CPz (midline areas) show higher modulations than the other selected electrodes. A negative peak appears at about 240 ms in the error condition (Figure 2.A, black lines) in both FCz and CPz. After that, a positive peak is observed at about 330 ms with a following negative peak at about 420 ms in FCz and around 500 ms in CPz. In the correct condition (Figure 2.A, gray lines), both FCz and CPz include a positive peak at around 260 ms and a negative peak around 400 ms. Significant differences can be observed from 200 ms until 650 ms after the stimuli onset in both FCz and CPz. In the electrodes F3 and F4 (frontolateral sites), the most evident differences between correct and error are found at about 420 ms. At this time a negative deflection, lasting until about 500 ms, can be observed in the error condition (black line) but not in the correct condition (gray line). Significant differences could be found around 420 ms in both F3 and F4. These differences are larger at the left frontal areas (F3).

These results are consistent with previous studies of error monitoring with a similar protocol (Chavarriaga and Millán, 2010; Iturrate et al., 2014), and the negative peak in midline regions, particularly FCz, replicates negative ERP deflections reported by other error monitoring experiments (van Schie et al., 2004; Milner et al., 2004; Ullsperger et al., 2014).

Figure 7.2.B illustrates the ERP (error - correct) of EEG topographies during (0 ms) and after the stimuli (ERP peaks: 240 ms, 330 ms and 490 ms). No evident difference could be found at 0 ms. In contrast, we found a larger negativity for the error condition in medial central regions at 240 ms, followed by higher activity at 330 ms. Finally a larger negativity is also observed for the error condition in medial frontal regions at 480 ms. The spectrogram of channels F3, F4, FCz and CPz, computed using the short-time Fourier transform with window size 250 ms and overlapping 98%, is shown in Figure 7.2.C, error - correct. Frontal central (FCz) theta occurring around 250 ms seems to be the most prominent pattern. It appears in other channels (CPz, F4 and F3) as well but exhibiting a smaller amplitude than in FCz. The theta modulations finish

before 500 ms. A second modulation, although not as strong as in the theta band, manifests in the lower beta band in FCz and CPz at around 400 ms. Statistically significant differences (Wilcoxon ranksum test, corrected by a 1000 random permutation test) were found in FCz, CPz and F3, between 200 and 500 ms in the [4-10] Hz frequency range.

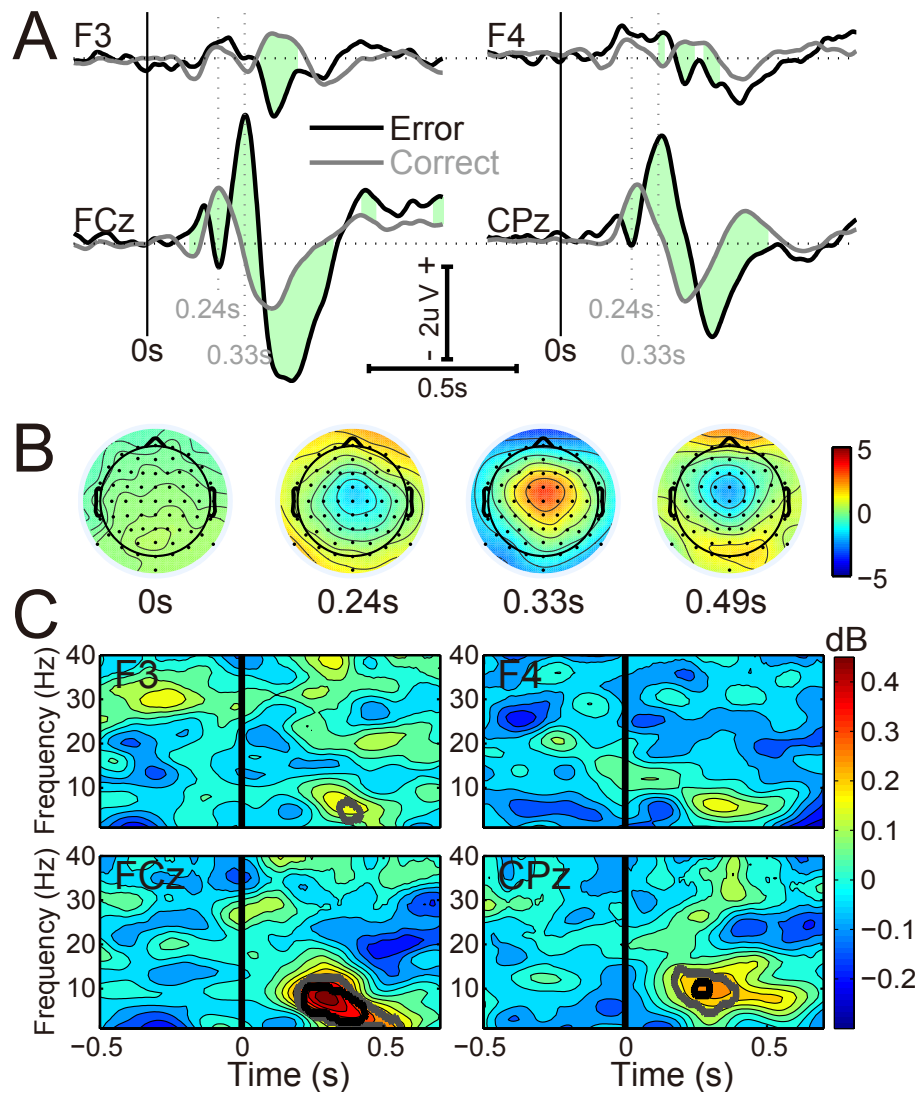


Figure 6.2: A. Grand average of the event-related potential (ERP). The black lines indicate the error condition, the gray lines show the correct condition, and green areas show the periods with significant differences between error and correct. Origin of the time axis, 0 s, represents the onset of the visual stimuli (i.e. cursor movement). Four EEG channels in frontolateral (F3 and F4) and midline central (FCz and CPz) areas are illustrated. B. Topographies of the ERP difference (error - correct) at selected time points, -0.2 s, 0 s, 0.24 s and 0.33 s. C. Differences of event related spectral perturbation of selected channels. The gray ($p < 0.05$) and black ($p < 0.01$) contours indicate the areas where significant differences between correct and error conditions were found.

6.3.2 Information inflow and outflow

Estimation of the information inflow and outflow in theta band shows that the error condition have stronger connectivity modulations than the correct condition (Figure 6.3). In the error condition, the frontal and frontocentral areas have the highest increased inflow. Most electrodes (gray circles, $p < 0.002$) in these regions show significant differences compared to the pre-stimulus activity, particularly in frontocentral and frontolateral channels, as shown by the black markers (Bonferroni correction). For the outflow patterns, the essential brain regions are frontocentral and centroparietal. In addition, given previous evidences that MFC is the generator of the error-related ERP (Holroyd and Coles, 2002; Taylor et al., 2007; Milner et al., 2004) and the contribution of frontoparietal interaction in the attention network (Ptak, 2012), we therefore choose frontocentral (defined as the combination of FC1, FCz and FC2 electrodes), frontolateral (F5, F3 and F1; and F6, F4 and F2 for left and right ones respectively) and centroparietal (CP1, CPz and CP2) regions for further analyses. We averaged the brain connectivity of electrode pairs between these regions after the computation of the SdDTE, e.g. the connectivity from frontocentral to left frontolateral is the mean value among all pairs from electrodes FC1, FCz and FC2 to electrodes F1, F3 and F5.

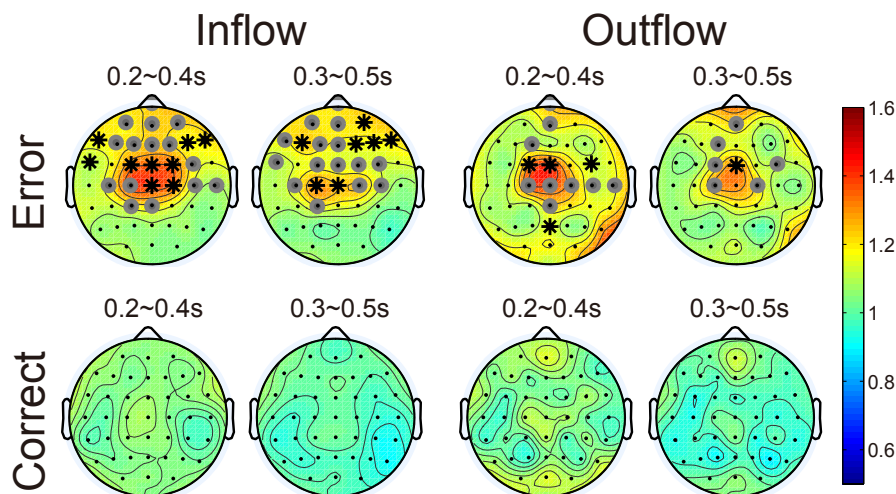


Figure 6.3: Grand average of information inflow and outflow for all electrodes in theta band. Results were referenced by dividing the mean value of the pre-stimulus time window (-875 ms to -125 ms) and averaged for all subjects. Values equal to 1 denote no change from pre-stimulus levels. Greater values indicate an increase in inflow/outflow, while smaller values represents a decrease. Gray circles indicate $p < 0.002$, and the black markers denote statistical significance using Bonferroni correction.

6.3.3 Multi-trial brain connectivity patterns

Figures 6.4.A, C and E illustrate the dynamics of directional brain connectivity patterns in the time-frequency domains. This figure shows the connectivity patterns by SdDTF for both

directions, e.g., Figure 6.4.A indicates causal connection from frontocentral to left frontolateral (first row) and from left frontolateral to frontocentral (second row). The statistical tests (Wilcoxon signed rank test) between baseline (-875 ms to -125 ms) and monitoring periods at a subject level are shown in Figure 6.4.B, D and F. As can be observed, significant differences only appeared in the error condition, specifically in the theta band.

In lower frequencies, i.e. theta and alpha, brain connectivity increases. In error trials, significant increases ($p < 0.05$) appear in the information flow from frontocentral to both left and right frontolateral areas in the theta band, starting at about 200 ms and ending at about 400 ms. Significant connectivity pattern between frontocentral and left frontolateral areas (Figure 6.4.A, 6.4.B, 6.4.C and 6.4.D) could also be observed. In contrast, no significant modulation appears after correct trials. The pattern of information flow in the opposite direction (i.e. from frontolateral to frontocentral sites) exhibits an increase in the theta and alpha band, and is significant from the right hemisphere ($p < 0.05$). In the correct condition, the brain connectivity in both directions does not change significantly neither in the theta nor alpha band ($p > 0.05$) with respect to the baseline period. The information flow from centroparietal to frontocentral areas shows an early increase (starting at about 100 ms) in connectivity in the theta band for the error condition, as displayed in Figures 6.4.E and F. This modulation precedes those observed between frontocentral and frontolateral regions, and may be related to perceptual processes. An increase in connectivity from frontocentral to centroparietal areas appears in the alpha and theta bands as well.

In higher frequency bands, i.e. beta and gamma, we observe a significant decrease in the information flow from frontolateral to frontocentral areas in the error condition. This pattern slightly precedes the increase observed in lower frequencies. This pattern is significant in the error condition ($p < 0.05$) between baseline and after onset: starting at 100 ms to 300 ms from left side in beta and gamma and later from the right hemisphere. As before, no significant modulations appear in the correct condition.

Information flow in the opposite direction, from frontocentral to frontolateral areas, decreases as compared to the baseline level for both conditions, but no significant change could be found. The connectivity patterns between frontocentral and centroparietal regions also decrease in the error condition, with a significant reduction from centroparietal to frontocentral in the gamma band ($p < 0.05$). As before, the modulations in the correct condition are much lower and show no significant difference with respect to baseline levels.

Chapter 6. Brain Connectivity Patterns of Performance Monitoring at Average and Single-trial Levels

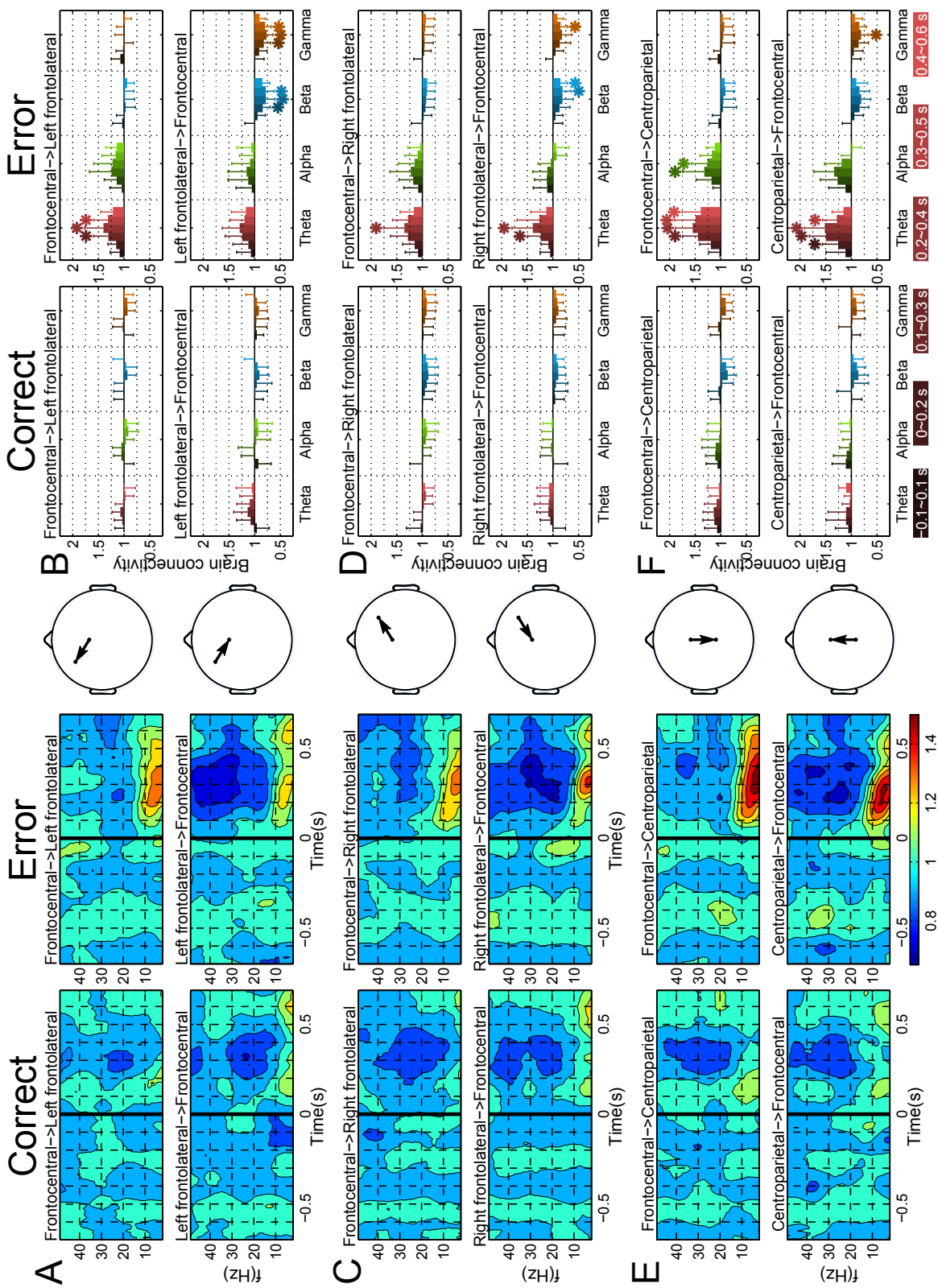


Figure 6.4: Brain connectivity between frontocentral, frontolateral and centroparietal areas.

Figure 6.4: A, C and E represent SdDTF in the time-frequency domain. Colors in the figure represent the ratio with respect to pre-stimulus level (average between -875 s and -125 ms). Values equal to 1 represents no difference (equivalent as pre-stimulus level) in brain connectivity. Smaller values indicate depressed brain connectivity, and, conversely, values greater than 1 denotes enhanced cross-regional interactions. The two columns on the right side (B, D and F) show the mean values and standard deviations of the SdDTF for each window and frequency band across subjects. The duration of the six windows are indicated at the bottom of the two right-side columns ([-0.1, 0.1], [0.0, 0.2], [0.1, 0.3], [0.2, 0.4], [0.3, 0.5] and [0.4, 0.6]). They also indicate significant differences (Wilcoxon signed rank test, $p < 0.05$). The head maps in the center line indicate the brain regions that are analyzed: frontocentral and left frontolateral in A and B; frontocentral and right frontolateral in C and D; frontocentral and centroparietal in E and F.

6.3.4 Single trial connectivity and classification

Figure 6.5.A shows the estimation of the single trial modulation of brain connectivity patterns between F3, F4, FCz and CPz. The figure illustrates the grand average of all trials of the 15 subjects in the time window 200 ms to 400 ms as well as statistically significant values with respect to the baseline period (-800 to -200 ms).

The connectivity values of the correct condition (gray bars) show no significant modulation, in comparison to the baseline period. In the error condition, the results are consistent with the multi-trial analysis, i.e. information flows from frontocentral to frontolateral and centroparietal sites are enhanced in the theta band. A decrease in beta connectivity in the opposite direction is also observed, which is significant from frontolateral to frontocentral sites.

We computed the Fisher score for each connectivity feature, which measures how well that feature separates correct and error trials. Figure 6.5.B reports the averaged Fisher score of all pairs throughout the frequency domain for each time point. The Fisher score revealed that most of the discriminability between error and correct trials came from the time interval between 200 ms to 400 ms. Figure 6.5.C shows an equivalent analysis in the frequency domain. Low frequency bands (4-15 Hz, mainly theta and alpha) are the most dominant rhythms, with a smaller peak in beta (around 25 Hz). Discrimination power associated to spatial directionality (averaged in time window 0 s-0.7 s) are illustrated in Figures 6.5.D and 6.5.E for 4-15 Hz and 25-30 Hz, corresponding to the two peaks in Figure 6.5.C. The width of the arrows represents the normalized Fisher score. The information flows in the theta band from FCz to F3, F4 and CPz are much stronger than others, while a larger decrease is seen in the beta flows from F3, F4 and CPz to FCz. These results are consistent with the patterns obtained in the multi-trial analysis.

Chapter 6. Brain Connectivity Patterns of Performance Monitoring at Average and Single-trial Levels

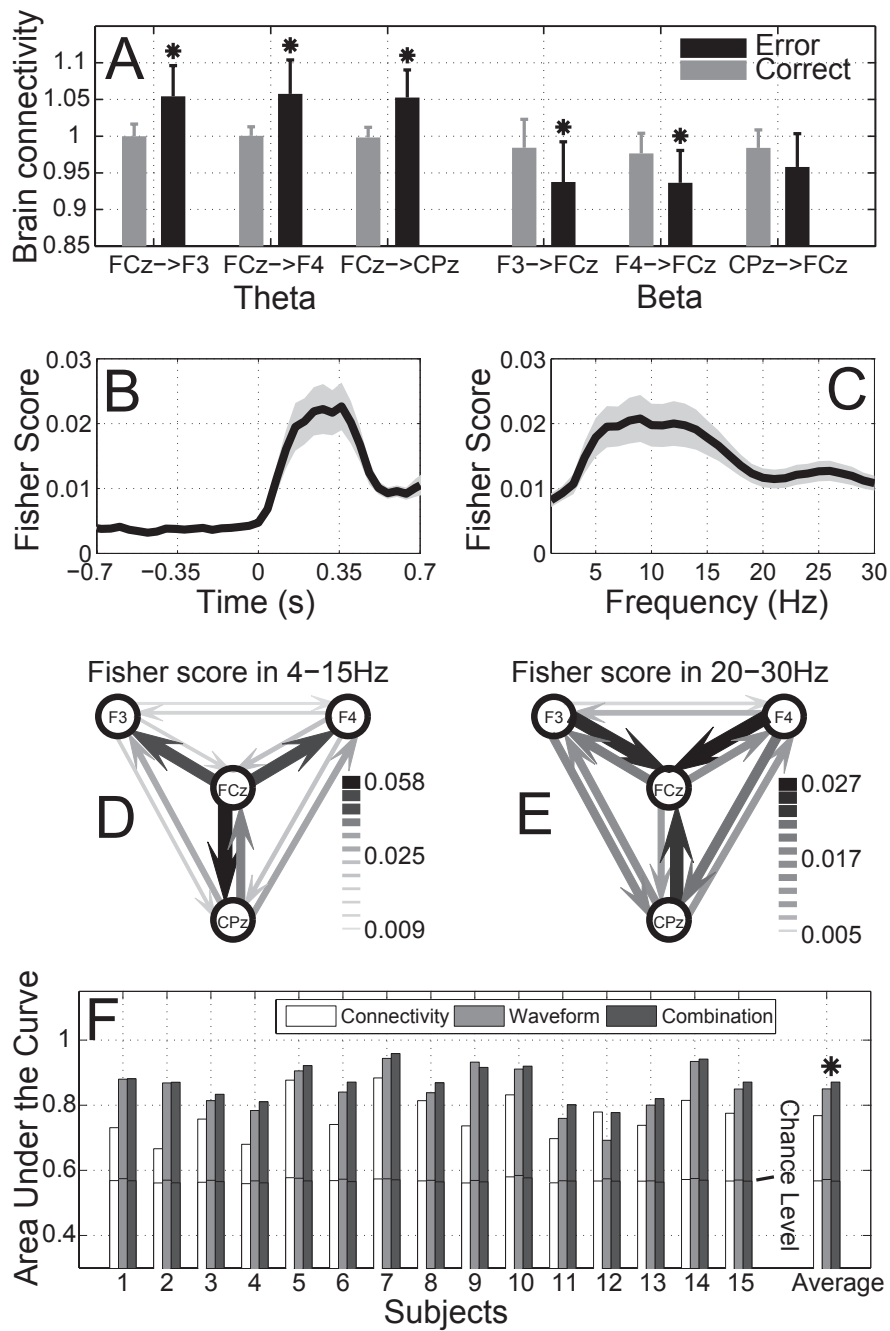


Figure 6.5: Single trial analysis of brain connectivity between F3, F4, FCz and CPz.

Figure 6.5: A. The columns represent the mean value between 200 ms and 400 ms for theta and beta bands. Asterisks indicate statistical significance ($p < 0.05$) between baseline (-800 ms to -200 ms) and after onset (200 ms to 400 ms). B. Discrimination power (Averaged Fisher score \pm standard error) of brain connectivity features in temporal domain. C. Discrimination power of brain connectivity features (Averaged Fisher score \pm standard error) in frequency domain. D and E: Spatial directionality of discrimination power in low (4-15 Hz) and high (25-30 Hz) frequency bands. The width of the arrows represents the normalized Fisher score. F. Classification performances of three feature sets: connectivity, temporal and the combination of them. The bars represent AUC for each subject, and the black lines indicate the 95% confidence chance of output from random classifiers. Asterisk indicates that, across all subjects, the combination of features yields a significant improvement ($p < 0.05$, see text for details).

Figure 6.5.F shows the classification performance (AUC) for the three types of features used: connectivity, temporal and combined features. Besides the AUC for each subject it also shows the mean AUC across all subjects. Chance level estimated using a permutation test (95% confidence interval) is indicated by the black line in the bar. In all subjects the three types of features yielded classification performance significantly higher than chance level (paired Wilcoxon signed rank test $p < 0.05$). The performance using connectivity-based features (AUC = 0.7682) was lower than for temporal features (AUC = 0.8502). However, the combination of the two features resulted in significantly higher performance (AUC = 0.8709) than using temporal features alone (paired Wilcoxon signed rank test, $p < 0.05$). Overall, 14 out of 15 subjects had higher AUC with combined features. These results suggest that not only it is feasible to extract discriminant information from the connectivity patterns in single trials, but also that this information is complementary to the customary temporal features.

6.3.5 Methodological Considerations

The brain activity at source level is particularly interesting. For this, inverse solution methods are usually used to estimate the source activity prior to the connectivity analysis (Schoffelen and Gross, 2009; Hipp et al., 2011). As a methodological check, we include it in this study. Among the existent inverse solution methods, beamforming is one of the most frequently used methods. This method maps the EEG signals into electric activities within specific regions of interest (ROI) by maximizing the variance ratio inside and outside the ROI (Grosse-Wentrup et al., 2009). We replicated the previous analysis using this technique. The processing followed the computational steps in (Grosse-Wentrup et al., 2009), and we used the generic MNI-based leadfield matrix for all subjects. ROIs were selected as the 10 closest voxels (within 1.5 cm radius sphere from the closet point in the cortex under the surface electrode) to each of the 41 EEG electrodes. Particularly, the beamformer was derived for each subject using 100 trials (-1 s to 1 s) in both conditions together. Figure 6.6.A shows the averaged source topographies

Chapter 6. Brain Connectivity Patterns of Performance Monitoring at Average and Single-trial Levels

(error - correct) at the ERP peaks, 240 ms and 330 ms.

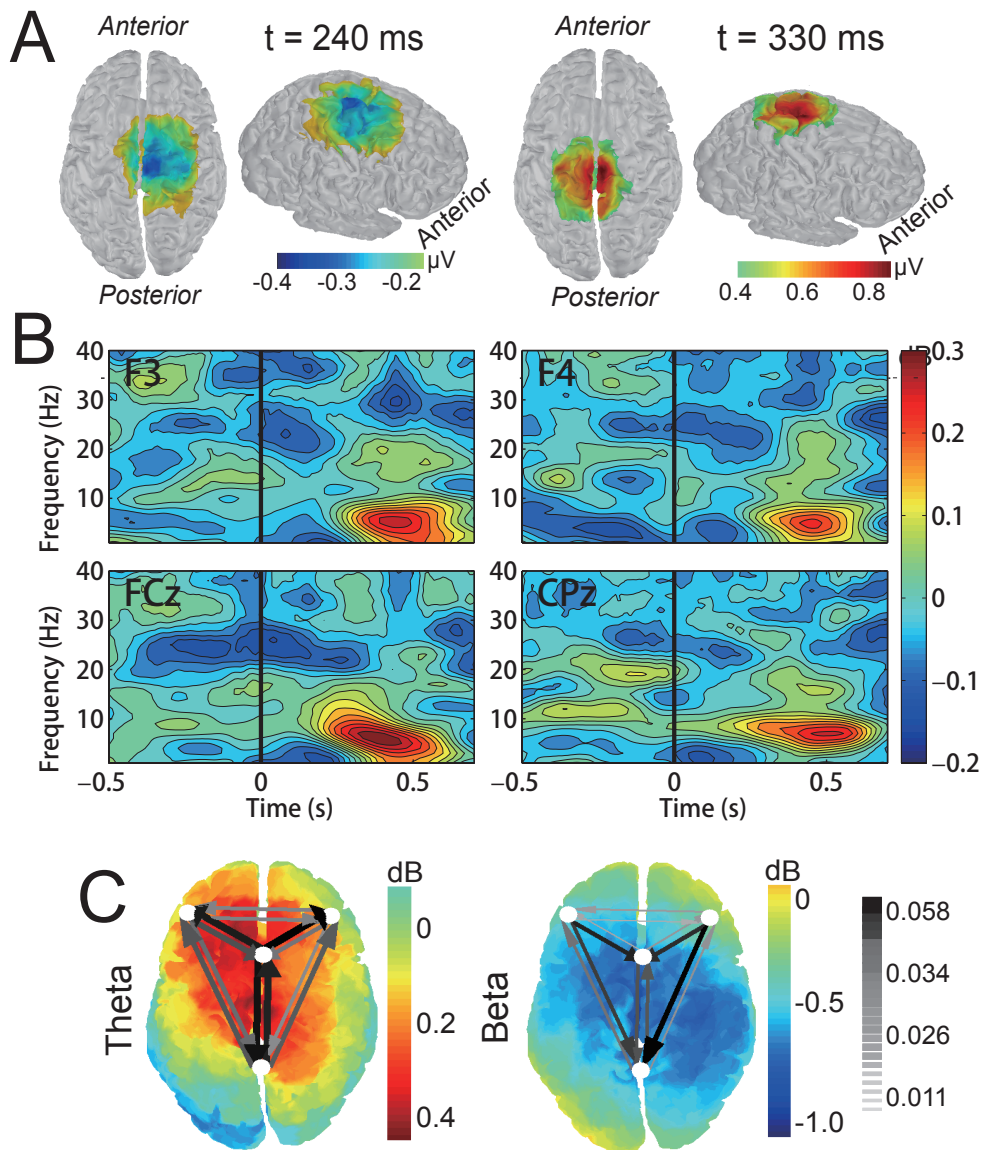


Figure 6.6: A. The difference (error - correct) of topographies in source level at 240 ms and 330 ms after visual stimuli, using beamforming of 41 ROIs under 41 central EEG electrodes. The values are thresholded at -0.2 μV for the negative peak and 0.4 μV for the positive peak. B. Time-frequency spectrogram (error - correct) of four brain sources under electrodes F3, F4, FCz and CPz. C. Fisher score of brain connectivity patterns between four selected brain sources, in two frequency bands, 4-15 Hz and 20-30 Hz. The values of the Fisher score are represented by the color and the thickness of the arrows. Power spectrum density (error - correct) of the brain sources at 240 ms is indicated by the color.

Consistent patterns with the EEG topographies were found (Figure 7.2.B), i.e. negativity at

240 ms and positivity at 330 ms in medial central areas. The spectrogram (error - correct) of the four selected ROIs, under F3, F4, FCz and CPz, are illustrated in Figure 6.6.B, showing higher theta modulation in the error condition from about 200 ms after stimulus onset. We also estimated single-trial connectivity patterns between the four selected ROIs, i.e. left and right frontolateral, medial frontal and centroparietal regions, using DTF. This yielded similar brain connectivity patterns (measured by the Fisher scores, Figure 6.6.C), particularly in the theta band. The colors of the head model indicate the differences (error - correct) of the band power, theta (left) and beta (right) in all 41 ROIs, showing higher theta and lower beta power in the error condition.

6.4 Discussion and conclusion

The results of the current work show that specific modulations of directional brain connectivity patterns are elicited when subjects are monitoring external erroneous events. In particular, there is an increase of information transfer at the theta band between frontal and parietal regions and from frontocentral to frontolateral areas; as well as a suppression of brain interactions from frontolateral and centroparietal to frontocentral areas at the beta band. Previous studies using intracranial and surface EEG, as well as hemodynamics neuroimaging techniques have pointed out that the information transfer patterns between the frontolateral and frontocentral regions are associated with the monitoring of self-generated errors (Cavanagh et al., 2009; Brázdil et al., 2009; Debener et al., 2005). In addition, there are consistent reports of MFC activation due to erroneous information both from internal and external sources (Holroyd et al., 2004; Cavanagh et al., 2012). We report patterns similar to those obtained for monitoring self-generated errors, further supporting the existence of a common mechanism of monitoring processes in the brain, irrespective of the modality of the error.

Theta dynamics in the MFC relates to focused attention, working memory and action control (Klimesch, 1999; Klimesch et al., 2001; Sauseng et al., 2004; Gevins and Smith, 2000; Buzsáki and Draguhn, 2004), particularly error monitoring and feedback processing in both human (Trujillo and Allen, 2007; Cavanagh et al., 2009; Cohen et al., 2008; Wang et al., 2005) and primates (Tsujimoto et al., 2010; Womelsdorf et al., 2010; Kuwabara et al., 2014), and organize cross-regional brain interactions for cognitive control processes (Cohen and Cavanagh, 2011; Cohen et al., 2009A). Further studies report the MFC theta as a common temporal neural pattern during endogenous and exogenous monitoring processes (Cavanagh et al., 2012; Ullsperger et al., 2014). We report increased theta connectivity patterns during error monitoring. In particular, the directional information transfers from frontocentral to frontolateral regions possibly reflect the communication from MFC to lateral regions as further cognitive reaction after the error detection in MFC, consistent with the patterns elicited by self-generated errors as measured by electrophysiological (Luks et al., 2002; Brázdil et al., 2007; Cavanagh et al., 2009; Brázdil et al., 2009), and fMRI (Debener et al., 2005; Agam et al., 2011) techniques. This highlights the role of theta dynamics in frontal areas as a common cognitive mechanism between different performance monitoring processes, i.e., external erroneous

Chapter 6. Brain Connectivity Patterns of Performance Monitoring at Average and Single-trial Levels

events and self-generated errors (Cavanagh et al., 2012).

Interestingly, we found stronger information flow from frontocentral to left frontolateral than from frontocentral to right regions, illustrated in Figure 4. The lateralization phenomenon is also observable in ERP amplitudes, the F3 has lower negative peak than F4, as shown in Figure 2. A. Larger inter-channel theta synchrony between left frontal hemisphere and frontocentral sites – with respect to right frontolateral sites – have been previously reported in an action monitoring tasks, c.f., Figure 3 in (Cavanagh et al., 2009). It has been suggested that the left dorsal prefrontal cortex is more related to participant's expectation regarding the nature of the upcoming trial, whereas the right dorsal prefrontal cortex is associated with the online macro-adjustments in a conflict-driven context (Vanderhasselt et al., 2009). It might be possible that the pattern of lower interactions with right frontocentral areas is caused by the fact that the monitoring process in our experiments does not require any further behavioral adjustments. However, it is yet to be elucidated the exact mechanisms that govern this lateralization pattern.

We also observed significant information flows between centroparietal and frontocentral areas starting as early as 100 ms. This pattern appears before the activation of the network in frontal regions (i.e., between frontocentral and frontolateral), and may be linked to perception processes. Since the cursor moving directions are balanced in both error and correct conditions, this pattern is not correlated with specific moving directions. An interpretation of this frontoparietal interaction is that the sensory representation towards visual perception in the parietal cortex has already been biased by the contents in the working memory, modulating the information flow after stimulus onset, and reported as an integration between bottom-up perception and top-down control process (Ptak, 2012). However, modulations of connectivity patterns between frontal and parietal regions have not been reported in the studies of monitoring self-generated errors. A previous study was unable to find significant modulation of phase synchrony between FCz and parietal regions (Cavanagh et al., 2009). However, in these studies the EEG data is time-locked to the behavioral responses, and stimulus-locked parietal patterns – more related to sensory processes – may be wash out after trial averaging given the variability of the reaction time.

Besides modulations in the theta band, we also observed decreased connectivity patterns in the beta and gamma bands. The beta band activity is associated with the maintenance of the current sensorimotor or cognitive state (Engel and Fries, 2010). Decreased beta power and beta synchronization are usually related with the changes of cognitive conditions (Pfurtscheller et al., 2005; Jurkiewicz et al., 2006). Also, beta modulation is expressed more strongly if the maintenance of the status quo is intended or predicted than after novel or erroneous events (Engel et al., 2001; Engel and Fries, 2010). Accordingly, greater beta power in frontocentral areas has been reported after correct feedback in reinforcement learning tasks (Cavanagh et al., 2012). This effect has been attributed to increased coactivation of MFC and motor cortices during feedback processing (Cohen and Ranganath, 2007). In turn, other studies reported stronger beta depression and rebound in MEG signals after error trials in a monitoring task (Koelewijn et al., 2008). Together with our results, this shows that the beta modulations

are also sensitive to the errors in absence of motor responses. Rather than reflecting low-level automatic motor resonance, the beta desynchronization corresponds to the discontinuation of the current cognitive states as a high level role, not restricted to motor related intentions (Koelewijn et al., 2008; van Schie et al., 2004). This study supports this theory, since no specific movement reaction is required in the task but the continuation of the cognitive state maintenance is no longer sustained after the perception of erroneous events.

Currently, there is an increased interest in the possibility of performing single-trial, spatio-temporal analysis of the neural correlates of monitoring processes (Debener et al., 2005; Cavanagh et al., 2009; Heike et al., 2010; Cohen and Cavanagh, 2011; Cavanagh et al., 2012). This allows to elucidate phenomena that is hardly observable using averaging-based methods. Here we show that cross-regional interaction patterns can be estimated at the single-trial level. These patterns are obtained with a regression model, and thus are not linearly dependent with original EEG channels, possibly providing discriminant information for decoding whether a trial corresponds to monitoring the correct or erroneous condition. Notably, significant differences and discrimination capability (Fisher score) in the single trial modulations further verified that the obtained brain interaction patterns during error cognition are coincident with the modulation patterns obtained at the subject level. The estimation of connectivity patterns in a single-trial basis shows that the network dynamics do convey information about the brain modulations of the monitoring process. Importantly, this information is complementary to the one provided by standard ERP analysis for the use of recognizing error trials, both in the temporal and spectral domain.

Recent studies of EEG-based brain-computer interface show that the classification performance of motor imagery tasks using brain connectivity features, either DTF (Billinger et al., 2013) or instantaneous phase difference (Hamner et al., 2011), is comparable to the use of customary band power features. Connectivity-based features have also been used for continuous decoding of arm trajectories from electrocorticography signals showing increased estimation accuracy with respect to spectral features (Benz et al., 2012). However, most of these classification or regression models are mainly data driven, extracting features through optimization algorithms, without providing an explicit interpretation about the selected features. The current work provides evidence that discriminant connectivity-based features not only allows pattern recognition, but are also consistent with the current knowledge about the dynamics of the brain network involved in monitoring processes.

It should be noticed that the single-trial connectivity estimation required larger analysis windows than the multi-trial analysis. This increases the reliability of the parameter estimation, but decreases temporal resolution. Further work can explore alternative algorithms to overcome this limitation, for instance, adaptive DTF based on adaptive estimation of autoregressive parameters (Wilke et al., 2008).

To summarize, modulations of brain connectivity patterns appear in both low and high frequency bands in the process of monitoring external events through the recording of scalp

Chapter 6. Brain Connectivity Patterns of Performance Monitoring at Average and Single-trial Levels

EEG. In particular, strong theta modulations are obtained both at average and single-trial level. These results, consistent with modulations elicited after the monitoring of self-generated errors, support the parsimonious role of theta activity in MFC in coordinating cross-regional activity during various monitoring processes. Importantly, since our protocol does not involve motor response, these network patterns appear to be related to intrinsic mechanisms of the function of error cognition in human brain, instead of being exclusively linked to co-activation with motor areas. Furthermore, the temporal evolution of the EEG connectivity modulations – i.e., activation of frontoparietal network precedes increased frontolateral interactions – suggests a possibly hierarchical organization of the monitoring cognition: Early frontoparietal interaction may reflect modulation of neural activities by bottom-up sensory inputs, whereas frequency-specific interactions between frontocentral and frontolateral areas reflect the perturbation of cognitive states in the working memory and the preparation for potential top-down adjustment. Future work will be devoted to investigate the causal dependences between these two modulation patterns, as well as trial-by-trial changes in different response and feedback tasks.

7 EEG-based Decoding of Error-Related Brain Activity in a Real-World Driving Task

7.1 Introduction

Driving a vehicle requires multiple cognitive processes, e.g., sustaining current vehicle conditions, monitoring environmental events, and action decisions. Currently, driving assistant systems are mainly based on monitoring the vehicle conditions, e.g., the parameters of the car (steering, braking and accelerating), vehicle's location, complexity of the environment, and distance from other automobiles. Recently, it has also been proposed that these systems can also monitor driver's condition through the recording of EEG, ECG and EOG signals (Chuang et al., 2010; Haufe et al., 2011; Haufe et al., 2014).

Brain computer interfaces (BCI) have been developed to restore communication capabilities for patients, or healthy individuals (Lebedev and Nicolelis, 2006; Millán and Carmena, 2010), i.e., in-car assistant system. These BCI systems will decode driver's brain activity to estimate his/her cognitive states or action intentions. For instance, the system can verify whether the driver is paying attention to the driving behavior (Simon et al., 2011), estimate mental workload (Dijksterhuis et al., 2013), or predict driver's intention of action (e.g., braking, traffic lights, and lane changes) (Haufe et al., 2011; Khaliliardali et al., 2012; Gheorghe et al., 2013a; Haufe et al., 2014; Kim et al., 2015).

The present study investigates another modality for a brain-dependent driving assistance system tested in a real car. It relies on the error-related brain activity. Error-related processing is a basic brain function related to learning and regulating goal-directed behavior (Holroyd and Coles, 2002; Taylor et al., 2007). It is considered as an underlying monitoring process for both endogenous and exogenous conflict information, e.g., expectation mismatch or erroneous motor commission (Cavanagh et al., 2012). The error-related brain activity can be reflected in scalp recordings in the form of phase locked event related potentials (ERP), around 50 ms after erroneous motor responses (Gehring et al., 1993; Holroyd and Coles, 2002; Cavanagh et al., 2012), or 250 ms after the stimuli presence in the case of monitoring external errors (van Schie et al., 2004; Chavarriaga and Millán, 2010; Chavarriaga et al., 2014). This ERP pattern has been used in BCI for detecting error activity while human subjects either

Chapter 7. EEG-based Decoding of Error-Related Brain Activity in a Real-World Driving Task

control moving objects (Parra et al., 2003; Ferrez and Millán, 2008) or monitor an external system (Chavarriaga and Millán, 2010; Iturrate et al., 2014). This information can then be used to correct user's erroneous decision (Parra et al., 2003), improve the information transfer rate of BCI system (Ferrez and Millán, 2008), or detect subject's intentional preferred target (Chavarriaga and Millán, 2010; Zhang et al., 2012). See (Chavarriaga et al., 2014) for a review.

The current study try to detect error-related brain activity during driving. In the experiments, a driving assistant system presents a directional cue indicating a turning direction before reaching intersections, and single trial classification is performed to recognize error-related brain activity to verify whether the directional cue corresponds to driver's intention. Some of the results in this chapter has been previously published in (Zhang et al., 2013).

7.2 Materials and Methods

7.2.1 Participants

Twenty-two subjects (three female, age 26.79 ± 3.51) participated in the experiments in the car simulator. Seven of them (one female, age 27.86 ± 1.95) participated in the evaluation of online decoding. Seventeen subjects in the experiment in the car simulator had driving licenses and 9 of them were driving recently.

Eight subjects (two female, age 28.62 ± 2.72) participated in the real car experiments. Seven of them (two female, age 28.42 ± 2.88) participated in the online evaluation. All subjects in the real car experiment hold valid driving licenses and were active drivers. The experimental protocols were approved by the local ethical committee and subjects provided written informed consent. All subjects, in both car simulator and real car experiments, had normal or corrected-to-normal vision, and did not report any known neurological or psychiatric diseases.

7.2.2 Experimental settings in car simulator

The first phase of the experiments was performed on a custom-made simulated car, shown in Figure 7.1.A, corresponding to a realistic vehicle with normal-sized car seat, steering wheel, accelerate and brake pedals. For the experiments, we designed a 3D virtual environment of a small town including six north-to-south and five east-to-west roads arranged in a rectangular grid using the software *Blender* (<http://www.blender.org/>). The protocol was run in a customized open source driving simulation program *VDrift* (<http://vdrift.net/>). The virtual driving environment was presented in three 27 inch 3D monitors, which were about 120 cm away from subject's eyes. The monitors allowed to present the scene from 8 directions and do not require the user to wear 3D glasses. During the experiment, the car control signals (steering, pedal positions), vehicle dynamics and its position in the virtual environment are continuously recorded at a sampling rate of 256 Hz.

Subjects were instructed to drive following street boards located on top of the intersections as shown in Figure 7.1.B. The speed of the vehicle was limited to 60 Km/h. When the car approaches an intersection (at approx 80 m) a *visual cue* composed of three gray arrows (pointing left, up and right) appeared at the lower part of the wind shield. One second later, still before the car reached the intersection, one of the arrows was highlighted in green, indicating one of the possible driving directions (*directional cue*). This cue was supposed to show the turning direction inferred by another driving assistance system. All cues disappeared 500 ms after the directional cue.

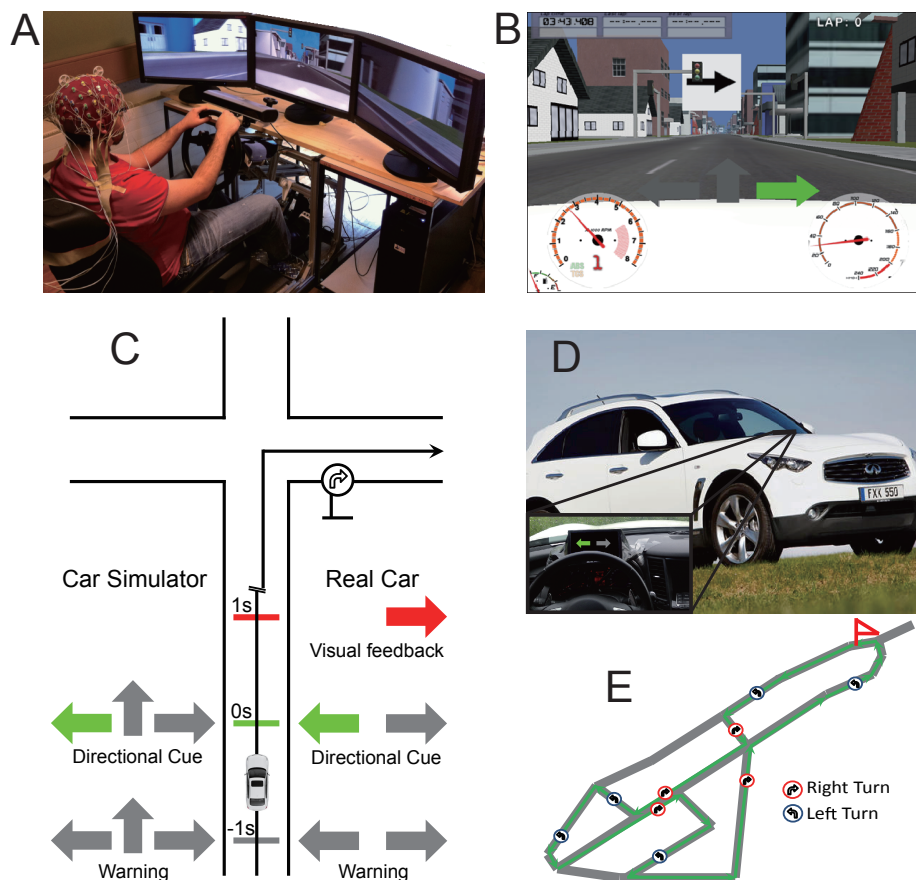


Figure 7.1: Experimental settings and protocols. A. Setup of experiments in car simulator with EEG recording. B. Virtual environment as perceived by the driver in the car simulator. Directional signs (white panel with black arrow in the center) shows the direction of turning; while information from the driving assistant are shown over the dashboard (gray and green arrows). C. Timings for experimental protocol. A visual cue is shown to notify subjects that a new trial is starting, and the directional cue informs a possible turning direction to elicit error-related brain activity if conflicted with subject's preference, and the visual feedback indicates whether the system have detected error activity. The arrows disappear at 500 ms. D. Vehicle Infiniti FX30 used for the real car experiments. The inset shows the monitor displaying the experimental cues. E. The closed track used for the real car experiments. The red flag indicates the start point of the lap.

Chapter 7. EEG-based Decoding of Error-Related Brain Activity in a Real-World Driving Task

During the experiment, the probability of directional cue (green arrow) pointing to the same direction as the street board was 70%. Twenty-two subjects performed one offline recording composed of 5 runs, where each run was composed of 30 trials, i.e., 30 intersections, and lasted about 9 to 12 minutes. Seven of these subjects participated in subsequent online recordings, which contained 4 to 6 runs depending on the subject. This yielded 150 trials (i.e., intersections) for offline runs and an average of 158.57 ± 14.64 trials for the online analysis.

7.2.3 Experimental settings in the real car

The real car experiments were performed in an Infiniti FX30 vehicle, shown in Figure 7.1.D. Subjects were requested to use the automatic gearshift and keep their hand on the steering wheel to limit their arm movements. We disabled the built-in driving assistance systems during the experiments, i.e., intelligent cruise control, lane departure prevention, and vehicle dynamic control. Similarly to the car simulator, the vehicle was equipped with a driving logger (provided by the manufacturer) that recorded steering and pedal positions at a sampling rate of 256 Hz. A 7 inch screen was placed on the dashboard in front of the subject (behind the steering wheel) to show the task-related arrows during the experiments. For safety reasons, the real driving experiments were performed in a closed road without any other vehicle or pedestrians.

Subjects drove the car following direction signs placed along the road, as shown in Figure 7.1.C and E. Based on the topology of the real road used for the experiments, the options of turning were reduced to left and right, thus only these two arrows were shown as directional cues. The timings of the visual cues were exactly the same as in the car simulator. Subjects were asked to drive normally as in a secondary road and limit their speed to 60 km/h. Each run of the real car recording consisted of 5 laps (9 trials per lap), i.e., 45 trials per run, which lasted around 15 to 20 minutes, depending on the speed of the car. We recorded 3 runs for each subject corresponding to 135 trials. Eight subjects performed offline experiments on the first day, and seven of them participated in a second recording day to test online decoding. Six subjects performed directly the online runs using a classifier trained in offline data from the previous day. The offline data (first day) of the remaining subject was contaminated by artifacts, therefore she performed two offline runs on the second day, followed by one online runs.

In most runs of the online experiment with the real car (normally from the second run), subjects were given additional visual feedback 1 s after showing the directional cue (green arrow). The visual feedback was a red arrow, only shown when an error potential was detected from the EEG (Figure 7.1.C), pointing to the opposite direction as the green arrow. No visual feedback was shown when the EEG signal was recognized as a correct trial. The term “*visual feedback*” is used to indicate the red arrow after classification.

7.2.4 Data acquisition and pre-processing

Unless specified, the processing of physiological signals was the same for both simulated and real driving experiments. EEG signals were recorded from 64 locations according to the extended 10/20 system using a Biosemi Active Two system with a sampling rate of 2048 Hz. Ground and reference electrodes were replaced by the Common Mode Sense (CMS) active electrode and the Driven Right Leg (DRL) active electrode. Signals were referenced to the CMS electrode placed 1 cm to the left of POz. EOG signals were simultaneously recorded using electrodes positioned above the nasion and below the outer canthi of both eyes. Experimental events (timing and type of the visual cues) were marked in both EEG data and the driving log file via hardware triggers sent from parallel port.

For the data obtained in the car simulator, we analyzed the temporal waveform of the ERP after filtering the raw signal spatially, common average reference (CAR), and in the frequency domain, 4_{th} order non-causal Butterworth filter with cutoff [1 10] Hz. The choice of this frequency band is based on the fact that the main oscillatory signature of error-related brain activity is in the theta band (Holroyd and Coles, 2002; Taylor et al., 2007; Chavarriaga et al., 2014). We kept the same processing for the online experiment in the car simulator, except using a causal filter. In addition to the analysis of the temporal waveform, we also computed the PSD of the signal in a broader band, namely [1 50] Hz for car simulator and [1 30] Hz for the real car. This difference was motivated by the presence of vehicle specific electrical noise at 30 Hz.

For the real car experiment, the offline analysis was the same as in the car simulator. Prior to applying CAR, the EEG data was visually inspected to discard noisy channels. The signal in those channels was replaced by the average of neighbors. Contaminated electrodes were mainly located in parietal regions, which are [FC5 PO4 P2] for subject 1, [FC5] for subject 4, [P1 Pz P2 P3 CP2 CP4 CP6 FC6 O2] for subject 5, and [P1 PO4] for subject 7.

For the online processing of the real car data, the CAR was not performed for the reason that the signals were more prone to contamination in some of the electrodes, and the contaminated signal will affect the other channels in the case of applying CAR. Among all subjects, one of them (Subject 4) had substantial level noise in the real car experiments on the first day. For this reason, we discarded the subject's data on that day and only used the data from the second day.

After preprocessing, we extracted correct and error trials according to the onset of the directional cue ($t = 0$ s). Epochs were defined to include data from one second before ($t = -1$ s) to one second after ($t = 1$ s).

7.2.5 Classification

EEG activity was decoded in order to infer whether the user perceived the directional cue as 'correct', i.e., in agreement with the intended direction showed by the traffic sign, or 'erroneous',

Chapter 7. EEG-based Decoding of Error-Related Brain Activity in a Real-World Driving Task

otherwise. Classification between correct and error was performed based on the ERP time signal in the period, between 0.2 s and 0.7 s after the onset from 41 EEG electrodes: AF3, F1, F3, F5, FC5, FC3, FC1, C1, C3, C5, CP5, CP3, CP1, P1, P3, P5, PO3, POz, Pz, CPz, AF4, AFz, Fz, F2, F4, F6, FC6, FC4, FC2, FCz, Cz, C2, C4, C6, CP6, CP4, CP2, P2, P4, P6 and PO4¹. The 50 most discriminant features (channel and time point) were selected for classification. The discriminant power of each feature was estimated using the Fisher score: $\frac{|m_1 - m_2|}{(s_1 + s_2)}$, where m_i and s_i are the mean value and variance of the samples from the i^{th} class.

We used Linear Discriminant Analysis (LDA) to classify correct and error trials. The offline performance was evaluated using 10-fold cross validation, where the folds were generated keeping the temporal structure of the data. Feature selection was performed separately per each fold using the training data. Since the trial numbers for the two classes were not balanced, i.e., about 30% of them were error trials, we report the results in terms of both accuracy, and sensitivity-specificity in the receiver operating characteristic (ROC) space.

Furthermore, the results were compared with chance level, which was computed empirically by shuffling the training labels, and building a classifier with such training data. The chance level corresponds to the average performance of repeating the shuffling process 1000 times. We also controlled that the discriminative information was actually related to error processing in the brain and not caused by signal contamination due to eye movements. For this, we trained a classifier using the 3 EOG channels in the offline dataset for both car simulator and real car. The EOG channels were preprocessed in the same way as the EEG signal.

The online classification followed the same processing as the offline data. In the case of the car simulator, the classifier was trained using the data obtained so far on that day, i.e., the classifiers were trained on the data of the preceding runs. So, the first run was offline, as no data was available for training a classifier. In the real car experiments, with the exception of Subject 4, we trained the classifier using the data recorded on the first day. The fact of training and testing the classifier on different days allowed us to further assess the consistence of the error-related patterns across time.

7.3 Results

7.3.1 Event-related potentials

Frontal central areas are considered as the main brain source for error-related brain activity (Holroyd and Coles, 2002; Taylor et al., 2007). We observe clear error-related modulations over these areas in offline datasets, as illustrated in the grand average ERP at FCz, Figure 7.2. The ERP from car simulator (Figure 7.2.A) exhibits similar amplitude as the real car data (Figure 7.2.B). The signal is smoother in the car simulator, which can be due to the larger number of participants and trials and the lower noise level in this environments.

¹Peripheral electrodes were excluded to reduce signal contamination

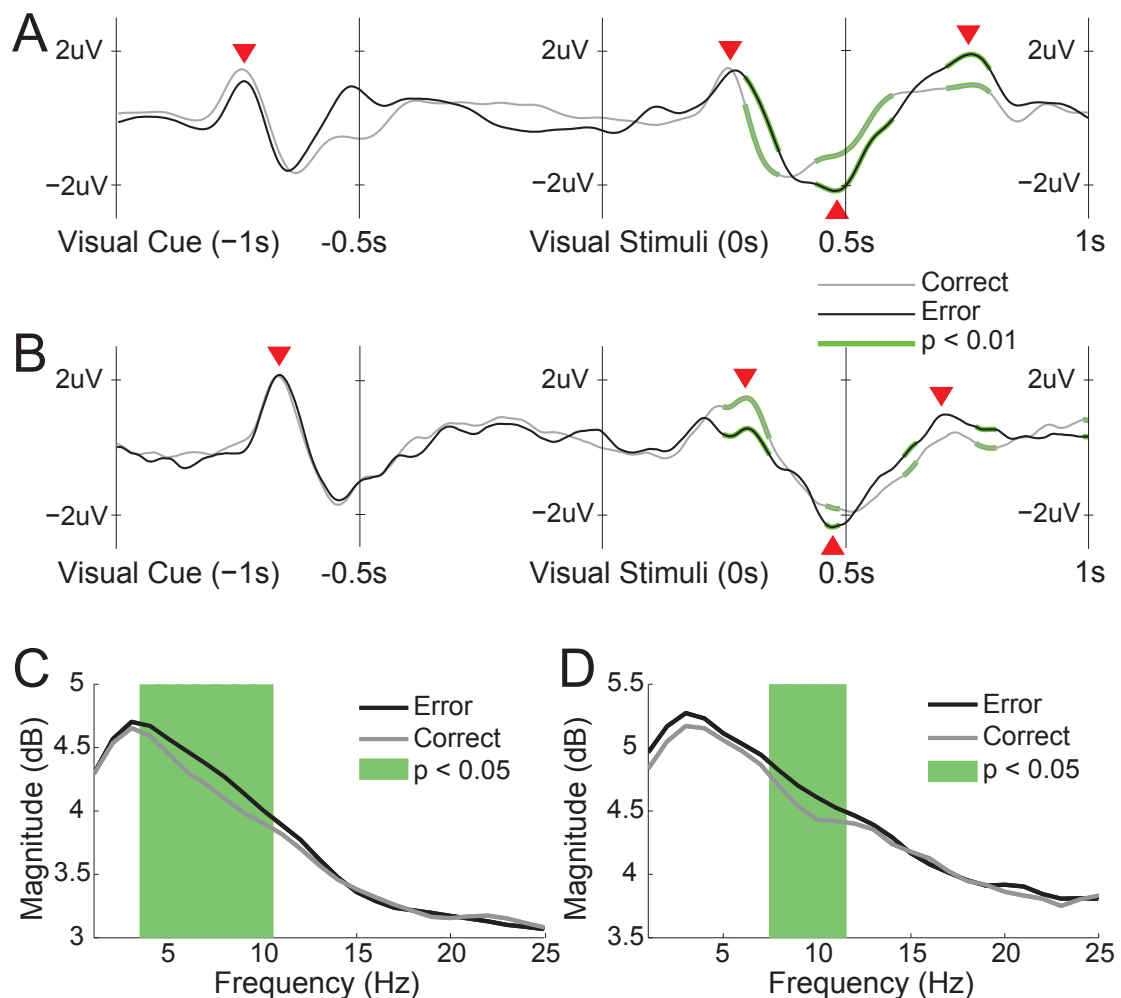


Figure 7.2: Grand average of ERP and PSD at FCz. EEG trials are epoched according to the directional cue (0 s), from -1 s (presence of the three gray arrows) to 1 s. A. ERP of the car simulator data. B. ERP of the real car data. Significant differences ($p < 0.01$) across time samples between error and correct trials are found by two-sample t -test for all trials, which are shown as green thick lines. The red triangles indicate the time points selected for the illustration of topography in Figure 7.3. C. PSD of the car simulator data. D. PSD of the real car data. PSD is computed in time window [200 400] ms. Statistical tests are performed by a two-sample t -test for all trials, and the significances ($p < 0.05$) are shown as the green area.

The ERP elicited in both experiments showed a positive peak after the visual cue, peaking at about 760 ms before the directional cue in the car simulator data (670 ms in the real car condition). No statistically significant difference was found ($p > 0.01$, two-sample t -tests, corrected by a 1000 random permutation test) between error and correct trials in the period before the directional cue ('visual stimulus' in Figure 7.2.A). After the appearance of the directional cue (0 ms), another positive peak is found for both the car simulator and real car data. It appears around 260 ms for the car simulator and 200 ms for the real car case. Again,

Chapter 7. EEG-based Decoding of Error-Related Brain Activity in a Real-World Driving Task

this peak does not show statistical difference between correct and error conditions, suggesting that none of these peaks is related with brain error processing. Specifically for the first peak (at -760 ms and -670 ms respectively), the directional cue (containing the information required to assess correct or erroneous conditions) has not yet been shown. In the experiments, the trials were randomly generated and balanced, i.e., left, right and straight arrows (left and right in the real car case) occurred equally often in both error and correct conditions, so we could infer that these two peaks are not correlated with the perception of spatial patterns of the stimuli.

A positive peak at 290 ms in the real car data can be found, which is significant ($p < 0.01$) between the error and correct. We observed a negative peak at about 480 ms. The error condition has significantly lower amplitude than the correct condition ($p < 0.01$) for both the car simulator and the real car datasets. Significant differences between error and correct could also be found at around 700 ms after the directional cue with higher amplitude in the error condition. In summary, the two experiments showed consistent ERP patterns and significant differences between the two conditions.

Topographies of the 41 electrodes considered in this study are shown in Figure 7.3. They show the scalp wide activity at the onset of the directional cue (0 s) and at the time of the ERP peaks. Frontal regions show a positive modulation after visual cue (-760 ms for car simulator and -670 ms for real car case) and the directional cue (260 ms for car simulator and 290 ms for real car). High activity is observed after the visual cue, probably due to the fact that the subjects perceived suddenly the first visual cue (three gray arrows), which was also the purpose of presenting this visual cue, informing the subjects the forthcoming directional cue in order to reduce the effect of visual surprising from brain error processing. Error and correct trials showed similar patterns at -760 ms, confirming that no error-related information is contained. Topographies at the onset of directional cue (0 ms) showed no specific modulation patterns, amplitudes being close to zero for all electrodes. We observed frontal negative deflections at about $t = 480$ ms ($t = 475$ ms for the real car case) for error and correct conditions, and the error trials have lower amplitude. Further, at about $t = 750$ ms ($t = 700$ ms for the real car case) we can see a positive pattern in frontal regions, especially in the error condition, relating to the positive peak in FCz in Figure 7.2.

The increase of theta band in medial frontal cortex (MFC) is considered as the main oscillatory modulation pattern of error monitoring (Holroyd and Coles, 2002; Taylor et al., 2007; Cavanagh and Frank, 2014). Figure 7.2.C and D illustrate the power spectrum density (PSD) in the period [200 400] ms after the directional cue for electrode FCz. For both error and correct trials, the PSD curves decrease gradually, and drop faster after 12 Hz. Both experiments showed higher theta power in the error condition. Specifically, significant differences ($p < 0.05$, two-sample t -test for all trials, corrected by a 1000 random permutation test) are found between 4-11 Hz (Figure 7.2.C) in the car simulator and between 7-9 Hz in the real car (Figure 7.2.D) case. No difference could be found in higher frequency ranges.

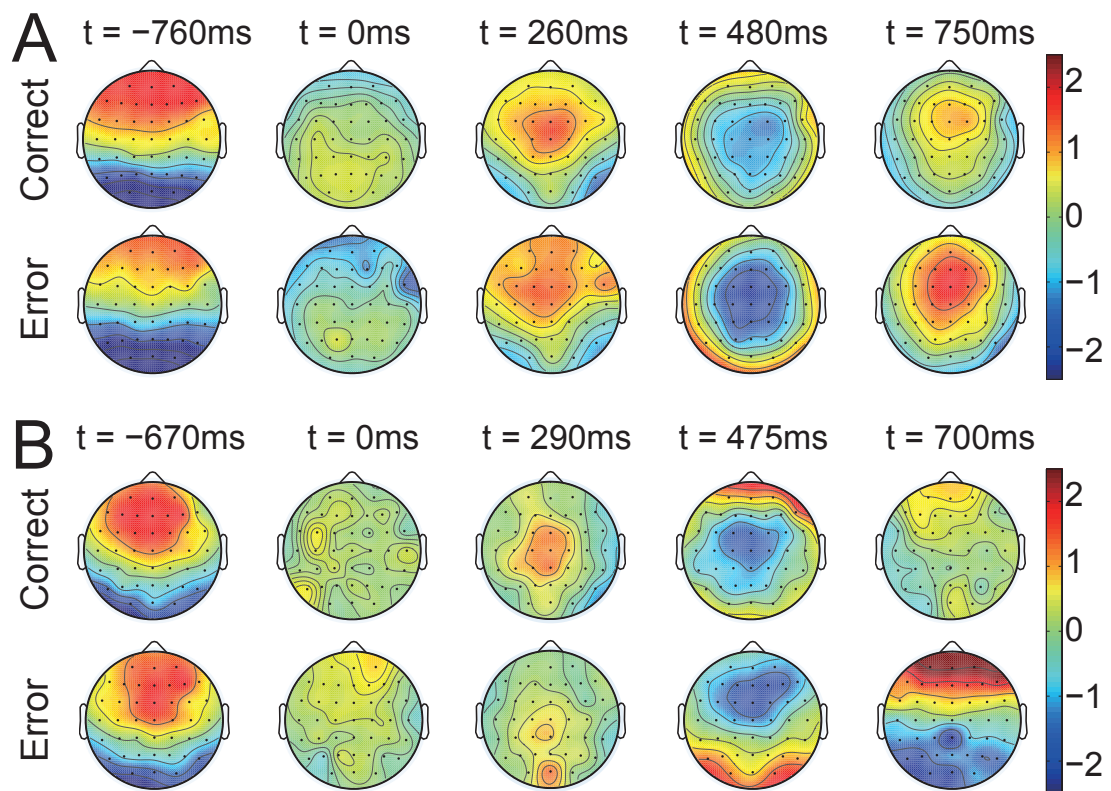


Figure 7.3: Topographic illustration of brain activity at time points of ERP peaks and $t = 0$ ms (onset of the directional cue). A. Car simulator dataset. B. Real car dataset. 41 central electrodes are shown in the figure, excluding the peripheral regions.

7.3.2 Offline classification results

The results of offline classification are depicted in Figure 7.4. Each curve in Figure 7.4.A and B represents the result of one subject, averaged across 10 folds. In both experiments, car simulator ($N=22$) and real car ($N=8$), most of the subjects have a classification performance above 0.5 (diagonal dash line). The average accuracy across subjects is 0.698 ± 0.065 and 0.6823 ± 0.059 for the car simulator ($N = 22$) and real car ($N = 8$) experiments, respectively. The sensitivity-specificity of the decoder using the area under the ROC curve (AUC) was of 0.729 ± 0.086 and 0.6824 ± 0.086 for the car simulator and real car experiments. Although the accuracy and AUC are lower in the real car, no significant difference (two sample t -test, $p > 0.05$) was found between the two experimental settings.

The performance of using EOG features is illustrated as gray boxplots in Figure 7.4.C and D, which were significantly lower (one sample t -test, $p < 0.05$) than using EEG features for both accuracy (0.614 ± 0.082 for the car simulator and 0.589 ± 0.106 for the real car) and AUC (0.616 ± 0.116 for the car simulator and 0.574 ± 0.142 for the real car). Furthermore, we computed the chance level for both experimental settings, shown with the white boxplot in Figure 7.4.C.

Chapter 7. EEG-based Decoding of Error-Related Brain Activity in a Real-World Driving Task

This yielded an accuracy of 0.523 ± 0.042 (car simulator) and 0.554 ± 0.030 (real car), and AUC of 0.494 ± 0.050 (car simulator) and 0.526 ± 0.051 (real car). Significant differences ($p < 10^{-4}$, paired t -test) were found between the chance level (blank boxes) and the EEG classification for both accuracies and AUC.

7.3.3 Online classification

For the experiments in the car simulator, since the classifier was updated after every run, we report online performance for each run, from runs 2 to run 5, illustrated in Figure 7.5.A.

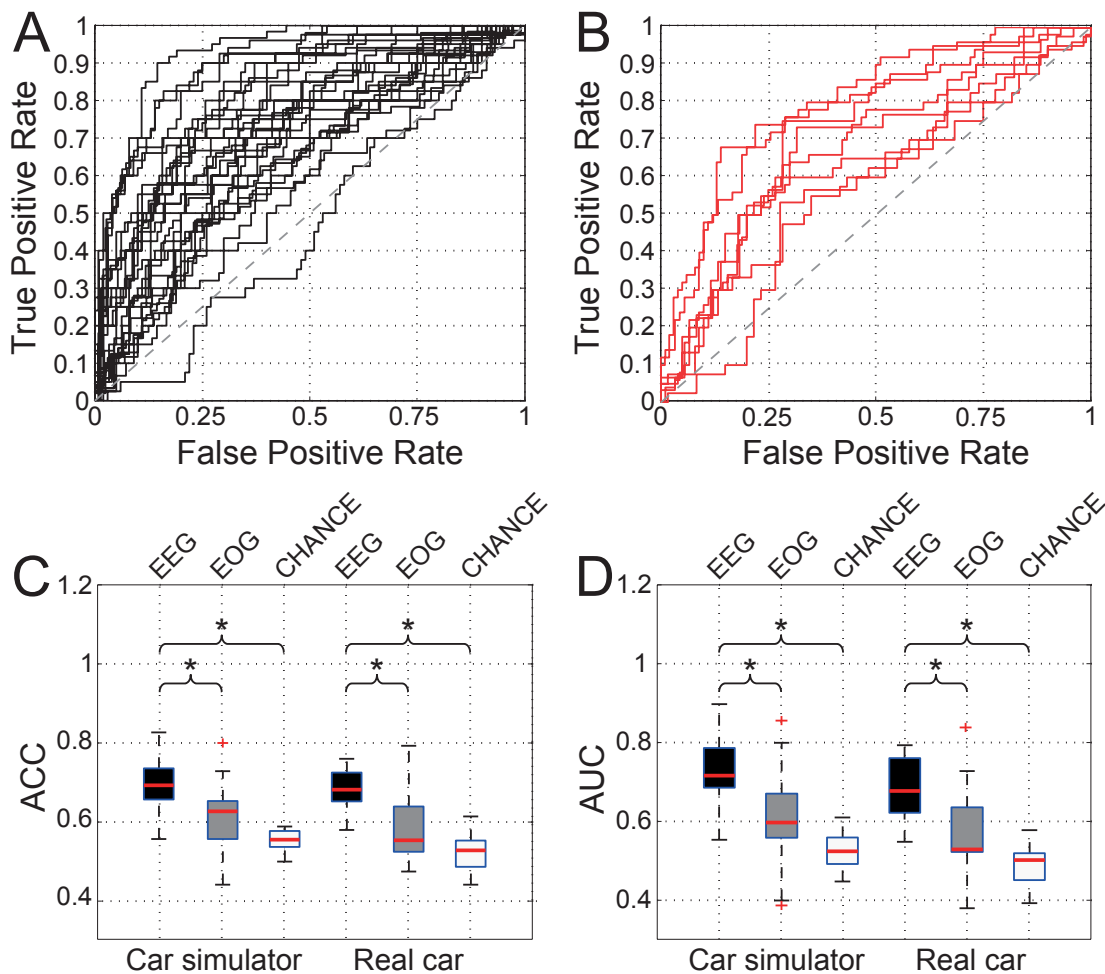


Figure 7.4: Offline classification performance of both car simulator ($N=22$) and real car data ($N=8$). A. Results in ROC space for the car simulator, i.e., quantified by false positive rate and true positive rate. Each curve shows results of one subject (10-fold cross validation) B. Results in ROC space for the real car. C and D. Median and 25th/75th percentiles of accuracy and area under the curve in car simulator and real car datasets. Black boxes show the results of using EEG signal, gray boxes show the results of using EOG signal, and the empty boxes indicate the chance levels. Asterisk indicates significant difference using t -test.

The later run has higher accuracy than the early runs; thus, the 5th run (0.733 ± 0.150) has higher accuracy than the 2nd run (0.567 ± 0.101), which is statistically significant ($p < 0.05$, paired t-test). The false positive rate and true positive rate of each run for the seven subjects are illustrated in Figure 7.5.B, showing that the performance exceeds chance level in most runs. We could also observe substantial differences between subjects, e.g., the subject corresponding to blue diamond shows better performance than that of green hexagrams, which might be due to the diversity of the signal quality, the experience of performing similar experiments and the attention level during the recording.

Similarly, the results of online real car experiments are shown in Figure 7.6. Since the online experiments have different number of runs across subjects, we present the results of each run for each participant separately. Five subjects did the first online run without the visual feedback, i.e., the red arrow one second after detecting the error-related brain activity. Excepting subject 4, the classifiers were trained based on the data collected in the previous recording day, and no further update of the classifier was done during online experiments. As shown in Figure 7.6.A, the classification performance increases across runs, particularly the first run was never the highest for any subject. Again, variations in performance exist across participants, e.g., subject 2 has much better performance (0.786 ± 0.060) than the others, and subject 3 (0.545 ± 0.068) has performance close to random level except for the last run. As mentioned in the section 7.2.3, subject 4 has only one online run using the training data of the same day. This might be one of the reasons why this subject has relatively higher performance (0.773) than other subjects.

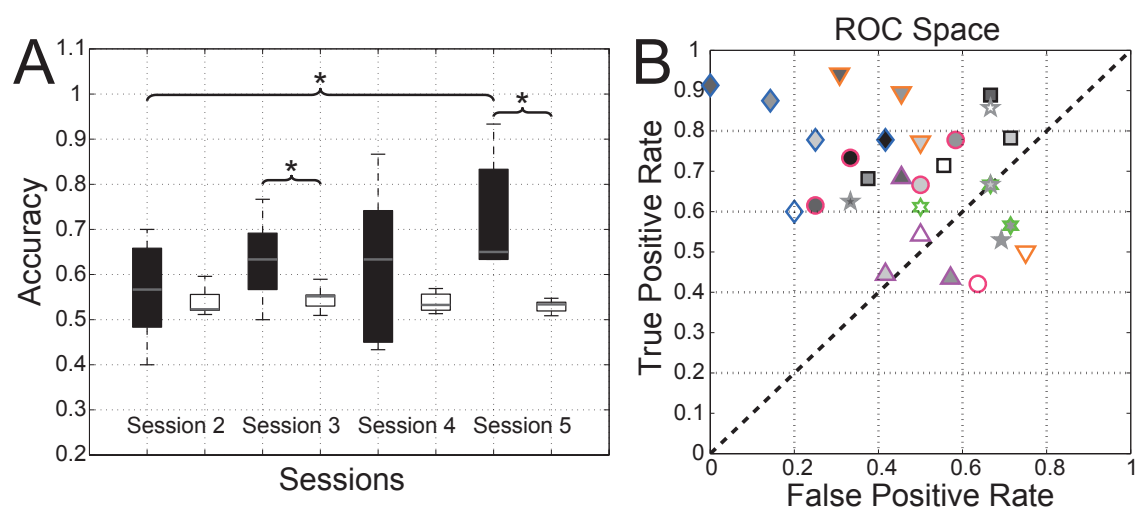


Figure 7.5: Performance of online experiments in the car simulator (N=7). A. Classification accuracies in the online runs (from 2 to 5), averaged across participants. Error bars represents the standard deviation. B. False positive and true positive rate of all online runs for. Each type of marker represents one specific subject and the face color (white to black) indicates the run order, i.e., lighter markers correspond to earlier runs than darker markers.

Chapter 7. EEG-based Decoding of Error-Related Brain Activity in a Real-World Driving Task

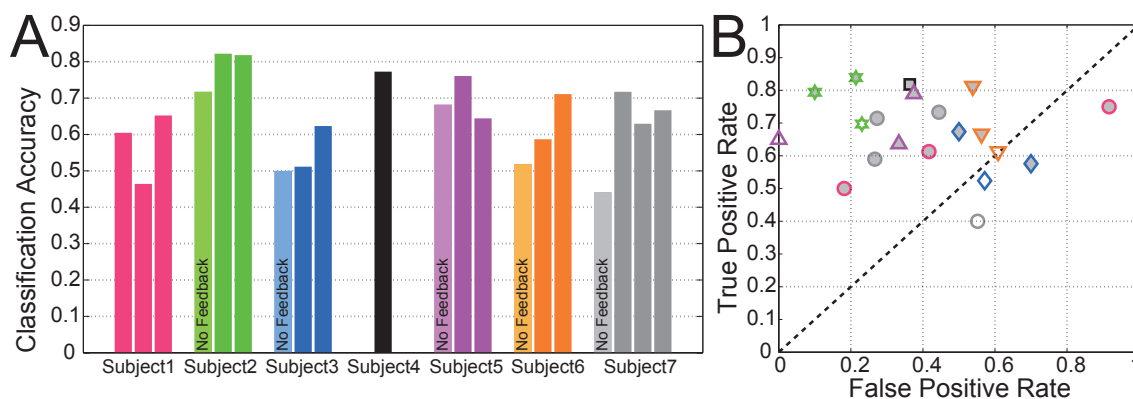


Figure 7.6: Online performance of real car experiments (N=7). A. Classification accuracy for each subject with different number of runs. Runs that did not deliver visual feedback was labeled as 'No Feedback'. B. False positive and true positive rate of all runs. Subjects are represented by marker types, and the color convention is the same as in A. The runs with feedback are indicated with filled markers.

7.4 Discussions

In this study, we have analyzed and decoded error-related brain activity while driving a simulated and a real car. Classification of the EEG signals in a single trial basis yielded performances significantly above chance level for most subjects and therefore can be used to obtain information about the driver's appraisal of the presented stimuli, e.g., to validate inferences made by a driving assistant system. This study extends our previous work from car simulator to real car experiments. The consistency of ERP grand averages and classification performance between the car simulator and real car experiments supports the idea of using BCI systems to assist in driving tasks. More importantly, the current study also evaluated decoding of these signals in an online manner, showing similar performance between the two experimental setups, further proving the feasibility of such systems in realistic applications.

Unsurprisingly, the EEG signals were more prone to artifact contamination in the real car situation than in the simulated condition. The environmental noise, e.g., moving and shaking of the automobile as well as the movements of the subject's eyes and head, are some of the factors that decrease the quality of the EEG data in this condition. Concerning these aspects, the robustness and reliability should be taken into account in the design of in-car BCI systems. The error-related EEG activity has been reported to be largely independent from the stimuli type (e.g., visual, auditory or tactile) and spatial position of stimuli, modulated only when subjects perceive conflicting information (Chavarriga and Millán, 2010). This activity is mainly associated with modulations in theta band, thus the interest frequency range did not overlap with the vehicle specific electrical noise observed at 30 Hz in the real car experiments. Furthermore, as the brain sources of error-related activity is located in the medial frontal area (Holroyd and Coles, 2002; Taylor et al., 2007), we excluded the peripheral EEG channels

for analysis, which are more sensitive to eyes and muscular movement. Comparing the ERP (Figure 7.2) and topographies (Figure 7.3) between the car simulator and real car results, we could conclude that even though the signal quality is noisier in real world driving, the modulation of the brain patterns is kept the same as in the car simulator. The fact that EOG-based classification yielded low performance also supports the notion that the discriminative patterns are not originated from eye movements. Further studies may attempt to apply algorithms to remove eye movements and blinks automatically (Joyce et al., 2004).

The classification results showed performance variations across subjects and runs. In general, most subjects were naive to the protocol, both for the car simulator and the real car experiments. Only one subject performed the experiment in the car simulator before the real car recording. The performance variability across individuals and runs is possibly caused by the attention level and the adaptation to the protocol. As we see in the car simulator data (Figure 7.5.A), the performance gradually increases from run 2 to run 5 with significant improvement, which is also supported by the real car dataset where the later runs outperform the first one. These results suggest that certain adaptation is necessary for subject to obtain good and stable classification performance. Nevertheless, we cannot exclude that the increase in accuracy observed in the online car simulator experiments are not also due to the larger amount of data available for training the decoder. Further study may try to find the relative contribution of data amount and subject adaptation.

We compared this protocol with the previous study of error monitor without any behavior (Chavarriaga and Millán, 2010) (mean classification accuracy of 0.758 and 0.632 for correct and error trials, respectively), showing no obvious drop of the classification performance, and therefore proving that detecting the error-related brain activity in complex tasks is feasible and the accuracy is equivalent as pure monitoring.

In the current study, even though the classification performance is above chance level for most of the subjects, it may be not high enough for practical applications. To optimize the classification performance in future, we can improve the feature selection method in order to reduce redundancy in the selected features for classifiers (Brown et al., 2012). Additionally, the current study only uses the discriminative information from ERP patterns, or temporal waveforms, as classification features. Alternative features, e.g., spectral information and causal influences between electrodes, are likely to boost classification performance according to some reported studies on BCI (Wang et al., 2006; Zhang et al., 2012; Billinger et al., 2013; Omedes et al., 2014). Moreover, the online results in the car simulator data indicate that the prompt updating of the classifier seems to contribute to performance improvement, which might be further evaluated through the adaption of the parameters (i.e., mean and variance) in the LDA classifiers.

In summary, we have presented the first online BCI system in real car to detect error-related brain activity, as a first step in transferring error-related BCI technology from laboratory studies to the real-world driving tasks. Consistent brain signatures and classification performance

Chapter 7. EEG-based Decoding of Error-Related Brain Activity in a Real-World Driving Task

prove the feasibility of the approach in complex environments, as an extension of the previous study in a car simulator. Our future work will focus on investigating other machine learning methods to improve the performance of error detection, evaluating the possibility of using alternative stimuli, e.g., auditory or tactile, to evoke error-related brain activity without extra visual burden during driving, as well as testing the protocol in open roads as compared to driving in a closed track.

8 Estimating Brain Connectivity Patterns of Monitoring Error during Driving

8.1 Introduction

In Chapter 6, we reported brain connectivity patterns during error monitoring. These patterns are characterized by modulations in the theta and beta frequency bands, and localized in the medial frontal, parietal and frontolateral regions. That study explored the feasibility of exploiting connectivity information as classification features for single trial recognition. However, the study was performed in simple, well controlled experimental conditions, i.e., subjects were requested to not perform any movement while monitoring the moving direction of the cursor, which is ideal to minimize artifacts and to obtain clean brain signals, but it is not so realistic towards BCI applications.

In this chapter, we explore the preliminary results of implementing brain connectivity analysis during driving, both in a car simulator and a real car. The data corresponds to the experiments described in Chapter 7, where the subjects were driving a vehicle, monitoring directional cues that were shown when the vehicle was about to enter the intersection, and comparing the intentional turning direction with the shown arrow direction. The connectivity computation was performed on single trials, providing features for classification. The methods are similar to those described in chapter 7. To be able to compute these patterns for each trial, a relatively long time window was used and a small number of electrodes were considered, with the purpose of increasing the reliability of the MVAR model. Classification was performed using a sliding window to calculate DTF and use Fisher score to choose the most separable connectivity pairs (c.f., Section 6.2.4).

The other aim of this study is to assess the characteristics of the connectivity features. Since the connectivity features are computed along a sliding window in the time domain, and the results of each window are in the frequency domain and across brain regions, the discrimination power of these features is expected to be consistent with the oscillatory modulation patterns found in Chapter 6 (See Figure 7.2.2.A).

8.2 Methods

8.2.1 Data preparation

Before the computation of connectivity, the EEG data was preprocessed through a bandpass spectral filter, cutoff between 1 and 50 Hz, which is the same as what we did for the moving cursor moving cursor, i.e., a 4th order Butterworth filter. The EEG trials were extracted from one second before to one second after the appearance of the direction cue (the green arrow that guesses the turning direction).

8.2.2 Computation of brain connectivity

The computation of brain connectivity was based on DTF, the detail description of which can be found in the Section 3.4. The parameter setting is similar to the computation for the moving cursor dataset (section 6.2.4 in Chapter 6), i.e., a sliding window was used to perform the computation of the MVAR model, thus DTF is also obtained in those windows as temporal modulations. The length of the sliding window was set to 400 ms, with an overlap of 360 ms. Since the trials were extracted from -1 s to 1 s, we finally got the DTF from -800 ms to 800 ms. Four EEG channels were included for the computation of brain connectivity, F3, F4, FCz and CPz, and the order of the MVAR model was set to 5, to trade off the lack of data in such single trial computation (see 6.2.4). The order satisfies the inequality $K(p+1)/(N_s n_t) < 0.1$, where the trial number (n_s) equals 1.

After computing the DTF, a 4-dimensional matrix is obtained for each trial, which is $4 \times 4 \times 30 \times 40$. The first two dimensions indicates the interaction among four channels, where the direction is from the second dimension to the first dimension. The third dimension represents the frequency range (from 1 to 30 Hz), and the last dimension indicates the time line of the sliding window. For further analysis we excluded the information in the diagonal of the first two dimensions, considering only the interaction between different channels. In the phase of classification, these connectivity pairs were converted into a vector.

8.2.3 Classification settings

In this study two types of features are used to compare with the classification performance based on the temporal waveform in Chapter 7. As it was the case in Chapter 6, the first type of features corresponds to the information from DTF values, and the second type is based on the combination of both DTF and temporal waveforms. Performance was estimated based on the 10-fold cross validation classification accuracy and the area under the curve. Connectivity features were selected by Fisher score. For the combined feature set, features in temporal waveform and connectivity matrices are selected and combined together as input of the classifier. These settings are the same for both car simulator and real car dataset.

8.3 Results

8.3.1 Feature analysis

The discrimination power of the connectivity features are analyzed in terms of their distributions in temporal and frequency domains, similar to Figure 6.5. As shown in Figure 8.1.A, the temporal distribution of the car simulator data is not as smooth as in the dataset of the moving cursor (Figure 6.5.B). However, we also observe highest discrimination power between 200 ms and 500 s after the directional cue. Similarly, the distribution of the discrimination power shows higher modulations in theta band (peaking at 7 Hz) and beta band (peaking at 20 Hz), shown in Figure 8.1.B.

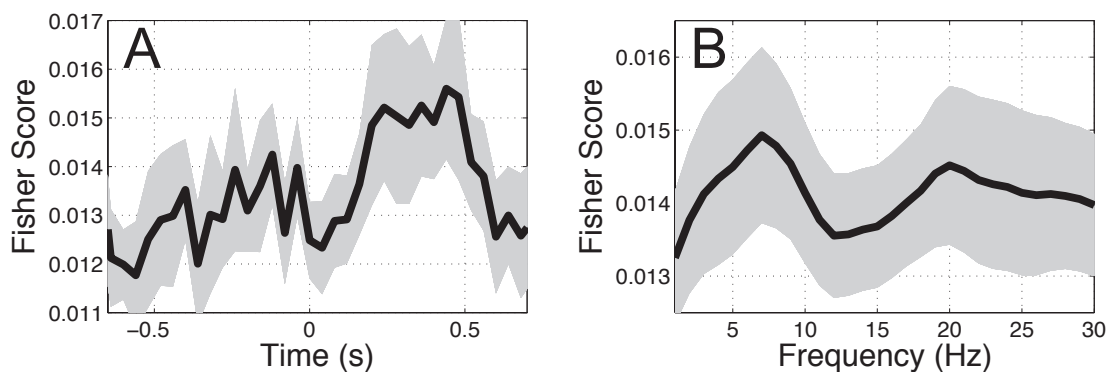


Figure 8.1: The distribution of the discrimination power of connectivity features for simulated driving. A. The distribution of the Fisher score in temporal domain. B. The distribution in the frequency domain, 1-30 Hz. The gray areas indicate the standard error across all subjects and the dark curves represent the grand average.

Similar results are found in the real car driving, i.e., high peak in the temporal domain after directional cue and two dominant peaks in the frequency domain in theta and beta bands (Figure 8.2). These results are consistent with the neural signature we found in Chapter 6, confirming the existence of similar timing and spectral attributes when we perform experiments in more complex and realistic situations, such as in simulated and real car driving.

We also obtained the discrimination power for connectivity patterns within the four electrodes considered, shown in Figure 8.3. The most discriminative pattern for the simulated driving was from F3 to FCz, and from F4 to FCz in the real car case. The obtained patterns were not as clear as those found in the simpler experiments (c.f. Figure 6.5), as discriminant power was more uniformly distributed. These differences may be due to the increased complexity of the task, and the smaller number of subjects that are considered in the real car study. Further analysis is required to better characterize these patterns.

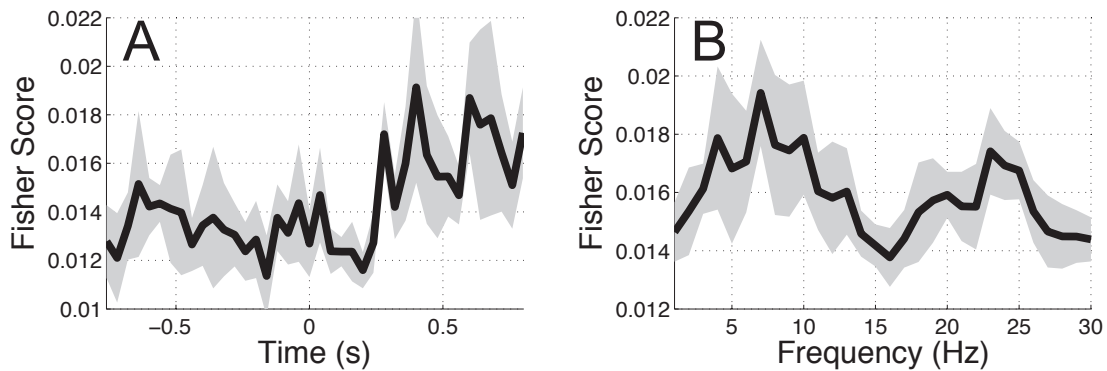


Figure 8.2: The distribution of the discrimination power of connectivity features for the real car experiments. A. The distribution of the Fisher score in the temporal domain. B. The distribution in the frequency domain, 1-30 Hz. The gray areas indicate the standard error across all subjects and the dark curves represent the grand average.

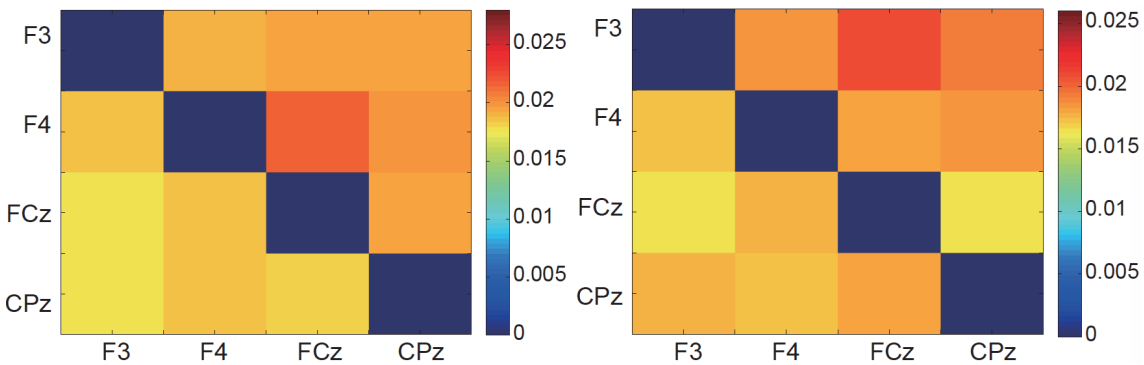


Figure 8.3: The discrimination power of connectivity patterns between 4-10 Hz, from 200 ms to 800 ms. A. Real car. B. Simulated driving. The information flow is from the vertical index to the horizontal index.

8.3.2 Classification performance

The classification performance can be found in Figure 8.4. The AUC for the dataset of car simulator was 0.746 ± 0.057 when only connectivity features were included, and raised to 0.813 ± 0.069 when we used the combination of both connectivity and waveform features. The results of using the combination was significantly better ($p < 5 \times 10^{-5}$, paired t-test) than using the waveform features alone, whereas no significance was found between the connectivity and waveform features, $p = 0.1915$.

For the dataset of real car experiments, all classification results showed ROC curves above chance level (dash line, AUC = 0.5). The AUC was 0.740 ± 0.058 and 0.711 ± 0.050 (mean \pm SD), respectively for connectivity and combined features, which were not statistically significant comparing with waveform features. However, six out of eight subjects had the highest AUC using connectivity features. Four of them had higher performance (comparing with waveform

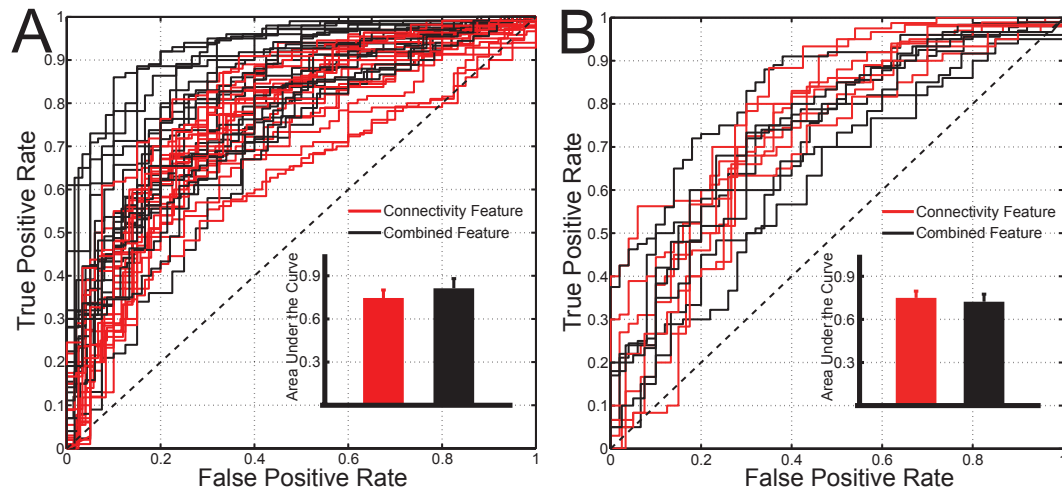


Figure 8.4: Classification performance of the datasets in the car simulator ($N = 22$) and the real car ($N = 8$). A. ROC curves for each subject using connectivity features (red trace) and combined features (black trace). The bar plots indicate the averaged and standard deviation of the AUC. B. The results of the dataset for real car.

features) using combined features.

8.4 Conclusion

The study in this chapter is a continuation of the study that we performed in Chapter 7, evaluating the feasibility of discriminating the error and correct trials during driving tasks. This study follows the analysis procedures for brain connectivity that were developed in Chapter 6, in which only the dataset of monitoring the moving cursor was considered. Here we further probe the method in a more realistic protocols.

The distribution of discriminative features we obtained in the driving protocols are not as clear as the results in the experiments of the moving cursor, where subjects remained still and avoided body movements. Nevertheless, the main patterns of the discriminative features in the temporal (positive peak after 200 ms) and frequency domains (high peaks in the theta and beta bands) remain the same, further proving the role of these frequency bands in the neural mechanism of brain error processing.

Even though we could not find similar brain connectivity patterns as in the protocol of the moving cursor, which were shown in Figures 8.3 and 6.5. In particular, the information flows from frontocentral to frontolateral regions in the theta band are not higher than others. Yet, one should notice that in the driving protocols, hand movements are necessary to steer (in order to adjust the position of the vehicle) and press the pedals (in order to sustain the driving speed), which may affect the cognitive processes in the human brain. In such a realistic task, it is not surprising that the connectivity patterns were not entirely consistent with the

Chapter 8. Estimating Brain Connectivity Patterns of Monitoring Error during Driving

results of the task in the laboratory environment, where only pure monitoring is requested without any motor action. In further studies we will assess the brain connectivity as a multi-trial basis, which could include larger brain regions and might diminish the environmental artifacts through the averaging of covariance matrices in the MVAR model. We could also use artifact-removal methods to clean the data before the connectivity analysis to find more stable patterns.

Another future research avenue opened by this study, is to explore online classification. The computation of the brain connectivity should be similar to what we have implemented in Chapter 4, using a sliding window to obtain DTF values with a certain overlap. Since we use only four EEG channels in this study, the computation will be faster than that in what we have found in Chapter 4 using 16 EEG channels.

9 Analysis of Neural Activity Related to Lane Changing Reaction Time

9.1 Introduction

Reaction time measures how fast people can respond to the presentation of a sensory stimulus (Donders, 1969). It depends on both stimulus characteristics and people's mental states. The task urgency is one of the important characteristics that affect the reaction time, which is correlated with the contextual environment and indicates the harmful situation. The translation between the task urgency and the motor reaction is modulated by afferent and cortical systems (Galton, 1890; Carlsen et al., 2004). Recent studies have shown evidences of the correlation between brain activities and reaction time (Galton, 1890), particularly frontal and parietal brain areas are associated with immediate response to urgent events (Kastner and Ungerleider, 2000; Gerson et al., 2005). More particularly, the parietal region is believed to be activated earlier than frontal during stimulus-driven behavior (Buschman and Miller, 2007).

However, these studies have mainly been performed using psychophysical protocols in well controlled situations, leaving open the question whether the same correlates of the underlying cognitive processes also appear in more complex tasks. At the same time, the analysis of the brain activity generated during driving has gained increased attention in recent years. This activity reflects cognitive processes taking place during the execution of this task and can potentially be exploited to improve driving assistance systems for intelligent cars (Lin et al., 2009; Khaliliardali et al., 2012; Gheorghe et al., 2013b). Recent studies during driving tasks have focused on detecting anticipated and emergency braking (Khaliliardali et al., 2012; Haufe et al., 2011), steering actions (Gheorghe et al., 2013b) as well as workload and levels of attention (Borghini et al., 2012). Particularly, the exploration of reaction time associated brain activity could possibly enable the prediction of behavior before the movement onset, and will be potentially implemented in intelligent car to improve the driving safety.

The present study attempts to investigate the neural correlates of reaction time in a driving task. 15 subjects participated the experiments in a simulated driving environment using a realistic car simulator, during which the subject needs to change lane to avoid collision from suddenly appearing obstacles. Scalp EEG is recorded during the experiment to obtain brain activities. We

analyzed event-related potentials (ERP) and spectral modulations elicited by the appearance of obstacles that trigger lane changes and their relation to the steering reaction. In particular, we focus on identifying reliable brain activity markers of the response variability. These obtained cortical patterns provide a fundamental understanding of the neural basis of stimulus driven behavior to salient events. Their correlation with the response speed may eventually uncover evidence linking the reaction time and brain activity, further supporting the possibility of predicting reaction before the behavior onset, and will be potentially implemented to improve the safety during driving.

9.2 Experimental setting and specification of data analysis

9.2.1 Experimental protocols

Fifteen subjects (three females, mean age 26.83 ± 3.04) participated in the experiments. They were all MSc or PhD students and had normal or corrected-to-normal vision. All subjects have valid driving license. None of them reported any known neurological or psychiatric disease. The experimental protocols were approved by the Research ethical committee of the EPFL Brain and Mind institute and all participants gave their informed consent.

In the experiment, subjects seated in a car simulator and were asked to drive at the highest speed (at about 95 KMH) along a 2-lane road. At any given moment an obstacle blocking one of the lanes could appear in front of the car, see Figure 9.1. If the obstacle was in the same lane, the subject was required to steer the car to the other lane to avoid the collision; otherwise, the subject should remain in the same lane. The probability of the obstacle to be in the same lane as the car was 25%. The distance between the vehicle and the obstacle at the moment of its appearance was variable in order to study different types of reaction, ranging from rapid, emergency responses when the obstacle appears at close distance to self-paced, slower responses if it is far ahead. Given the protocol, drivers were expected to maintain high levels of vigilance during the experiment.

To allow subjects to successfully avoid collisions throughout the experiment, the distance between the car and the obstacle at its appearance was chosen randomly from an uniform distribution between 40 m and 70 m. The inter-trial interval (i.e. time between the appearance of two consecutive obstacles) was at least 5 sec (corresponding to a distance of 150 m.).

We recorded six sessions, where each of them comprised the appearance of 87 obstacles (i.e. trials). The duration of one session was about 9 minutes and 30 seconds, resulting in a total recording time of about one hour. Overall, we obtained 522 trials yielding 137.6 ± 15.2 trials where the subject was required to change lanes. Those trials where the subject steered before the appearance of the obstacle were removed and not included in later analysis. We uniformly selected 100 trials for each subject and ordered them by the reaction time for the further analysis.

9.2. Experimental setting and specification of data analysis

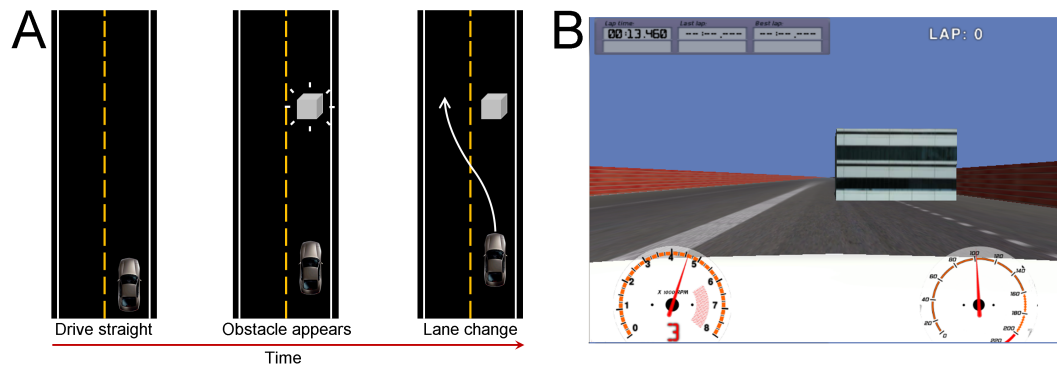


Figure 9.1: Experimental protocol. A. Timing of the protocol. Subject drives straight in a two lane motor way. An obstacle will appear either in the same lane (rare condition, 20%) or the other lane (frequent condition, 80%). The subject need to change lane immediately if the obstacle is in the same lane to avoid collision. B. The screenshot of the 3D environment.

9.2.2 Experimental setup

The experimental set-up consists of a realistic car simulator as shown in Figure 7.2.2.A. Car related data (e.g. steering, braking, accelerating and location) from the driving simulator was logged at 256 Hz. The simulated driving environment was built using the software, *Blender* (<http://www.blender.org>) and presented using a customized open source racing program (*Vdrift*) on three 27" 3D monitors. Subjects seated at about 120 cm from the screens and were not required to wear 3D glasses.

9.2.3 Specifications for signal processing and data analysis

9.2.3.1 Data recording and processing

The driver's reaction time was estimated as the time it takes for the steering values to exceed a threshold within 1 s after the obstacle appearance. The threshold was determined by empirical experience. In this analysis we used the absolute value of steering data to define lane changes, thus the direction of the change (i.e. left-to-right or right-to-left was not taken into account). The steering data values range from 0.0 to 0.3 (a.u.) in our experiments, corresponding to the range from straight driving to sharp steering turns.

Scalp EEG was recorded from 64 electrodes (Biosemi Active Two, The Netherlands) with an extended 10-20 system montage at a sampling rate of 2048 Hz. The most peripheral electrodes were discarded from the analysis to reduce the influence of artifact contamination, yielding a total of 41 channels. EEG and car-related recordings were synchronized for off-line analysis using a 4 Hz square signal sent from the driving simulator to the EEG recording device via parallel port.

For analysing ERPs, we filtered the EEG data in the frequency band [1 10] Hz with a 4th

order non-causal Butterworth filter, whereas the spectral analysis was performed in the range [1 50] Hz. Common spatial filter was used as re-reference of the EEG signals to remove common brain activities across all electrodes. Power spectral density (PSD) of the single trials was computed by 1024-point discrete Fourier transform with a sliding Hamming window of 250 ms, and 218.75 ms overlapping was used in order to balance the smoothness and resolution in the time domain. For analysing ERPs and PSDs, EEG was segmented into epochs spanning from -1 s to 1.5 s with respect to the obstacle appearance ($t=0$). The PSD for each trial was reference by the baseline activity in the time window [-375 0] ms. Trials in which the driver was not driving straight during the period before the obstacle onset were excluded from the analysis.

9.2.3.2 Source analysis

In this study, we employed beamforming to find activities of brain sources. The beamforming constructs spatial filters that extract sources originating in pre-defined regions of interest (ROIs), maximizing the ratio of variances of sources inside and outside the ROI, with the assumption that only variance changes can provide information on the subject's intention 3.5. A template of a lead field matrix includes with 3013 sources was adopted to construct the source activity for all subjects. Each source was 1 cm (for all three dimensions, i.e. x, y and z axis) away from the neighbors. The beamformer (spatial filter) was estimated for each subject individually. To avoid spurious effects when two conditions are compared, we averaged the spatial covariance matrices of 250 trials from two conditions (Hipp et al., 2011), by randomly selecting 125 trials from each. We analyzed the brain connectivity at the single trial level. Since the data amount was limited, only frontal and parietal regions were selected for analysis on the ground that frontoparietal network is modulated in stimulus-driven reactions (Corbetta and Shulman, 2002; Brass et al., 2005).

9.2.3.3 Analysis of brain connectivity

The brain connectivity was estimated for each single trial using the directed transfer function (DTF) (Kamiński and Blinowska, 1991), which is based on multivariate autoregressive (MVAR) model. The coefficient matrices of the MVAR model were transferred to the frequency domain by the fast Fourier transform to explore the causal influences in the frequency domain. The DTF was computed with a sliding window of 300 ms (95% overlapping) for the 2 ROIs (frontal and parietal) obtained by beamforming source localization.

9.3 Main results

9.3.1 Behavior analysis

Figure 9.2.A shows the driver steering profiles after obstacle appearance for all subjects. Trials were binned according to the initial distance between the car and the obstacle, each trace in the figure shows the average steering curve for each bin, color coded from shorter to larger distances (from light to dark tones, respectively). Unsurprisingly, trials in which the obstacle appeared at shorter distances (dark traces) exhibited a faster reaction time and larger steering amplitude than those with farther obstacles.

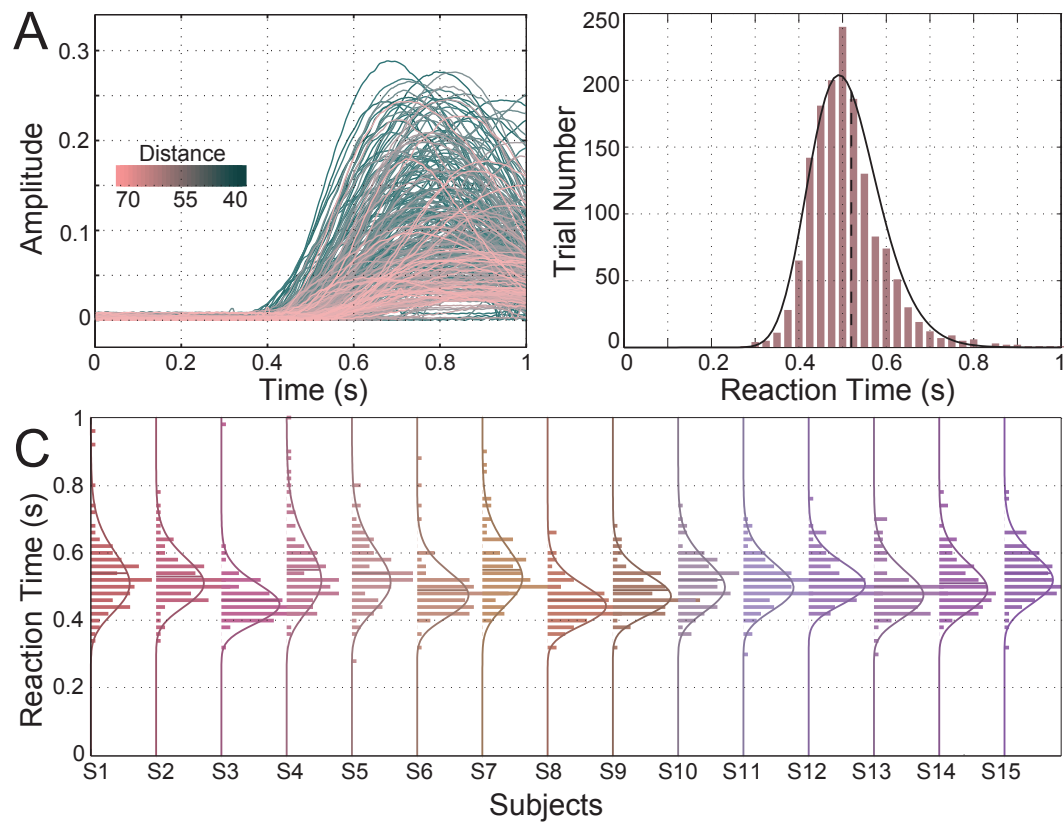


Figure 9.2: Analysis of lane changing behaviors in the rare condition (an obstacle appeared in front of the car, thus requiring a lane change). A. Steering curves are averaged across all subjects for each distance level between the car and the obstacles. Distances are represented by the gray scales of the curves. B. Histogram of the reaction time for all rare trials. Trial number was calculated from all subjects. C. Histogram of the reaction time for each subject for all rare trials. The curves are the fitted lognormal distribution.

Figure 9.2.B and C illustrate the distribution of reaction among all subjects and individually, respectively. Data are fitted with lognormal distribution, and the mean values are indicated by the dash lines. Based on this results we set the steering threshold to estimate the reaction time

to the value of 0.01. The distribution of the reaction time is shown in Figure 9.2.B. The median value for all the trials is 0.496 s, and the mean value (\pm standard deviation) is $0.519 \text{ s} \pm 0.109 \text{ s}$. For the EEG analysis we discarded the extremes of the distributions, corresponding to trials with reaction times smaller than 400 ms or larger than 650 ms, amounting to 6.88% of all the recorded trials. More than 100 trials remained for further analysis for each subject.

9.3.2 Event-related potential

Event-related potentials (ERPs) of channels FCz and CPz are shown in Figures 9.3.A and C, respectively. The reaction time of the trials is indicated by the darkness of the curves, the darker the faster. Each curve indicates the averaged ERP across all subjects binned based on the reaction time, i.e., from 0.4 s to 0.65 s after the appearance of obstacles.

FCz electrode shows a positive peak at about 270 ms followed by a negative peak at about 515 ms. Slower trials (light traces) appear to have later peaks than the faster ones). A more marked pattern appears in channel CPz, where a large negative deflection appears at about 300 ms. As before, the peak latency of this component seems modulated by the driver's reaction time. Significant correlation between the peak latency of the early peak –appearing before action onset– and the driver's reaction time was found for both channels, shown in Figures 9.3.C and D. The latency of the positive peak in FCz had a correlation coefficient of 0.427 ($p < 10^{-4}$), while the negative peak in CPz yielded a correlation of 0.683 ($p < 10^{-13}$). The p value was obtained using Student's t-distribution with the assumption of bivariate normal distribution. The grand average of trials with no lane change (frequent case: obstacle on the other side of the road) is shown as green curves, where a negative peak can be observed after 200 ms, and followed by a positive peak.

Consistently with the ERPs, scalp-wide grand average activity at 300 ms exhibits a strong negative modulation in parietal areas, with a broader positivity over frontal areas, as shown in Figure 9.3.E. The topography of no lane change condition is shown in Figure 9.3.G, which also has negative modulation in the parietal regions, but with much smaller amplitude. Similarly, figure 9.3.F shows the correlation between the peak latency of the early ERP component (prior to 400 ms) for each electrode. The results show positive correlations in both parietal and frontal regions, with highest correlation value in the former area. These spatial specific correlation patterns suggest that these sites are modulated in the stimulus-driven reaction and are informative about the behavioral reaction time.

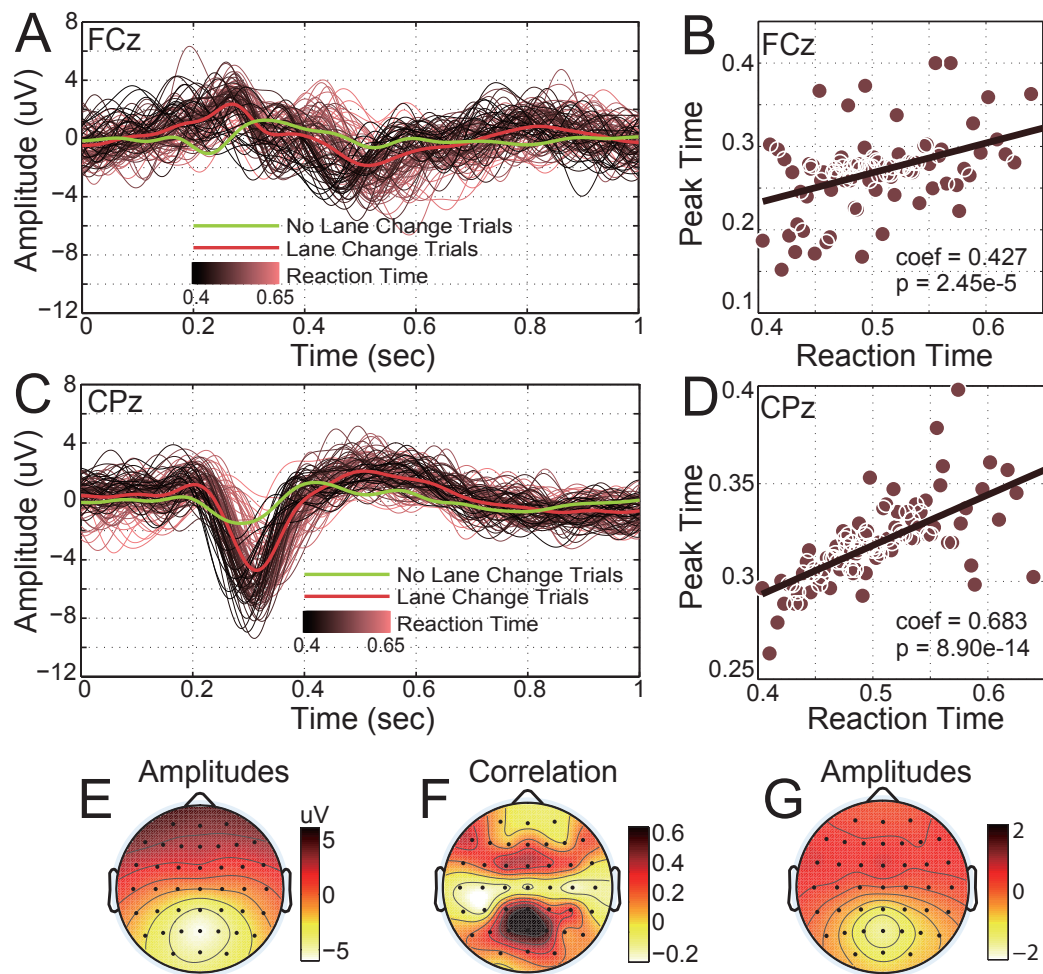


Figure 9.3: Event-related potentials and their correlation with reaction time. A and C: Event-related potentials in FCz and CPz. Reaction time of a trial is color coded (the darker the faster), and the grand average is shown by the thick red curve. B and D: Correlation between reaction time and the peak time. To compute the correlation, we chose an ERP peak before the steering reaction: First positive peak for FCz and first negative peak for CPz. E: Topography of ERP amplitude for all trials at 300 ms for lane change trials. F: Topography of correlation coefficients. G: Topography of ERP amplitude for all trials at 300 ms for no lane change trials.

9.3.3 Power spectral density

The grand average of the PSD in FCz and CPz are shown in Figure 9.4.A and B, for no lane change and lane change conditions, respectively. For both cases, we found no evident modulation before 200 ms following the obstacle appearance. In contrast, both electrodes show increased theta power (4-8 Hz) after this period, where the lane change case has much higher power. In particular, theta power increases sharply at around 200 ms, peaking at 300 ms, before the steering onset in lane change trials

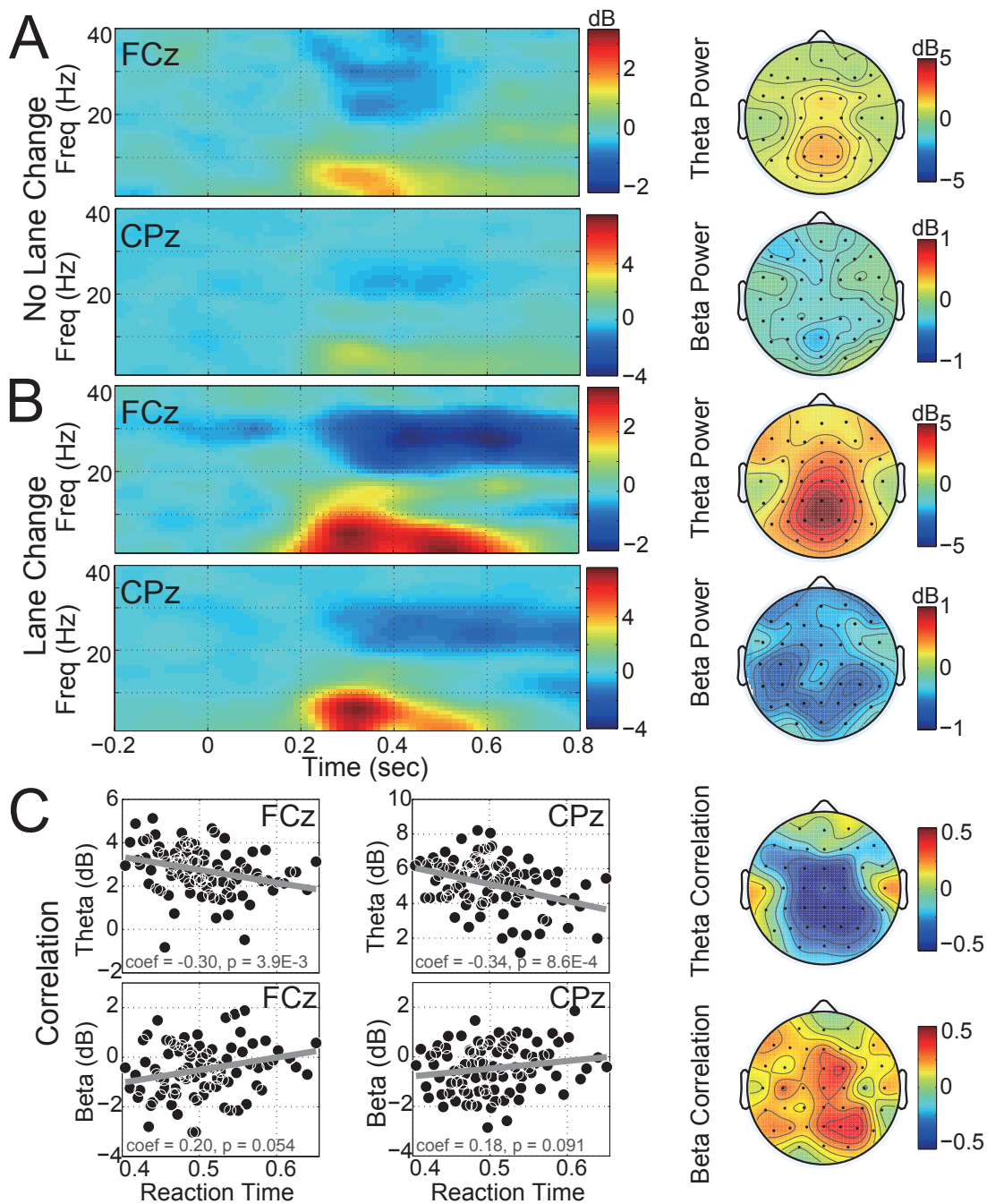


Figure 9.4: Analysis of power spectrum density. A and B. PSD of the electrode FCz and CPz in no lane change and lane change cases, respectively, and the topographies of theta and beta power (200 ms to 400 ms). C: Linear fitting between the reaction time and the band power, theta (4-8 Hz) and beta bands (20-35 Hz), for electrodes FCz and CPz, and the topographies of correlation coefficients for theta power and beta power.

A decrease in the beta power (20-35 Hz) is also clear in these two conditions in both electrodes,

appearing at about 300 ms, which continues during lane change behavior in the lane change trials. The pattern disappears around 500 ms in the condition of no lane changes, and the modulation amplitude is also much smaller comparing with the lane change case. In addition, a late increase at about 500 ms can be observed in the low frequency (1-4 Hz) activity in FCz. This pattern is not obvious in CPz, nor in the trials of no lane change.

Right side of Figure 9.4 also illustrates the topographical analysis of spectral modulations for the theta and beta bands. Each plot shows the average band power in the window from 200 ms to 400 ms. The two conditions present similar modulation patterns, but the amplitude is much higher in the case of lane change. The theta power increase is stronger at parietal areas for both cases, peaking at CPz and Pz, also appearing in frontocentral and frontolateral regions. The pattern for the beta band shows broader modulations, particularly in parietal regions. The medial central (electrode Cz) and lateral frontal regions do not show evident beta modulation.

The correlation between the band power (theta and beta) and the reaction time of the steering are analyzed as well, which is similar to that reported in the section of ERP analysis. The average band power in the time window between 200 ms to 400 ms was computed and used to obtain the correlation coefficient between the reaction time. The reaction time and the power modulation in the theta band is significantly correlated, with correlation coefficient -0.3 in FCz ($p < 0.005$) and -0.34 in CPz ($p < 0.001$). The correlation coefficients in theta are negative, which indicate that the trials with faster reaction are accompanied by a stronger increase in theta. The beta power is positively correlated with the reaction time (the correlation coefficient is 0.2 and 0.18 for FCz and CPz respectively), i.e., the faster reaction the more decrease in beta, however, these correlations are not statistically significant ($p > 0.05$).

In the topography of correlation coefficients, we observe that both frontocentral (except Cz) and parietal regions are highly correlated with reaction time. The coefficients in frontolateral regions are close to 0.2, but much lower than frontocentral and parietal regions. In the beta band, the most correlated regions are also frontal and parietal.

9.3.4 Frontoparietal network

The frontoparietal network is computed by DTF on the ROIs obtained by beamforming source localization. The directional correlations are shown in Figure 9.5.A. The connectivity patterns seem similar between the two directions, from frontal to parietal and from parietal to frontal in the case of performing lane change.

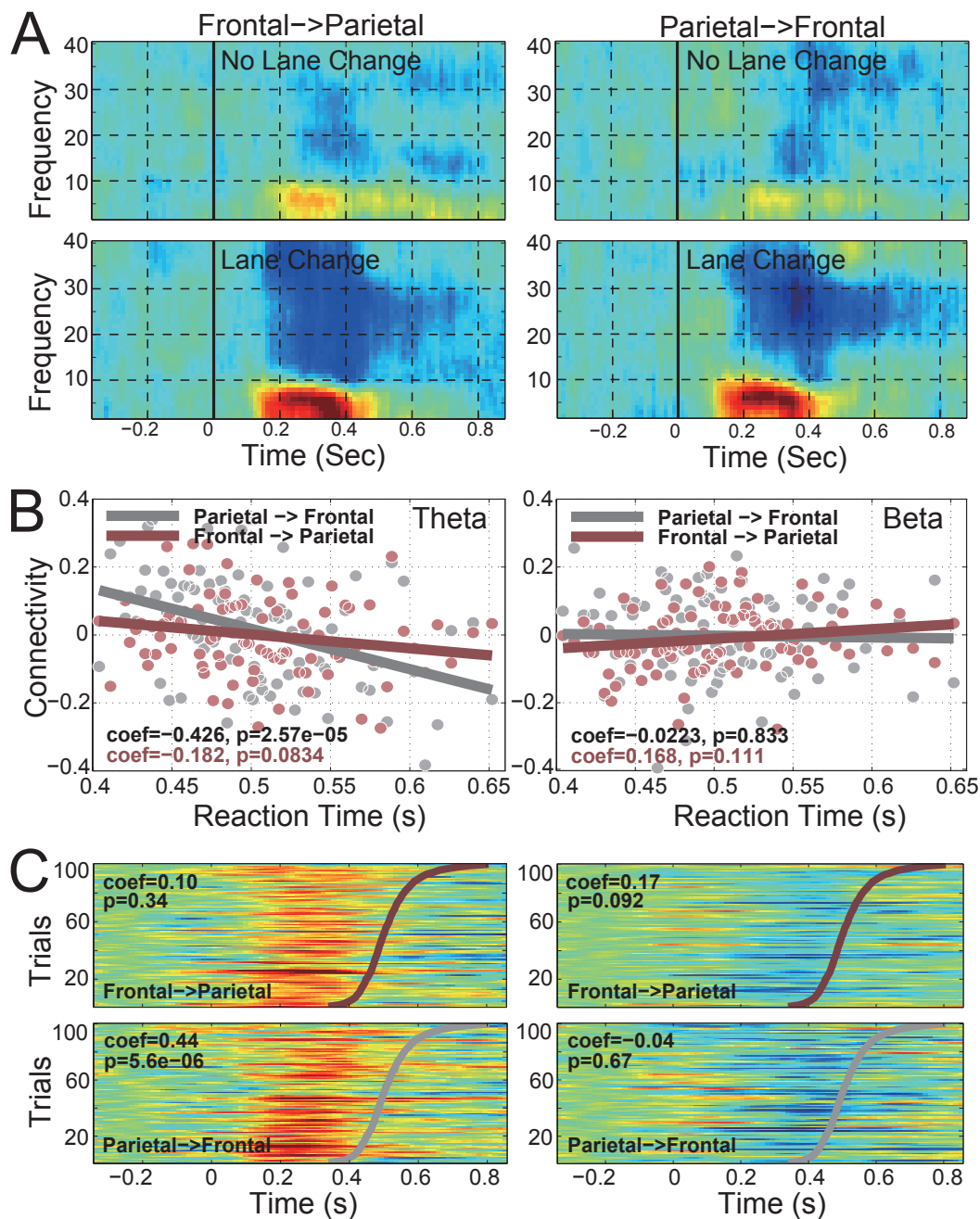


Figure 9.5: Analysis of frontoparietal network. A: Directional connectivity patterns between frontal and parietal regions in time-frequency domain. B: Linear fitting between reaction time and the averaged connectivity in theta and beta bands. C: Correlation analysis between the reaction time and the peak timing of directional connectivity pattern in theta and beta bands.

In the case of lane change trials, no specific modulation can be observed before 150 ms. Information flows in both directions increased in the frequency range below 9 Hz, starting at about 150 ms and ending at 450 ms. This increase pattern is more intensive in 4-8 Hz than

below 4 Hz. A positive peak can be observed around 5-6 Hz between 300 ms and 350 ms. From 350 ms to 400 ms, we can observe a power increase in low frequency range, 1-4 Hz. In higher frequency ranges (above 10 Hz), decreased interaction power could be found. After 450 ms, only the frequency range 10-30 s remain modulated, particularly 20-30 Hz in the pattern from parietal to frontal. The condition of no lane change has similar but much smaller modulation, and the information flow from frontal to parietal has higher amplitude than the opposite direction.

Similarly, the band power of the connectivity results are fitted with the reaction time using linear regression model. The theta power (4-8 Hz) in the time window 200 ms to 400 ms is negatively correlated (faster reaction accompanies with higher increased theta influence) with the reaction time, Figure 9.5.B. The correlation coefficient is -0.426 for the direction from parietal to frontal, which is statistically significant ($p < 0.05$) and much higher than from frontal to parietal, -0.182 that is not significant ($p > 0.05$). For the modulation in beta band (20-30 Hz), no significant correlation ($p > 0.05$) can be found either from parietal to frontal, where the coefficient is -0.0223, or from frontal to parietal, with coefficient = 0.168 and $p > 0.05$.

Furthermore, the timing of the peak was also fitted to the reaction time based on linear models, as shown in Figure 9.5.C. Trials were ordered according to the reaction time with a resolution of 100 levels, from fastest to slowest (bottom to top), and the thick curves indicate the reaction time for the trials. For each trial, the connectivity in theta (left columns) and beta (right columns) bands were considered. The peak timings of the theta connectivity were mainly from 100 ms to 400 ms, whereas the peak timings of the beta connectivity were mainly from 200 ms to 600 ms, which is closer to the curves. The results show that only the peak timing of the information flow from parietal to frontal in theta band (left bottom) is significantly correlated with the reaction time, with correlation coefficient 0.44 and $p < 0.05$.

9.4 Discussion and conclusion

This study provides evidence of reliable neural markers of the driver's response variability. Significant correlation was found between the driver's response and the brain activity prior to the steering action, both at the level of the ERP peak latency and power modulations in the theta band. In agreement with previous studies performed in simpler experimental protocols (Gerson et al., 2005), these correlations can be observed in parietal and frontal areas.

In our experiments, the intensity of the visual stimuli is varied from trial to trial, due to the distance between the vehicle and the suddenly appearing obstacle. The shorter distance leads to higher demand of lane change, not only from the visual perception of closer object (larger) but also the higher temporal urgency of the task, which requires faster reactions to prevent potential harm to the subject and the vehicle (Pins and Bonnet, 1996; Bell et al., 2006; Gage et al., 2007; Lakhani et al., 2011; Lakhani et al., 2012). Current debates exist about the mechanism of the reduction of response latency in urgent situations, either caused by different

Chapter 9. Analysis of Neural Activity Related to Lane Changing Reaction Time

CNS pathways or a common pathway but more rapid response latency (Gage et al., 2007; Lakhani et al., 2011). The brain patterns obtained in the present study are similar across trials no matter the diversity of reaction times, in terms of ERP peaks and oscillatory power modulations. This is not so surprising given that all trials required an emergency action to be taken. In fact, these patterns are extremely weak when no emergency response is necessary. On the other side, the intensity of these patterns varied and are correlated with the response speed. Thus, our results seem to support the hypothesis of a common CNS pathway. To further probe this hypothesis, the driving experiment could be extended with an additional condition of stimulus-driven lane change that would not cause any harm if not executed.

The frontal and parietal regions are activated during attentional tasks in both human subjects and monkeys (Buzsáki, 2005; Gregoriou et al., 2009), and particularly the frontal-parietal coherence reflects the transformation from the sensory representation in parietal cortex into the adjusting behavioral responses in frontal regions (Herzog et al., 2014). The findings in this study show a correlation of responding speed in both frontal and parietal regions, i.e., intensive modulation is associated with faster behavior. Recent evidences show earlier and more dominant neural association in parietal in such exogenous processing comparing with frontal area (Buschman and Miller, 2007; Arcizet et al., 2011), which is consistent with our results of cross-regional connectivity analysis, where the information flow in theta band from parietal to frontal lobe is significantly increased when the subjects react faster. Future study may focus on full brain connectivity pattern to search for interaction patterns with a higher spatial resolution.

Concluding, the current findings complement recent studies that have identified correlates of other cognitive processes in realistic driving, including drowsiness (Lin et al., 2009; Lin et al., 2011; Khushaba et al., 2011; Chuang et al., 2014), emergency braking (Haufe et al., 2011; Haufe et al., 2014), error-awareness (Zhang et al., 2013), anticipation of self-motivated steering (Gheorghe et al., 2013b) and braking actions (Khaliliardali et al., 2012), as well as visual attention (Renold et al., 2014). We reckon that future driving assistive systems can exploit information derived from this signals –decoded through a brain-machine interface system–, in combination with information from in-car sensors to tailor the support they provide both to the perceived conditions of the environment as well as the internal state of the driver (Saeedi et al., 2013).

10 Conclusions and future directions

10.1 Summary

Brain connectivity analysis has been increasingly applied over the last decade for investigating different aspects of human cognitions. In this thesis, we followed this approach -using non-invasive recording techniques to advance our understanding of the dynamics related to cognitive processes, i.e., error processing, motor imagery and reaction speed. Additionally, we investigated the potential use of brain connectivity patterns in BCI applications: on one hand, to improve single-trial decoding performance, and on the other hand, to assess the stroke recovery during BCI therapy.

The study of brain error processing is one of the main components of this thesis, covering not only the assessment of its underlying neural correlates (Chapter 6), single trial estimation of these patterns (Chapter 6), but also potential applications during driving (Chapter 7 and 8). We studied the oscillatory connectivity patterns in a pure monitoring task, i.e., directional information flows among frontal, parietal and frontoparietal regions. This supports the existence of a common neural basis for monitoring self-generated and external errors. We also found significant improvements of decoding performance when the connectivity patterns are used in combination with traditional features. These findings provided evidences for the hypothesis that the monitoring processes in the human brain are independent from the type of error, internal or external, and validated the consistence of these patterns in single-trial analysis. The application during driving was initially evaluated in a simulated environment, then extended to a real car. The challenges come from the difficulties of multiple tasks, and the higher level of artifacts in EEG signals. In both settings, we decoded the error-related brain activity achieving decoding performances significantly higher than chance level, thus supporting the feasibility of online implementation. As before, the improvement of the recognition performance was further achieved by the inclusion of brain interaction patterns as classifier inputs.

We also investigated the neural correlates of reaction time in different driving situations. We found significant correlation between the reaction time and ERP latency and spectral modula-

tions, respectively, mainly involving the frontoparietal network. The directional information flow from parietal to frontal areas is significantly correlated with the reaction time, reflecting the cognitive transition from visual perception in parietal area to the movement adjustment in the frontal cortex. Our findings are consistent with the previous findings on the role of theta band in cognitive control process, and support the hypothesis that the stimulus driven bottom-up behavior relies on information transfer between frontal and parietal areas (Corbetta and Shulman, 2002; Brass et al., 2005).

This thesis also analyzed inter- and intra-hemispheric brain connectivity during motor imagery tasks (Chapter 4). Frequency specific information flows are discovered between two hemispheres. The findings are consistent with the theory that the desynchronization of the contralateral sensorimotor cortex is associated to limb movements. We also validated the feasibility of exploiting this information for BCI applications in offline and online experiments. Such inter/intra-hemisphere connectivity is particularly helpful for stroke and neglect patients, for whom the interaction between the two hemispheres is altered by the lesion. We therefore applied the method in stroke/neglect patients, and found significant changes in the information flows before and after rehabilitation therapy in long term recordings (Chapter 5).

Across these studies, we used MVAR based methods to estimate brain connectivity, whose feasibility and reliability are therefore proven for EEG signals. We used multi-trial analysis to investigate neural mechanisms, providing a more reliable and detailed estimation of brain connectivity, which can include broad brain regions and offer high resolution in temporal domain (Chapter 5 and 6). In our case, 41 EEG channels were included, covering the whole scalp apart from peripheral regions (Section 6.2.2), which allowed us to find associated brain areas according to the obtained information inflow/outflow patterns (Section 6.3.2). On the other hand, we also computed signal-trial connectivity for classification purposes. This requires to limit the analysis to fewer channels and has a relatively lower temporal resolution (Chapter 4, 6 and 8). Such decreased resolution is due to the limited amount of available data, according to estimation theory, i.e., 10 times of data amount should be assured for the estimation of parameters (Korzeniewska et al., 2008), which limits the number of channels, and the order of the MVAR model. In our studies, we increased the window size (data amount) in order to include more EEG channels and produce relatively more reliable estimations of the brain connectivity (Section 6.2.4).

In our studies we also estimated connectivity patterns at the source level, using beamforming source localization in Section 6.3.5 and 9.2.3.2. This method could estimate particular brain activity in pre-defined cortical sources. But it is quite depending on prior knowledge of associated brain areas. We adopted this methods as further validation after finding significant brain connectivity patterns using CSD (Section 6.3.5). We also managed to estimate single trial brain connectivity at the source level (Section 9.2.3.2) by defining two specific interesting brain sources, i.e., a fronto-parietal network. This method could possibly be applied in real time as a spatial filter, which may further contribute to improve classification performance by using only highly associated brain source, e.g., anterior cingulate cortex for classifying

error-related brain activity.

Concluding, as a main line of the thesis, brain connectivity analysis was applied to study several brain cognitive processes, finding cross-regional interaction patterns to uncover fundamental neural mechanisms. The significance of this thesis also comes from the combination of knowledge at both subject and single-trial levels. As another contribution, the implementation of estimating brain connectivity in real time enables its application in BCI systems, particularly, providing novel neural signatures as potential classification features.

10.2 Future work

Long term future studies may cover several aspects of potential application of brain connectivity analysis. For instance, given the feasibility of real time computation of connectivity patterns, a real-time visualization of connectivity feedback could be provided to BCI end-users, possibly promoting voluntary modulation of connectivity patterns in motor imagery task. As its significance in quantifying stroke recovery, the brain connectivity between healthy and lesioned cortices could possibly be exploited as a biomarker for recovery or pathologies. Another further work could aim to assess the consistence between different brain connectivity measurements, e.g., between linear and nonlinear methods (DTF and phase locked value). In addition, we can also exploit brain connectivity to monitor relatively long-term cognitive states, for instance the fatigue during driving using frontoparietal network. Future studies can also focus on developing a method to estimate brain connectivity at different time-scales, i.e., combining different brain signal acquisition modalities. For instance, the simultaneous recording of EEG and fMRI can provide high resolution brain activity for both time and space, allowing further investigation of the mechanisms of the human brain (Debener et al., 2006; Caballero-Gaudes et al., 2013).

In this thesis, limitations still exist in both data analysis and experimental designs. Therefore, we define three aspects of potential short-term future work:

First of all, it is necessary to improve the stability of the real time estimation of connectivity. In the study of motor imagery, we computed DTF using a sliding window of 1/16 s to update the brain connectivity patterns as the input of the classifier. Even though the size of the sliding window was 1000 ms, which is already relatively long comparing with the update rate, the stability of the MVAR estimation could not be fully confirmed, since a lot of EEG channels are included. As it is a common issue throughout this thesis, i.e., the lack of data or the extensive number of coefficients to be estimated in real time, we would propose three ways to improve the stability. The first way is to select a subset of EEG channels, which reduces the number of coefficients in the MVAR model, thus increasing the ratio between the input data and the model order. This solution is useful when the regions of interest can be defined, e.g., based on prior knowledge or multi-trial analysis, as shown in Chapter 6. The other approach is to repeat the computation of DTF in sub-windows for several times and obtain the averaged MVAR coefficients. We could set the size of sub-windows as 500 ms and overlap for 50%, as it is done

in the Welch's method in the estimation of power spectral density. However, this approach may require longer computation times, thus the numbers of sub-windows should be taken into account in the online decoding. The third way is to use an adaptive algorithm to update the MVAR coefficients without performing estimation in each time window (Möller et al., 2001; Wilke et al., 2008). This method is particularly suitable for the analysis of online time series and will potentially replace the sliding window based algorithms.

Second, concerning the studies related to driving tasks, some potential future works could be carried out to further validate the results we obtained. In the study of detecting error-related brain activity during driving, we have performed the experiments in both car simulator and real car situations, but on a closed-road. However, it is also necessary to execute the assessments when the vehicle is in the condition of realistic traffic. Moreover, we have proven the improvement of the decoding performance using novel features (brain connectivity patterns), but not yet tested in real time analysis. Therefore, this verification should also be done in the future. In another study of driving, we found the correlation between the reaction time of lane changes and brain correlates in emergency situation, which resulted with specific patterns in temporal/spectral domains, and the interactions between frontal and parietal regions. However, this conclusion is drawn from a dataset of stimulus-driven lane change in emergent situations. Thus a potential future work is comparing two conditions, i.e., emergency and self-paced, to re-confirm the brain patterns which are correlated with reaction time.

Last, in current studies we have found brain connectivity patterns in several frequency bands. For instance, both monitoring and motor imagery have specific patterns in theta and beta bands. Recent studies have provided evidences that the cross-frequency couplings may carry functional roles in communication and learning (Trujillo and Allen, 2007; Canolty and Knight, 2010). Particularly, the high frequency band reflects the local activity in cognitive processes, whereas the low frequency band acts across distributed brain areas. Thus the causality between different frequency bands might have profound implications for human cognitions. The future directions of this thesis also includes the investigation of interactions between different frequency bands and explored cognitive processes, i.e., monitoring error, motor imagery and reaction time.

Bibliography

Agam Y, Hämäläinen MS, Lee AKC, Dyckman KA, Friedman JS, Isom M, Makris N, Manoach DS (2011) Multimodal neuroimaging dissociates hemodynamic and electrophysiological correlates of error processing. *Proc Natl Acad Sci* 108:17556–17561.

Allison BZ, McFarland DJ, Schalk G, Zheng SD, Jackson MM, Wolpaw JR (2008) Towards an independent brain–computer interface using steady state visual evoked potentials. *Clinical neurophysiology* 119:399–408.

Arcizet F, Mirpour K, Bisley JW (2011) A pure salience response in posterior parietal cortex. *Cerebral Cortex* 21:2498–2506.

Arnhold J, Grassberger P, Lehnertz K, Elger C (1999) A robust method for detecting inter-dependences: application to intracranially recorded EEG. *Physica D: Nonlinear Phenomena* 134:419–430.

Arnold M, Milner X, Witte H, Bauer R, Braun C (1998) Adaptive AR modeling of nonstationary time series by means of Kalman filtering. *IEEE Trans Biomed Eng* 45:553–562.

Astolfi L, Cincotti F, Mattia D, Babiloni C, Carducci F, Basilisco A, Rossini P, Salinari S, Ding L, Ni Y et al. (2005) Assessing cortical functional connectivity by linear inverse estimation and directed transfer function: simulations and application to real data. *Clinical neurophysiology* 116:920–932.

Astolfi L, Cincotti F, Mattia D, de Vico Fallani F, Tocci A, Colosimo A, Salinari S, Marciani MG, Hesse W, Witte H et al. (2008) Tracking the time-varying cortical connectivity patterns by adaptive multivariate estimators. *Biomedical Engineering, IEEE Transactions on* 55:902–913.

Astolfi L, Cincotti F, Mattia D, Marciani MG, Baccala L, Fallani F, Salinari S, Ursino M, Zavaglia M, Babiloni F et al. (2006) Assessing cortical functional connectivity by partial directed coherence: simulations and application to real data. *Biomedical Engineering, IEEE Transactions on* 53:1802–1812.

Astolfi L, Cincotti F, Mattia D, Salinari S, Babiloni C, Basilisco A, Rossini PM, Ding L, Ni Y, He B et al. (2004) Estimation of the effective and functional human cortical connectivity with structural equation modeling and directed transfer function applied to high-resolution EEG. *Magnetic resonance imaging* 22:1457–1470.

Bibliography

- Babiloni F, Cincotti F, Babiloni C, Carducci F, Mattia D, Astolfi L, Basilisco A, Rossini P, Ding L, Ni Y et al. (2005) Estimation of the cortical functional connectivity with the multimodal integration of high-resolution EEG and fMRI data by directed transfer function. *Neuroimage* 24:118–131.
- Baccalá LA, Sameshima K (2001) Partial directed coherence: a new concept in neural structure determination. *Biological cybernetics* 84:463–474.
- Baccald L, de Medicina F (2007) Generalized partial directed coherence In *Digital Signal Processing, 2007 15th International Conference on*, pp. 163–166. IEEE.
- Bell A, Meredith M, Van Opstal A, Munoz D (2006) Stimulus intensity modifies saccadic reaction time and visual response latency in the superior colliculus. *Experimental Brain Research* 174:53–59.
- Bendat JS, Piersol AG (1980) Engineering applications of correlation and spectral analysis. *New York, Wiley-Interscience, 1980. 315 p.* 1.
- Benz HL, Zhang H, Bezerianos A, Acharya S, Crone NE, Zheng X, Thakor NV (2012) Connectivity analysis as a novel approach to motor decoding for prosthesis control. *IEEE Trans Neural Syst Rehabil Eng* 20:143–152.
- Biasiucci A (2014) Neurotechnology for brain repair: Imaging, enhancing and restoring human motor function. *PhD Thesis* .
- Biazoli Jr CE, Sturzbecher M, White TP, dos Santos Onias HH, Andrade KC, de Araujo DB, Sato JR (2013) Application of partial directed coherence to the analysis of resting-state EEG-fMRI data. *Brain connectivity* 3:563–568.
- Billinger M, Brunner C, Müller-Putz G (2013) Single-trial connectivity estimation for classification of motor imagery data. *J Neural Eng* 10:046006.
- Birbaumer N, Cohen LG (2007) Brain–computer interfaces: communication and restoration of movement in paralysis. *The Journal of physiology* 579:621–636.
- Birbaumer N, Ghanayim N, Hinterberger T, Iversen I, Kotchoubey B, Kübler A, Perelmouter J, Taub E, Flor H (1999) A spelling device for the paralysed. *Nature* 398:297–298.
- Blinowska K, Kus R, Kamiński M, Janiszewska J (2010) Transmission of brain activity during cognitive task. *Brain topography* 23:205–213.
- Blinowska KJ (2011) Review of the methods of determination of directed connectivity from multichannel data. *Med Biol Eng Comput* 49:521–529.
- Borghini G, Astolfi L, Vecchiato G, Mattia D, Babiloni F (2012) Measuring neurophysiological signals in aircraft pilots and car drivers for the assessment of mental workload, fatigue and drowsiness. *Neurosci Biobehav Rev* .

- Brass M, Ullsperger M, Knoesche TR, Von Cramon DY, Phillips NA (2005) Who comes first? the role of the prefrontal and parietal cortex in cognitive control. *Journal of cognitive neuroscience* 17:1367–1375.
- Brázdil M, Babiloni C, Roman R, Daniel P, Bares M, Rektor I, Eusebi F, Rossini PM, Vecchio F (2009) Directional functional coupling of cerebral rhythms between anterior cingulate and dorsolateral prefrontal areas during rare stimuli: a directed transfer function analysis of human depth EEG signal. *Hum Brain Mapp* 30:138–146.
- Brázdil M, Mikl M, Mareucek R, Krupa P, Rektor I (2007) Effective connectivity in target stimulus processing: A dynamic causal modeling study of visual oddball task. *Neuroimage* 35:827–835.
- Bressler SL (1995) Large-scale cortical networks and cognition. *Brain Research Reviews* 20:288–304.
- Brookhuis KA, de Waard D (2010) Monitoring drivers mental workload in driving simulators using physiological measures. *Accident Analysis & Prevention* 42:898–903.
- Brown G, Pocock A, Zhao MJ, Luján M (2012) Conditional likelihood maximisation: a unifying framework for information theoretic feature selection. *J Mach Learn Res* 13:27–66.
- Brown JW, Braver TS (2005) Learned predictions of error likelihood in the anterior cingulate cortex. *Science* 307:1118–1121.
- Brunner C, Scherer R, Graimann B, Supp G, Pfurtscheller G (2006) Online control of a brain-computer interface using phase synchronization. *Biomedical Engineering, IEEE Transactions on* 53:2501–2506.
- Buch E, Weber C, Cohen LG, Braun C, Dimyan MA, Ard T, Mellinger J, Caria A, Soekadar S, Fourkas A et al. (2008) Think to move: a neuromagnetic brain-computer interface (bci) system for chronic stroke. *Stroke* 39:910–917.
- Bullmore E, Sporns O (2009) Complex brain networks: graph theoretical analysis of structural and functional systems. *Nat Rev Neurosci* 10:186–198.
- Buschman TJ, Miller EK (2007) Top-down versus bottom-up control of attention in the prefrontal and posterior parietal cortices. *Science* 315:1860–1862.
- Buttfield A, Ferrez PW, Millán JdR (2006) Towards a robust bci: error potentials and online learning. *Neural Systems and Rehabilitation Engineering, IEEE Transactions on* 14:164–168.
- Buzsáki G (2005) Theta rhythm of navigation: Link between path integration and landmark navigation, episodic and semantic memory. *Hippocampus* 15:827–840.
- Buzsáki G, Draguhn A (2004) Neuronal oscillations in cortical networks. *science* 304:1926–1929.

Bibliography

- Caballero-Gaudes C, Van de Ville D, Grouiller F, Thornton R, Lemieux L, Seeck M, Lazeyras F, Vulliemoz S (2013) Mapping interictal epileptic discharges using mutual information between concurrent EEG and fMRI. *Neuroimage* 68:248–262.
- Canolty RT, Knight RT (2010) The functional role of cross-frequency coupling. *Trends in cognitive sciences* 14:506–515.
- Carlsen AN, Chua R, Inglis JT, Sanderson DJ, Franks IM (2004) Can prepared responses be stored subcortically? *Experimental brain research* 159:301–309.
- Carmena JM, Lebedev MA, Crist RE, O’Doherty JE, Santucci DM, Dimitrov DE, Patil PG, Henriquez CS, Nicolelis MA (2003) Learning to control a brain–machine interface for reaching and grasping by primates. *PLoS biology* 1:e42.
- Carter CS, Macdonald AM, Botvinick M, Ross LL, Stenger VA, Noll D, Cohen JD (2000) Parsing executive processes: strategic vs. evaluative functions of the anterior cingulate cortex. *PNAS* 97:1944–1948.
- Cavanagh JF, Cohen MX, Allen JJB (2009) Prelude to and resolution of an error: EEG phase synchrony reveals cognitive control dynamics during action monitoring. *J Neurosci* 29:98–105.
- Cavanagh JF, Frank MJ (2014) Frontal theta as a mechanism for cognitive control. *Trends Cogn Sci* 18:414–421.
- Cavanagh JF, Zambrano-Vazquez L, Allen JJB (2012) Theta lingua franca: a common mid-frontal substrate for action monitoring processes. *Psychophysiology* 49:220–238.
- Chang HC, Deng H, Lee P, Wu CH, Shyu KK (2010) Real-time control of an ssvep-actuated remote-controlled car In *SICE Annual Conference*, pp. 1884–1887.
- Chavarriaga R, Millán JdR (2010) Learning from EEG error-related potentials in noninvasive brain-computer interfaces. *IEEE Trans Neural Syst Rehabil Eng* 18:381–388.
- Chavarriaga R, Sobolewski A, Millán JdR (2014) Errare machinale est: the use of error-related potentials in brain-machine interfaces. *Front Neurosci* 8:208.
- Chen C, Kiebel SJ, Friston KJ (2008) Dynamic causal modelling of induced responses. *Neuroimage* 41:1293–1312.
- Chuang CH, Ko LW, Jung TP, Lin CT (2014) Kinesthesia in a sustained-attention driving task. *Neuroimage* 91:187–202.
- Chuang CH, Lai PC, Ko LW, Kuo BC, Lin CT (2010) Driver’s cognitive state classification toward brain computer interface via using a generalized and supervised technology In *The 2010 International Joint Conference on Neural Networks*, pp. 1–7.
- Cohen MX, Axmacher N, Lenartz D, Elger CE, Sturm V, Schlaepfer TE (2009A) Nuclei accumbens phase synchrony predicts decision-making reversals following negative feedback. *J Neurosci* 29:7591–7598.

- Cohen MX, Cavanagh JF (2011) Single-trial regression elucidates the role of prefrontal theta oscillations in response conflict. *Front Psychol* 2:30.
- Cohen MX, Ranganath C (2007) Reinforcement learning signals predict future decisions. *J Neurosci* 27:371–378.
- Cohen MX, Ridderinkhof KR, Haupt S, Elger CE, Fell J (2008) Medial frontal cortex and response conflict: evidence from human intracranial EEG and medial frontal cortex lesion. *Brain Res* 1238:127–142.
- Connor J, Whitlock G, Norton R, Jackson R (2001) The role of driver sleepiness in car crashes: a systematic review of epidemiological studies. *Accid Anal Prev* 33:31–41.
- Corbetta M, Shulman GL (2002) Control of goal-directed and stimulus-driven attention in the brain. *Nature reviews neuroscience* 3:201–215.
- Daly I, Nasuto S, Warwick K (2012) Brain computer interface control via functional connectivity dynamics. *Pattern Recogn* 45:2123 – 2136.
- Daunizeau J, Kiebel SJ, Friston KJ (2009) Dynamic causal modelling of distributed electromagnetic responses. *NeuroImage* 47:590–601.
- David O, Friston KJ (2003) A neural mass model for MEG/EEG:: coupling and neuronal dynamics. *NeuroImage* 20:1743–1755.
- David O, Harrison L, Friston KJ (2005) Modelling event-related responses in the brain. *NeuroImage* 25:756–770.
- David O, Kiebel SJ, Harrison LM, Mattout J, Kilner JM, Friston KJ (2006) Dynamic causal modeling of evoked responses in EEG and MEG. *NeuroImage* 30:1255–1272.
- de Bruijn ERA, de Lange FP, von Cramon DY, Ullsperger M (2009) When errors are rewarding. *J Neurosci* 29:12183–12186.
- de Vico Fallani F, Astolfi L, Cincotti F, Mattia D, Marciani MG, Tocci A, Salinari S, Witte H, Hesse W, Gao S et al. (2008) Cortical network dynamics during foot movements. *Neuroinformatics* 6:23–34.
- De Waard D, Brookhuis KA (1991) Assessing driver status: a demonstration experiment on the road. *Accident analysis & prevention* 23:297–307.
- Debener S, Ullsperger M, Siegel M, Engel AK (2006) Single-trial EEG–fMRI reveals the dynamics of cognitive function. *Trends in cognitive sciences* 10:558–563.
- Debener S, Ullsperger M, Siegel M, Fiehler K, von Cramon DY, Engel AK (2005) Trial-by-trial coupling of concurrent electroencephalogram and functional magnetic resonance imaging identifies the dynamics of performance monitoring. *J Neurosci* 25:11730–11737.

Bibliography

- Decety J (1996) The neurophysiological basis of motor imagery. *Behavioural brain research* 77:45–52.
- Decety J, Perani D, Jeannerod M, Bettinardi V, Tadary B, Woods R, Mazziotta JC, Fazio F (1994) Mapping motor representations with positron emission tomography .
- Dijksterhuis C, de Waard D, Brookhuis KA, Mulder BLJM, de Jong R (2013) Classifying visuomotor workload in a driving simulator using subject specific spatial brain patterns. *Front Neurosci* 7:149.
- Do AH, Wang PT, King CE, Chun SN, Nenadic Z (2013) Brain-computer interface controlled robotic gait orthosis. *J Neuroeng Rehabil* 10:111.
- Dobkin BH (2009) Progressive staging of pilot studies to improve phase iii trials for motor interventions. *Neurorehabilitation and Neural Repair* 23:197–206.
- Donchin E, Spencer KM, Wijesinghe R (2000) The mental prosthesis: assessing the speed of a p300-based brain-computer interface. *Rehabilitation Engineering, IEEE Transactions on* 8:174–179.
- Donders FC (1969) On the speed of mental processes. *Acta psychologica* 30:412–431.
- Engel AK, Fries P, Singer W (2001) Dynamic predictions: oscillations and synchrony in top-down processing. *Nat Rev Neurosci* 2:704–716.
- Engel AK, Fries P (2010) Beta-band oscillations—signalling the status quo? *Curr Opin Neurobiol (Lond)* 20:156–165.
- Eoh HJ, Chung MK, Kim SH (2005) Electroencephalographic study of drowsiness in simulated driving with sleep deprivation. *International Journal of Industrial Ergonomics* 35:307–320.
- Fan XA, Bi LZ, Chen ZL (2010) Using EEG to detect drivers' emotion with bayesian networks In *Machine Learning and Cybernetics (ICMLC), 2010 International Conference on*, Vol. 3, pp. 1177–1181. IEEE.
- Farwell LA, Donchin E (1988) Talking off the top of your head: toward a mental prosthesis utilizing event-related brain potentials. *Electroencephalography and clinical Neurophysiology* 70:510–523.
- Ferrez PW, Millán JDR (2005) You are wrong! automatic detection of interaction errors from brain waves In *In Proceedings of the 19th International Joint Conference on Artificial Intelligence*.
- Ferrez PW, Millán JdR (2008) Error-related EEG potentials generated during simulated brain-computer interaction. *IEEE Transactions on Biomedical Engineering* 55:923–929.
- Fetz EE (1969) Operant conditioning of cortical unit activity. *Science* 163:955–958.

- Franaszczuk PJ, Bergey GK, Kamiński MJ (1994) Analysis of mesial temporal seizure onset and propagation using the directed transfer function method. *Electroencephalography and clinical neurophysiology* 91:413–427.
- Friston KJ (2009) Modalities, modes, and models in functional neuroimaging. *Science* 326:399–403.
- Friston KJ (2011) Functional and effective connectivity: a review. *Brain connectivity* 1:13–36.
- Friston KJ, Harrison L, Penny W (2003) Dynamic causal modelling. *Neuroimage* 19:1273–1302.
- Gage W, Zabjek K, Hill S, McIlroy W (2007) Parallels in control of voluntary and perturbation-evoked reach-to-grasp movements: Emg and kinematics. *Experimental Brain Research* 181:627–637.
- Gainotti G, D’Erme P, Bartolomeo P (1991) Early orientation of attention toward the half space ipsilateral to the lesion in patients with unilateral brain damage. *Journal of Neurology, Neurosurgery & Psychiatry* 54:1082–1089.
- Galán F, Nuttin M, Lew E, Ferrez PW, Vanacker G, Philips J, Millán JdR (2008) A brain-actuated wheelchair: asynchronous and non-invasive brain–computer interfaces for continuous control of robots. *Clinical Neurophysiology* 119:2159–2169.
- Galovski TE, Malta LS, Blanchard EB (2006) *Road rage: Assessment and treatment of the angry, aggressive driver*. American Psychological Association.
- Galton F (1890) Exhibition of instruments (1) for testing perception of differences of tint, and (2) for determining reaction-time. *The Journal of the Anthropological Institute of Great Britain and Ireland* 19:pp. 27–29.
- Ganguly K, Carmena JM (2009) Emergence of a stable cortical map for neuroprosthetic control. *PLoS biology* 7:e1000153.
- Gehring WJ, Goss B, Coles MGH, Meyer DE, Donchin EA (1993) Neural system for error-detection and compensation. *Psychol Sci* 4:385–90.
- Gerson AD, Parra LC, Sajda P (2005) Cortical origins of response time variability during rapid discrimination of visual objects. *Neuroimage* 28:342–353.
- Gevins A, Smith ME (2000) Neurophysiological measures of working memory and individual differences in cognitive ability and cognitive style. *Cereb Cortex* 10:829–839.
- Geweke J (1982) Measurement of linear dependence and feedback between multiple time series. *Journal of the American Statistical Association* 77:304–313.
- Geweke JF (1984) Measures of conditional linear dependence and feedback between time series. *Journal of the American Statistical Association* 79:907–915.

Bibliography

- Gheorghe L, Chavarriaga R, Millán JdR (2013a) Steering timing prediction in a driving simulator task. *Conf Proc IEEE Eng Med Biol Soc* 2013:6913–6916.
- Gheorghe LA, Chavarriaga R, Millán JdR (2013b) Steering Timing Prediction in a Driving Simulator Task In *Proceedings of the 35th Annual International Conference of the IEEE Engineering in Medicine and Biology Society*, pp. 6913–6916.
- Ginter J, Blinowska KJ, Kamiński M, Durka PJ (2001) Phase and amplitude analysis in time-frequency space—application to voluntary finger movement. *J Neurosci Meth* 110:113–124.
- Göhring D, Latotzky D, Wang M, Rojas R (2013) Semi-autonomous car control using brain computer interfaces In *Intelligent Autonomous Systems 12*, pp. 393–408. Springer.
- Grandjean E (1979) Fatigue in industry. *British Journal of Industrial Medicine* 36:175–186.
- Grandjean E (1989) *Fitting the task to the man: a textbook of occupational ergonomics* Taylor & Francis/Hemisphere.
- Granger CW (1969) Investigating causal relations by econometric models and cross-spectral methods. *Econometrica: Journal of the Econometric Society* pp. 424–438.
- Gregoriou GG, Gotts SJ, Zhou H, Desimone R (2009) Long-range neural coupling through synchronization with attention. *Progress in brain research* 176:35–45.
- Grosse-Wentrup M (2008) Understanding brain connectivity patterns during motor imagery for brain-computer interfacing. In *NIPS*, pp. 561–568.
- Grosse-Wentrup M, Liefhold C, Gramann K, Buss M (2009) Beamforming in noninvasive brain-computer interfaces. *Biomedical Engineering, IEEE Transactions on* 56:1209–1219.
- Guo F, Hong B, Gao X, Gao S (2008) A brain-computer interface using motion-onset visual evoked potential. *Journal of neural engineering* 5:477.
- Gusnard DA, Raichle ME (2001) Searching for a baseline: functional imaging and the resting human brain. *Nature Reviews Neuroscience* 2:685–694.
- Gysels E, Renevey P, Celka P et al. (2007) Fast feature selection to compare broadband with narrowband phase synchronization in brain-computer interfaces. *Methods Inf Med* 46:160–163.
- Gysels E, Celka P (2004) Phase synchronization for the recognition of mental tasks in a brain-computer interface. *Neural Systems and Rehabilitation Engineering, IEEE Transactions on* 12:406–415.
- Gysels E, Renevey P, Celka P (2005) Svm-based recursive feature elimination to compare phase synchronization computed from broadband and narrowband EEG signals in brain-computer interfaces. *Signal Processing* 85:2178–2189.
- Häkkinen H, Summala H (2000) Sleepiness at work among commercial truck drivers. *Sleep* 23:49–57.

- Hamner B, Leeb R, Tavella M, Millán JdR (2011) Phase-based features for motor imagery brain-computer interfaces. *Conf Proc IEEE Eng Med Biol Soc* 2011:2578–2581.
- Haufe S, Treder MS, Gugler MF, Sagebaum M, Curio G, Blankertz B (2011) EEG potentials predict upcoming emergency brakings during simulated driving. *J Neural Eng* 8:1–11.
- Haufe S, Kim JW, Kim IH, Sonnleitner A, Schrauf M, Curio G, Blankertz B (2014) Electrophysiology-based detection of emergency braking intention in real-world driving. *J Neural Eng* 11:056011.
- Haufe S, Treder MS, Gugler MF, Sagebaum M, Curio G, Blankertz B (2011) EEG potentials predict upcoming emergency brakings during simulated driving. *J Neural Eng* 8:056001.
- Heike E, Hilde J, Markus U, Tom E (2010) Maladaptation of event-related EEG responses preceding performance errors. *Front Hum Neurosci* 4:12.
- Heilman KM, Van Den Abell T (1980) Right hemisphere dominance for attention the mechanism underlying hemispheric asymmetries of inattention (neglect). *Neurology* 30:327–327.
- Hennessy DA, Wiesenthal DL (1999) Traffic congestion, driver stress, and driver aggression. *Aggressive behavior* 25:409–423.
- Herbert BM, Pollatos O, Schandry R (2007) Interoceptive sensitivity and emotion processing: an EEG study. *International Journal of Psychophysiology* 65:214–227.
- Herzog L, Salehi K, Bohon KS, Wiest MC (2014) Pre-stimulus frontal-parietal coherence predicts auditory detection performance in rats. *Journal of Neurophysiology* .
- Hesse W, Möller E, Arnold M, Schack B (2003) The use of time-variant EEG granger causality for inspecting directed interdependencies of neural assemblies. *Journal of neuroscience methods* 124:27–44.
- Hipp JF, Engel AK, Siegel M (2011) Oscillatory synchronization in large-scale cortical networks predicts perception. *Neuron* 69:387–396.
- Hirvonen K, Hasan J, Häkkinen V, Värri A, Loula P (1997) The detection of drowsiness and sleep onset periods from ambulatory recorded polygraphic data. *Electroencephalogr Clin Neurophysiol* 102:132–137.
- Hochberg LR, Serruya MD, Friehs GM, Mukand JA, Saleh M, Caplan AH, Branner A, Chen D, Penn RD, Donoghue JP (2006) Neuronal ensemble control of prosthetic devices by a human with tetraplegia. *Nature* 442:164–171.
- Höhne J, Holz E, Staiger-Sälzer P, Müller KR, Kübler A, Tangermann M (2014) Motor imagery for severely motor-impaired patients: evidence for brain-computer interfacing as superior control solution. *PLoS one* 9:e104854.

Bibliography

- Holroyd CB, Coles MGH (2002) The neural basis of human error processing: Reinforcement learning, dopamine, and the error-related negativity. *Psychol Rev* 109:679–709.
- Holroyd CB, Nieuwenhuis S, Yeung N, Nystrom L, Mars RB, Coles MGH, Cohen JD (2004) Dorsal anterior cingulate cortex shows fMRI response to internal and external error signals. *Nat Neurosci* 7:497–498.
- Hood D, Joseph D, Rakotonirainy A, Sridharan S, Fookes C (2012) Use of brain computer interface to drive: preliminary results In *Proceedings of the 4th International Conference on Automotive User Interfaces and Interactive Vehicular Applications*, pp. 103–106. ACM.
- Horne JA, Reyner LA (1995) Sleep related vehicle accidents. *BMJ* 310:565–567.
- Hosoya Y (2001) Elimination of third-series effect and defining partial measures of causality. *Journal of time series analysis* 22:537–554.
- Hu S, Zheng G (2009) Driver drowsiness detection with eyelid related parameters by support vector machine. *Expert Systems with Applications* 36:7651–7658.
- Idogawa K (1991) On the brain wave activity of professional drivers during monotonous work. *Behaviormetrika* 18:23–34.
- Iturrate I, Chavarriaga R, Montesano L, Minguez J, Millán JdR (2014) Latency correction of event-related potentials between different experimental protocols. *J Neural Eng* 11:036005.
- James L (2000) *Road rage and aggressive driving: Steering clear of highway warfare* Prometheus Books.
- Jansen BH, Rit VG (1995) Electroencephalogram and visual evoked potential generation in a mathematical model of coupled cortical columns. *Biological cybernetics* 73:357–366.
- Jeong J, Gore JC, Peterson BS (2001) Mutual information analysis of the EEG in patients with alzheimer's disease. *Clinical Neurophysiology* 112:827–835.
- Joyce CA, Gorodnitsky IF, Kutas M (2004) Automatic removal of eye movement and blink artifacts from EEG data using blind component separation. *Psychophysiology* 41:313–325.
- Jurkiewicz MT, Gaetz WC, Bostan AC, Cheyne D (2006) Post-movement beta rebound is generated in motor cortex: evidence from neuromagnetic recordings. *Neuroimage* 32:1281–1289.
- Kamiński M, Ding M, Truccolo WA, Bressler SL (2001) Evaluating causal relations in neural systems: Granger causality, directed transfer function and statistical assessment of significance. *Biol Cybern* 85:145–157.
- Kamiński MJ, Blinowska KJ (1991) A new method of the description of the information flow in the brain structures. *Biol Cybern* 65:203–210.

- Kamiński M, Blinowska K, Szelenberger W (1997) Topographic analysis of coherence and propagation of EEG activity during sleep and wakefulness. *Electroencephalography and clinical neurophysiology* 102:216–227.
- Kastner S, Ungerleider LG (2000) Mechanisms of visual attention in the human cortex. *Annu Rev Neurosci* 23:315–341.
- Katsis CD, Katertsidis N, Ganiatsas G, Fotiadis DI (2008) Toward emotion recognition in car-racing drivers: A biosignal processing approach. *Systems, Man and Cybernetics, Part A: Systems and Humans, IEEE Transactions on* 38:502–512.
- Kayser J, Tenke CE (2006) Principal components analysis of laplacian waveforms as a generic method for identifying ERP generator patterns: I. evaluation with auditory oddball tasks. *Clin Neurophysiol* 117:348 – 368.
- Kecklund G, Akerstedt T (1993) Sleepiness in long distance truck driving: an ambulatory EEG study of night driving. *Ergonomics* 36:1007–1017.
- Kerns JG, Cohen JD, MacDonald AW, Cho RY, Stenger VA, Carter CS (2004) Anterior cingulate conflict monitoring and adjustments in control. *Science* 303:1023–1026.
- Khaliliardali Z, Chavarriaga R, Gheorghe LA, Millán JdR (2012) Detection of anticipatory brain potentials during car driving. *Conf Proc IEEE Eng Med Biol Soc* 2012:3829–3832.
- Khushaba RN, Kodagoda S, Lal S, Dissanayake G (2011) Driver drowsiness classification using fuzzy wavelet-packet-based feature-extraction algorithm. *IEEE Trans Biomed Eng* 58:121–131.
- Kiebel SJ, David O, Friston KJ (2006) Dynamic causal modelling of evoked responses in EEG/meg with lead field parameterization. *NeuroImage* 30:1273–1284.
- Kiebel SJ, Garrido MI, Friston KJ (2007) Dynamic causal modelling of evoked responses: the role of intrinsic connections. *Neuroimage* 36:332–345.
- Kiebel SJ, Klöppel S, Weiskopf N, Friston KJ (2007) Dynamic causal modeling: a generative model of slice timing in fMRI. *Neuroimage* 34:1487–1496.
- Kim IH, Kim JW, Haufe S, Lee SW (2015) Detection of braking intention in diverse situations during simulated driving based on EEG feature combination. *J Neural Eng* 12:016001.
- Kinsbourne M (1993) Orientational bias model of unilateral neglect: evidence from attentional gradients within hemispace. *Unilateral neglect: Clinical and experimental studies* pp. 63–86.
- Klimesch W (1999) EEG alpha and theta oscillations reflect cognitive and memory performance: a review and analysis. *Brain Research Reviews* 29:169–195.
- Klimesch W, Doppelmayr M, Yonelinas A, Kroll NE, Lazzara M, Röhm D, Gruber W (2001) Theta synchronization during episodic retrieval: neural correlates of conscious awareness. *Cognitive Brain Research* 12:33–38.

Bibliography

- Koelewijn T, van Schie HT, Bekkering H, Oostenveld R, Jensen O (2008) Motor-cortical beta oscillations are modulated by correctness of observed action. *Neuroimage* 40:767–775.
- Korzeniewska A, Crainiceanu CM, Kuś R, Franaszczuk PJ, Crone NE (2008) Dynamics of event-related causality in brain electrical activity. *Hum Brain Mapp* 29:1170–1192.
- Korzeniewska A, Mańczak M, Kamiński M, Blinowska KJ, Kasicki S (2003) Determination of information flow direction among brain structures by a modified directed transfer function (dDTF) method. *J Neurosci Meth* 125:195–207.
- Kramer AF (1990) Physiological metrics of mental workload: A review of recent progress Technical report, DTIC Document.
- Krusiński DJ, McFarland DJ, Wolpaw JR (2012) Value of amplitude, phase, and coherence features for a sensorimotor rhythm-based brain–computer interface. *Brain research bulletin* 87:130–134.
- Krusiński DJ, Sellers EW, McFarland DJ, Vaughan TM, Wolpaw JR (2008) Toward enhanced p300 speller performance. *Journal of neuroscience methods* 167:15–21.
- Kuś R, Ginter JS, Blinowska KJ (2005) Propagation of EEG activity during finger movement and its imagination. *Acta neurobiologiae experimentalis* 66:195–206.
- Kuś R, Blinowska KJ, Kamiński M, Basińska-Starzycka A (2008) Transmission of information during continuous attention test. *Acta neurobiologiae experimentalis* 68:103.
- Kuwabara M, Mansouri FA, Buckley MJ, Tanaka K (2014) Cognitive control functions of anterior cingulate cortex in macaque monkeys performing a wisconsin card sorting test analog. *J Neurosci* 34:7531–7547.
- Lachaux JP, Lutz A, Rudrauf D, Cosmelli D, Le Van Quyen M, Martinerie J, Varela F (2002) Estimating the time-course of coherence between single-trial brain signals: an introduction to wavelet coherence. *Neurophysiologie Clinique/Clinical Neurophysiology* 32:157–174.
- Lachaux JP, Rodriguez E, Martinerie J, Varela FJ et al. (1999) Measuring phase synchrony in brain signals. *Human brain mapping* 8:194–208.
- Lakhani B, Ooteghem KV, Miyasike-daSilva V, Akram S, Mansfield A, McIlroy WE (2011) Does the movement matter? determinants of the latency of temporally urgent motor reactions. *Brain Research* 1416:35 – 43.
- Lakhani B, Vette AH, Mansfield A, Miyasike-daSilva V, McIlroy WE (2012) Electrophysiological correlates of changes in reaction time based on stimulus intensity. *PLoS ONE* 7.
- Lal SK, Craig A (2001) A critical review of the psychophysiology of driver fatigue. *Biological psychology* 55:173–194.

- Lal SK, Craig A (2002) Driver fatigue: electroencephalography and psychological assessment. *Psychophysiology* 39:313–321.
- Lal S, Craig A (2000) Psychophysiological effects associated with drowsiness: driver fatigue and electroencephalography In *International Journal of Psychophysiology*, Vol. 35, pp. 39–39. ELSEVIER SCIENCE BV PO BOX 211, 1000 AE AMSTERDAM, NETHERLANDS.
- Lebedev MA, Nicolelis MA (2006) Brain–machine interfaces: past, present and future. *TRENDS in Neurosciences* 29:536–546.
- Leeb R, Perdakis S, Tonin L, Biasiucci A, Tavella M, Creatura M, Molina A, Al-Khodairy A, Carlson T, Millán JdR (2013) Transferring brain-computer interfaces beyond the laboratory: Successful application control for motor-disabled users. *Artif Intell Med* 59:121 – 132.
- Lenné MG, Triggs TJ, Redman JR (1997) Time of day variations in driving performance. *Accid Anal Prev* 29:431–437.
- Leuthardt EC, Schalk G, Wolpaw JR, Ojemann JG, Moran DW (2004) A brain–computer interface using electrocorticographic signals in humans. *Journal of neural engineering* 1:63.
- Lin CT, Chang CJ, Lin BS, Hung SH, Chao CF, Wang IJ (2010) A real-time wireless brain–computer interface system for drowsiness detection. *Biomedical Circuits and Systems, IEEE Transactions on* 4:214–222.
- Lin CT, Chen SA, Chiu TT, Lin HZ, Ko LW (2011) Spatial and temporal EEG dynamics of dual-task driving performance. *J Neuroeng Rehabil* 8:11.
- Lin CT, Ko LW, Sheng TK (2009) Computational intelligent brain computer interaction and its applications on driving cognition. *IEEE Computational Intelligence Magazine* 4:32–46.
- Lin CT, Wu RC, Liang SF, Chao WH, Chen YJ, Jung TP (2005) EEG-based drowsiness estimation for safety driving using independent component analysis. *Circuits and Systems I: Regular Papers, IEEE Transactions on* 52:2726–2738.
- Lorenz EN (1963) Deterministic nonperiodic flow. *Journal of the atmospheric sciences* 20:130–141.
- Luks TL, Simpson GV, Feiwell RJ, Miller WL (2002) Evidence for anterior cingulate cortex involvement in monitoring preparatory attentional set. *Neuroimage* 17:792–802.
- Lupton D (2002) Road rage: drivers’ understandings and experiences. *Journal of Sociology* 38:275–290.
- Luu P, Flaisch T, Tucker DM (2000) Medial frontal cortex in action monitoring. *J Neurosci* 20:464–469.
- Luu S, Chau T (2009) Decoding subjective preference from single-trial near-infrared spectroscopy signals. *Journal of neural engineering* 6:016003.

Bibliography

- Maglione A, Borghini G, Aricò P, Borgia F, Graziani I, Colosimo A, Kong W, Vecchiato G, Babiloni F (2014) Evaluation of the workload and drowsiness during car driving by using high resolution EEG activity and neurophysiologic indices. *Conf Proc IEEE Eng Med Biol Soc* 2014:6238–6241.
- Marreiros A, Kiebel SJ, Friston KJ (2008) Dynamic causal modelling for fMRI: a two-state model. *Neuroimage* 39:269–278.
- Marreiros AC, Kiebel SJ, Daunizeau J, Harrison LM, Friston KJ (2009) Population dynamics under the laplace assumption. *Neuroimage* 44:701–714.
- Mason MF, Norton MI, Van Horn JD, Wegner DM, Grafton ST, Macrae CN (2007) Wandering minds: the default network and stimulus-independent thought. *Science* 315:393–395.
- Mazaheri A, Nieuwenhuis ILC, van Dijk H, Jensen O (2009) Prestimulus alpha and mu activity predicts failure to inhibit motor responses. *Hum Brain Mapp* 30:1791–1800.
- McFarland DJ, McCane LM, David SV, Wolpaw JR (1997) Spatial filter selection for EEG-based communication. *Electroencephalography and clinical Neurophysiology* 103:386–394.
- McFarland DJ, Miner LA, Vaughan TM, Wolpaw JR (2000) Mu and beta rhythm topographies during motor imagery and actual movements. *Brain topography* 12:177–186.
- Mellinger J, Schalk G, Braun C, Preissl H, Rosenstiel W, Birbaumer N, Kübler A (2007) An MEG-based brain–computer interface (bci). *Neuroimage* 36:581–593.
- Middendorf M, McMillan G, Calhoun G, Jones KS et al. (2000) Brain-computer interfaces based on the steady-state visual-evoked response. *IEEE Transactions on Rehabilitation Engineering* 8:211–214.
- Millán J, Renkens F, Mourino J, Gerstner W (2004) Noninvasive brain-actuated control of a mobile robot by human EEG 51:1026–1033.
- Millán JdR (2002) Brain-computer interfaces Technical report, The MIT Press.
- Millán JdR, Carmena J (2010) Invasive or noninvasive: understanding brain-machine interface technology. *IEEE Engineering in Medicine and Biology Magazine* 29:16–22.
- Millán JdR, Ferrez PW, Seidl T (2009) Validation of brain–machine interfaces during parabolic flight. *International review of neurobiology* 86:189–197.
- Miller EK, Cohen JD (2001) An integrative theory of prefrontal cortex function. *Annual Review of Neuroscience* 24:167–202.
- Milner WHR, Brauer J, Hecht H, Trippe R, Coles MGH (2004) Parallel brain activity for self-generated and observed errors. *Errors, Conflicts, and the Brain. Current Opinions on Performance Monitoring* pp. 124–129.

- Möller E, Schack B, Arnold M, Witte H (2001) Instantaneous multivariate EEG coherence analysis by means of adaptive high-dimensional autoregressive models. *Journal of neuroscience methods* 105:143–158.
- Moran RJ, Kiebel SJ, Stephan K, Reilly R, Daunizeau J, Friston KJ (2007) A neural mass model of spectral responses in electrophysiology. *NeuroImage* 37:706–720.
- Moran RJ, Stephan KE, Kiebel SJ, Rombach N, O'Connor W, Murphy K, Reilly R, Friston KJ (2008) Bayesian estimation of synaptic physiology from the spectral responses of neural masses. *NeuroImage* 42:272–284.
- Moran RJ, Stephan KE, Seidenbecher T, Pape HC, Dolan RJ, Friston KJ (2009) Dynamic causal models of steady-state responses. *NeuroImage* 44:796–811.
- Mormann F, Lehnertz K, David P, Elger CE (2000) Mean phase coherence as a measure for phase synchronization and its application to the EEG of epilepsy patients. *Physica D: Nonlinear Phenomena* 144:358–369.
- Morris C, Lecar H (1981) Voltage oscillations in the barnacle giant muscle fiber. *Biophysical journal* 35:193.
- Müller-Putz G, Scherer R, Brunner C, Leeb R, Pfurtscheller G (2008) Better than random: A closer look on bci results. *International Journal of Bioelectromagnetism* 10:52–55.
- Müller-Putz GR, Pfurtscheller G (2008) Control of an electrical prosthesis with an ssvep-based bci. *Biomedical Engineering, IEEE Transactions on* 55:361–364.
- Müller-Putz GR, Scherer R, Brauneis C, Pfurtscheller G (2005) Steady-state visual evoked potential (ssvep)-based communication: impact of harmonic frequency components. *Journal of neural engineering* 2:123.
- Musallam S, Corneil B, Greger B, Scherberger H, Andersen R (2004) Cognitive control signals for neural prosthetics. *Science* 305:258–262.
- Na SH, Jin SH, Kim SY, Ham BJ (2002) EEG in schizophrenic patients: mutual information analysis. *Clinical Neurophysiology* 113:1954–1960.
- Neuper C, Scherer R, Reiner M, Pfurtscheller G (2005) Imagery of motor actions: Differential effects of kinesthetic and visual-motor mode of imagery in single-trial EEG. *Cognitive Brain Research* 25:668–677.
- Nicolelis MA (2001) Actions from thoughts. *Nature* 409:403–407.
- Nicolelis MA (2003) Brain-machine interfaces to restore motor function and probe neural circuits. *Nature Reviews Neuroscience* 4:417–422.
- Nicolelis MA, Dimitrov D, Carmena JM, Crist R, Lehew G, Kralik JD, Wise SP (2003) Chronic, multisite, multielectrode recordings in macaque monkeys. *Proceedings of the National Academy of Sciences* 100:11041–11046.

Bibliography

- O'Donnell RD, Eggemeier FT (1986) Workload assessment methodology. .
- Omedes J, Iturrate I, Montesano L (2014) Brain connectivity in continuous error tasks In *Conf Proc IEEE Eng Med Biol Soc*.
- Omidvarnia A, Azemi G, Boashash B, O'Toole JM, Colditz PB, Vanhatalo S (2014) Measuring time-varying information flow in scalp EEG signals: orthogonalized partial directed coherence. *Biomedical Engineering, IEEE Transactions on* 61:680–693.
- Oya H, Poon PWF, Brugge JF, Reale RA, Kawasaki H, Volkov IO, Howard MA (2007) Functional connections between auditory cortical fields in humans revealed by granger causality analysis of intra-cranial evoked potentials to sounds: comparison of two methods. *Biosystems* 89:198–207.
- Papadelis C, Chen Z, Kourtidou-Papadeli C, Bamidis PD, Chouvarda I, Bekiaris E, Maglaveras N (2007) Monitoring sleepiness with on-board electrophysiological recordings for preventing sleep-deprived traffic accidents. *Clin Neurophysiol* 118:1906–1922.
- Papadelis C, Kourtidou-Papadeli C, Bamidis PD, Chouvarda I, Koufogiannis D, Bekiaris E, Maglaveras N (2006) Indicators of sleepiness in an ambulatory EEG study of night driving In *Engineering in Medicine and Biology Society, 2006. EMBS'06. 28th Annual International Conference of the IEEE*, pp. 6201–6204. IEEE.
- Papadelis CL, Lithari CD, Kourtidou-Papadeli C, Bamidis PD, Portouli E, Bekiaris E (2009) Monitoring driver's sleepiness on-board for preventing road accidents. In *MIE*, pp. 485–489.
- Parra LC, Spence CD, Gerson AD, Sajda P (2003) Response error correction—a demonstration of improved human-machine performance using real-time EEG monitoring. *IEEE Trans Neural Syst Rehabil Eng* 11:173–177.
- Pecora LM, Carroll TL (1990) Synchronization in chaotic systems. *Physical review letters* 64:821.
- Penny W, Litvak V, Fuentemilla L, Duzel E, Friston K (2009) Dynamic causal models for phase coupling. *Journal of neuroscience methods* 183:19–30.
- Penny WD, Stephan K, Mechelli A, Friston K (2004) Comparing dynamic causal models. *NeuroImage* 22:1157–1172.
- Pereda E, Quiroga RQ, Bhattacharya J (2005) Nonlinear multivariate analysis of neurophysiological signals. *Progress in neurobiology* 77:1–37.
- Pfurtscheller G, Brunner C, Schlögl A, Da Silva FL (2006) Mu rhythm (de) synchronization and EEG single-trial classification of different motor imagery tasks. *Neuroimage* 31:153–159.
- Pfurtscheller G, Neuper C, Brunner C, da Silva FL (2005) Beta rebound after different types of motor imagery in man. *Neurosci Lett* 378:156–159.

- Pfurtscheller G, Allison BZ, Brunner C, Bauernfeind G, Solis-Escalante T, Scherer R, Zander TO, Müeller-Putz G, Neuper C, Birbaumer N (2010) The hybrid bci. *Frontiers in neuroscience* 4.
- Pfurtscheller G, Andrew C (1999) Event-related changes of band power and coherence: methodology and interpretation. *Journal of clinical neurophysiology* 16:512.
- Pfurtscheller G, Da Silva FL (1999) Event-related EEG/meg synchronization and desynchronization: basic principles. *Clinical neurophysiology* 110:1842–1857.
- Pfurtscheller G, Neuper C (2001) Motor imagery and direct brain-computer communication. *Proceedings of the IEEE* 89:1123–1134.
- Philip P (2005) Sleepiness of occupational drivers. *Ind Health* 43:30–33.
- Pikovsky A, Rosenblum M, Kurths J, Hilborn RC (2002) *Synchronization: A universal concept in nonlinear sciences*, Vol. 2 Cambridge University Press Cambridge.
- Pikovsky A (1984) On the interaction of strange attractors. *Zeitschrift für Physik B Condensed Matter* 55:149–154.
- Pins D, Bonnet C (1996) On the relation between stimulus intensity and processing time: Piéron's law and choice reaction time. *Perception and Psychophysics* 58:390–400.
- Posner MI (1980) Orienting of attention. *Quarterly journal of experimental psychology* 32:3–25.
- Ptak R (2012) The frontoparietal attention network of the human brain: action, saliency, and a priority map of the environment. *Neuroscientist* 18:502–515.
- Ramoser H, Müller-Gerking J, Pfurtscheller G (2000) Optimal spatial filtering of single trial EEG during imagined hand movement. *IEEE Trans Rehabil Eng* 8:441–446.
- Rathbone DB, Huckabee JC (1999) Controlling road rage: A literature review and pilot study .
- Renold H, Chavarriaga R, Gheorghe LA, Millán JdR (2014) EEG correlates of active visual search during simulated driving: An exploratory study In *IEEE International Conference on Systems, Man, and Cybernetics*, San Diego, USA.
- Rissanen J, Wax M (1987) Measures of mutual and causal dependence between two time series (corresp.). *Information Theory, IEEE Transactions on* 33:598–601.
- Rubinov M, Sporns O (2010) Complex network measures of brain connectivity: uses and interpretations. *Neuroimage* 52:1059–1069.
- Saeedi S, Carlson T, Chavarriaga R, Millán JdR (2013) Making the most of context-awareness in brain-computer interfaces In *IEEE International Conference on Cybernetics*.

Bibliography

- Sakkalis V, Giurcaneanu CD, Xanthopoulos P, Zervakis ME, Tsiaras V, Yang Y, Karakonstantaki E, Micheloyannis S (2009) Assessment of linear and nonlinear synchronization measures for analyzing EEG in a mild epileptic paradigm. *Information Technology in Biomedicine, IEEE Transactions on* 13:433–441.
- Sakkalis V, Zervakis M, Micheloyannis S (2006) Significant EEG features involved in mathematical reasoning: evidence from wavelet analysis. *Brain topography* 19:53–60.
- Sato JR, Takahashi DY, Arcuri SM, Sameshima K, Morettin PA, Baccalá LA (2009) Frequency domain connectivity identification: an application of partial directed coherence in fMRI. *Human brain mapping* 30:452–461.
- Sauseng P, Klimesch W, Doppelmayr M, Hanslmayr S, Schabus M, Gruber WR (2004) Theta coupling in the human electroencephalogram during a working memory task. *Neurosci Lett* 354:123–126.
- Schalk G, Wolpaw JR, McFarland DJ, Pfurtscheller G (2000) EEG-based communication: presence of an error potential. *Clinical Neurophysiology* 111:2138–2144.
- Schelter B, Winterhalder M, Eichler M, Peifer M, Hellwig B, Guschlbauer B, Lücking CH, Dahlhaus R, Timmer J (2006) Testing for directed influences among neural signals using partial directed coherence. *Journal of neuroscience methods* 152:210–219.
- Schmidt E, McIntosh J, Durelli L, Bak M (1978) Fine control of operantly conditioned firing patterns of cortical neurons. *Experimental neurology* 61:349–369.
- Schneider T, Neumaier A (2001) Algorithm 808: Arfit matlab package for the estimation of parameters and eigenmodes of multivariate autoregressive models. *ACM T Math Software* 27:58–65.
- Schoffelen JM, Gross J (2009) Source connectivity analysis with MEG and EEG. *Hum Brain Mapp* 30:1857–1865.
- Serruya MD, Hatsopoulos NG, Paninski L, Fellows MR, Donoghue JP (2002) Brain-machine interface: Instant neural control of a movement signal. *Nature* 416:141–142.
- Shane MS, Stevens M, Harenski CL, Kiehl KA (2008) Neural correlates of the processing of another's mistakes: a possible underpinning for social and observational learning. *Neuroimage* 42:450–459.
- Siegel M, Donner TH, Engel AK (2012) Spectral fingerprints of large-scale neuronal interactions. *Nat Rev Neurosci* 13:121–134.
- Simon M, Schmidt EA, Kincses WE, Fritzsche M, Bruns A, Aufmuth C, Bogdan M, Rosenstiel W, Schrauf M (2011) EEG alpha spindle measures as indicators of driver fatigue under real traffic conditions. *Clin Neurophysiol* 122:1168–1178.

- Sitaram R, Zhang H, Guan C, Thulasidas M, Hoshi Y, Ishikawa A, Shimizu K, Birbaumer N (2007) Temporal classification of multichannel near-infrared spectroscopy signals of motor imagery for developing a brain-computer interface. *NeuroImage* 34:1416–1427.
- Sporns O (2007) Brain connectivity. *Scholarpedia* 2:4695.
- Stavrinou ML, Moraru L, Cimponeriu L, Della Penna S, Bezerianos A (2007) Evaluation of cortical connectivity during real and imagined rhythmic finger tapping. *Brain topography* 19:137–145.
- Stephan KE, Harrison LM, Kiebel SJ, David O, Penny WD, Friston KJ (2007) Dynamic causal models of neural system dynamics: current state and future extensions. *Journal of biosciences* 32:129–144.
- Stephan KE, Kasper L, Harrison LM, Daunizeau J, den Ouden HE, Breakspear M, Friston KJ (2008) Nonlinear dynamic causal models for fMRI. *Neuroimage* 42:649–662.
- Stephan KE, Penny WD, Moran RJ, den Ouden HE, Daunizeau J, Friston KJ (2010) Ten simple rules for dynamic causal modeling. *Neuroimage* 49:3099–3109.
- Stephan KE, Weiskopf N, Drysdale PM, Robinson PA, Friston KJ (2007) Comparing hemodynamic models with dcm. *Neuroimage* 38:387–401.
- Stoica P, Moses RL (1997) *Introduction to spectral analysis*, Vol. 1 Prentice hall Upper Saddle River.
- Sun Y, Zhang H, Feng T, Qiu Y, Zhu Y, Tong S (2009) Early cortical connective network relating to audiovisual stimulation by partial directed coherence analysis. *Biomedical Engineering, IEEE Transactions on* 56:2721–2724.
- Sutter EE (1992) The brain response interface: communication through visually-induced electrical brain responses. *Journal of Microcomputer Applications* 15:31–45.
- Taylor DM, Tillery SIH, Schwartz AB (2002) Direct cortical control of 3d neuroprosthetic devices. *Science* 296:1829–1832.
- Taylor SE, Stern ER, Gehring WJ (2007) Neural systems for error monitoring: Recent findings and theoretical perspectives. *Neuroscientist* 13:160–172.
- Tonin L (2014) Covert visuospatial attention brain-computer interface for control and rehabilitation. *PhD Thesis*.
- Tonin L, Leeb R, Sobolewski A, del R Millán J (2013) An online EEG bci based on covert visuospatial attention in absence of exogenous stimulation. *Journal of neural engineering* 10:056007.
- Tononi G, Sporns O, Edelman GM (1994) A measure for brain complexity: relating functional segregation and integration in the nervous system. *Proceedings of the National Academy of Sciences* 91:5033–5037.

Bibliography

Torsvall L, Akerstedt T (1987) Sleepiness on the job: continuously measured EEG changes in train drivers. *Electroencephalogr Clin Neurophysiol* 66:502–511.

Townsend G, LaPallo B, Boulay C, Krusienski D, Frye G, Hauser C, Schwartz N, Vaughan T, Wolpaw J, Sellers E (2010) A novel p300-based brain–computer interface stimulus presentation paradigm: moving beyond rows and columns. *Clinical Neurophysiology* 121:1109–1120.

Trujillo LT, Allen JJB (2007) Theta EEG dynamics of the error-related negativity. *Clin Neurophysiol* 118:645–668.

Tsuchida A, Bhuiyan MS, Oguri K (2009) Estimation of drowsiness level based on eyelid closure and heart rate variability In *Engineering in Medicine and Biology Society, 2009. EMBC 2009. Annual International Conference of the IEEE*, pp. 2543–2546. IEEE.

Tsujimoto T, Shimazu H, Isomura Y, Sasaki K (2010) Theta oscillations in primate prefrontal and anterior cingulate cortices in forewarned reaction time tasks. *J Neurophysiol* 103:827–843.

Ullsperger M, von Cramon DY (2001) Subprocesses of performance monitoring: a dissociation of error processing and response competition revealed by event-related fMRI and ERPs. *Neuroimage* 14:1387–1401.

Ullsperger M, Fischer AG, Nigbur R, Endrass T (2014) Neural mechanisms and temporal dynamics of performance monitoring. *Trends Cogn Sci* 18:259–267.

van Schie HT, Mars RB, Coles MGH, Bekkering H (2004) Modulation of activity in medial frontal and motor cortices during error observation. *Nat Neurosci* 7:549–554.

Vanderhasselt MA, Raedt RD, Baeken C (2009) Dorsolateral prefrontal cortex and stroop performance: tackling the lateralization. *Psychon Bull Rev* 16:609–612.

Varela F, Lachaux JP, Rodriguez E, Martinerie J (2001) The brainweb: phase synchronization and large-scale integration. *Nature reviews neuroscience* 2:229–239.

Velliste M, Perel S, Spalding MC, Whitford AS, Schwartz AB (2008) Cortical control of a prosthetic arm for self-feeding. *Nature* 453:1098–1101.

Vialatte FB, Maurice M, Dauwels J, Cichocki A (2010) Steady-state visually evoked potentials: focus on essential paradigms and future perspectives. *Progress in neurobiology* 90:418–438.

Vidal JJ (1977) Real-time detection of brain events in EEG. *Proceedings of the IEEE* 65:633–641.

Vidal JJ (1973) Toward direct brain-computer communication. *Annual review of Biophysics and Bioengineering* 2:157–180.

Walker G (1931) On periodicity in series of related terms. *Proceedings of the Royal Society of London. Series A, Containing Papers of a Mathematical and Physical Character* pp. 518–532.

- Wang C, Ulbert I, Schomer DL, Marinkovic K, Halgren E (2005) Responses of human anterior cingulate cortex microdomains to error detection, conflict monitoring, stimulus-response mapping, familiarity, and orienting. *J Neurosci* 25:604–613.
- Wang Y, Hong B, Gao X, Gao S (2006) Phase synchrony measurement in motor cortex for classifying single-trial EEG during motor imagery. *EMBC* 1:75–78.
- Wehling S, Simion C, Shimojo S, Bhattacharya J et al. (2007) Assessment of connectivity patterns from multivariate time series by partial directed coherence. *Chaos and Complexity Letters* 2:413–433.
- Weiskopf N (2012) Real-time fMRI and its application to neurofeedback. *Neuroimage* 62:682–692.
- Weiskopf N, Mathiak K, Bock SW, Scharnowski F, Veit R, Grodd W, Goebel R, Birbaumer N (2004) Principles of a brain-computer interface (bci) based on real-time functional magnetic resonance imaging (fMRI). *Biomedical Engineering, IEEE Transactions on* 51:966–970.
- Wilke C, Ding L, He B (2008) Estimation of time-varying connectivity patterns through the use of an adaptive directed transfer function. *IEEE Trans Biomed Eng* 55:2557–2564.
- Wolpaw JR, McFarland DJ (2004) Control of a two-dimensional movement signal by a noninvasive brain-computer interface in humans. *Proceedings of the National Academy of Sciences of the United States of America* 101:17849–17854.
- Wolpaw J, Birbaumer N, McFarland D, Pfurtscheller G, Vaughan T (2002) Brain-computer interfaces for communication and control. *Clin Neurophysiol* 113:767–791.
- Womelsdorf T, Johnston K, Vinck M, Everling S (2010) Theta-activity in anterior cingulate cortex predicts task rules and their adjustments following errors. *PNAS* 107:5248–5253.
- Yule GU (1927) On a method of investigating periodicities in disturbed series, with special reference to wolfer's sunspot numbers. *Philosophical Transactions of the Royal Society of London. Series A, Containing Papers of a Mathematical or Physical Character* pp. 267–298.
- Zhang H, Chavarriaga R, Gheorghe L, Millán JdR (2013) Inferring driver's turning direction through detection of error related brain activity. *Conf Proc IEEE Eng Med Biol Soc* 2013:2196–2199.
- Zhang H, Chavarriaga R, Goel MK, Gheorghe L, Millán JdR (2012) Improved recognition of error related potentials through the use of brain connectivity features. In *Conf Proc IEEE Eng Med Biol Soc*.
- Zhang H, Chavarriaga R, Millán JdR (2014) Towards implementation of motor imagery using brain connectivity features In *6th International Brain-Computer Interface Conference*, number EPFL-CONF-201757.

Bibliography

Zhang H, Chavarriaga R, Millán JdR (2015) Discriminant brain connectivity patterns of performance monitoring at average and single-trial levels. *NeuroImage* 120:64–74.

HUAIJIAN ZHANG

Email: huaijian.zhang@epfl.ch, **Phone:** 0041789201262,

Address: Rue du Vallon 32, Lausanne 1005, Switzerland

Date of Birth: 23/08/1985; **Gender:** Male; **Marital:** Single; **Nationality:** China

PROFILE

Implementation-oriented researcher with more than eight years experiences of neural signal processing and machine learning, proficient in handling multiple tasks, fast learning of new skills, working in teams and conducting independent achievements.

EDUCATION

Jun 2011-Sep 2015 Ph.D in Brain-Computer Interface

École polytechnique fédérale de Lausanne, Vaud, Switzerland

Sep 2008-Apr 2011 Master of Science in Biomedical Engineering

Zhejiang University, Hangzhou, Zhejiang, China

Dec 2010-Jun 2011 Visiting student in Biomedical Engineering

Johns Hopkins University, Baltimore, Maryland, USA

Sep 2003-Jun 2008 Bachelor of Science in Biomedical Engineering

Zhejiang University, Hangzhou, Zhejiang, China

SKILLS

Key Skills: Brain-Computer Interface, Neural Signal Processing and Machine Learning

Programming: Matlab, C/C++, R, Pascal/Delphi, Open GL and SQL/HIVE

Software: SPSS, SAS, MS Office Suite, Blender, Labview, LaTeX, and Mysql

Operating System: Windows, Linux (proficient) and Macintosh

Languages: English (Advanced, c1/c2), Chinese (native)

RESEARCH EXPERIENCE

● **May 2011-present École Polytechnique Fédérale de Lausanne, PhD**

Non-invasive Brain-Computer Interface, Collaborated with NISSAN Company.

– Design in-car BCI system to predict driver's turning direction in simulated and real car driving based on scalp EEG recording. Build simulated driving system based on an open source program (racing game, C++), blender and OpenGL.

– Brain connectivity analysis for error-related brain activity and motor imagery. Apply multivariate autoregressive model to find causal correlation between brain regions to improve classification performance. Adopt Kalman filter in real time to estimate brain connectivity adaptively.

– Design and test wireless EEG cap for driving tasks. Design the montage of the EEG cap to minimize the sensor number through the evaluation of classification performance. Test stability and usability of the EEG cap, and compare with existing commercial products.

- Explore correlation between reaction time and brain network during driving. Find patterns of lane change behavior in emergent situation. Use regression model to find the correlation between neural signatures and the fast/slow reactions.
- Exploit brain connectivity pattern as a recovery index for stroke/neglect patients. Analyze brain connectivity between healthy and damaged hemispheres before and after the stroke therapy. Use oscillatory information flows to quantify stroke recovery.
- Teaching assistance for courses: "Data Analysis and Model Classification" and "Neuroengineering". Lead weekly discussion of Matlab tutorial and exercises, and answer questions. Prepare Matlab code and design exercises/exams.

- **Dec 2009-Jun 2010 Johns Hopkins University, Visiting student**
Brain-Computer Interface based on ECoG recordings.

- Decode hand open-close trajectory based on ECoG data. Design spectral/spatial filters and regression models for ECoG based neural decoding. Adopt time-varying dynamic Bayesian network to find novel features to improve the regression performance.

- **Sept 2008-Apr 2011 Zhejiang University, Master projects**
Invasive Brain-Computer Interface.

- Data analysis for local field potential and action potentials. Detect and classify action potentials using linear/nonlinear classification methods. Decode moving trajectory of rats/primates based on spike firing rate and LFP signals. Implement real-time neural decoding for rats upper limb movements.

- **Sept 2003-Jun 2008 Zhejiang University, Bachelor projects**

- Signal processing and system design for ECG monitoring system. Design real time cardiac monitoring system based on Labview/LabJack. Implement signal processing and classification methods to detect abnormal heart rate and QRS patterns.
- Design and implement software system for a medical instrument (collaborated with 3F Medical Company). Design database and file storage based on Pascal and Mysql. Implement GUI design, text analysis and data extraction for medical instruments.

WORK EXPERIENCE

- **2014-2015 Analysis of Forex currency**

- Extract real time currency rate from multiple sources
- Predict currency rate through multivariate autoregressive model and regression models
- Simulate trading strategy/process for binary trading using Matlab

- **Jul 2010-Sept 2010 Alibaba Company, Data analyst**

- Extract specified data from Hadoop distributed file system using HIVE and JAVA.
- Utilize text analysis including URL parsing, keyword extraction and frequency analysis.
- Find statistical signatures and features of advertisement data in e-commerce websites.
- Predict advertisement price using regression models.

PUBLICATIONS

● Articles

“Discriminant brain connectivity patterns of performance monitoring at average and single-trial levels”. **Huaijian Zhang**, Ricardo Chavarriaga, José Del R. Millán. *NeuroImage*. 2015.

“EEG-based decoding of brain error monitoring in a real-world driving Task”. **Huaijian Zhang**, Ricardo Chavarriaga, Zahra Khaliliardali, Lucian Gheorghe, Inaki Iturrate and José Del R. Millán. *Journal of Neural Engineering*. Submitted.

“Brain-computer interface induces rebalance of cortical activity in spatial neglect”. Luca Tonin, Marco Pitteri, Robert Leeb, **Huaijian Zhang**, Emanuele Menegatti, Francesco Piccione, José Del R. Millán. *Scientific Report*. Submitted.

“Connectivity mapping of human brain by phased based evolution map approach”. **Huaijian Zhang**, Heather L Benz, Nitish V Thakor, Anastasios Bezerianos. *International Journal of Bifurcation and Chaos*. 2012.

“Development of an invasive brain-machine interface with a monkey model”. Qiaosheng Zhang, Shaomin Zhang, Yaoyao Hao, **Huaijian Zhang**, Junming Zhu, Ting Zhao, Jianmin Zhang, Yiwen Wang, Xiaoxiang Zheng, Weidong Chen. *Chinese Science Bulletin*. 2012.

“Connectivity analysis as a novel approach to motor decoding for prosthesis control”. Heather L Benz, **Huaijian Zhang**, Anastasios Bezerianos, Soumyadipta Acharya, Nathan E Crone, Xioaxiang Zheng, Nitish V Thakor. *IEEE transactions on neural systems and rehabilitation engineering*. 2011.

“A novel matched filter for neural action potential detection”. Jianhua Dai, **Huaijian Zhang**, Xiaochun Liu, Shaomin Zhang, Weidong Chen, Xiaoxiang Zheng. *Journal of Convergence Information Technology*. 2010.

“Neural decoding based on probabilistic neural network”. Yi Yu, Shaomin Zhang, **Huaijian Zhang**, Xiaochun Liu, Qiaosheng Zhang, Xiaoxiang Zheng, and Jianhua Dai. *Journal of Zhejiang University Science B*. 2010.

“Continuous neural decoding method based on general regression neural network”. Jianhua Dai, Xiaochun Liu, Shaomin Zhang, **Huaijian Zhang**, Qing Xu, Weidong Chen, Xiaoxiang Zheng. *International Journal of Digital Content Technology and its Applications*. 2010.

● Conferences

“Brain correlates of reaction time in the driving task of urgent lane change”. **Huaijian Zhang**, Ricardo Chavarriaga, Lucian Gheorghe, José Del R. Millán. *IEEE International Conference on Systems, Man, and Cybernetics*. 2015.

“Towards implementation of motor imagery using brain connectivity features”. **Huaijian Zhang**, Ricardo Chavarriaga, José Del R. Millán, *6th International Brain-Computer Interface Conference*. 2014.

“Inferring driver's turning direction through detection of error related brain activity”. **Huaijian Zhang**, Ricardo Chavarriaga, Lucian Gheorghe, José Del R Millán, Annual International Conference of the IEEE Engineering in Medicine and Biology Society. 2013.

“Improved recognition of error related potentials through the use of brain connectivity features”. **Huaijian Zhang**, Ricardo Chavarriaga, Mohit Kumar Goel, Lucian Gheorghe, José Del R Millán. *Annual International Conference of the IEEE Engineering in Medicine and Biology Society*. 2012.

“Self-paced movement intention detection from human brain signals: Invasive and non-invasive EEG”. Eileen Lew, Ricardo Chavarriaga, **Huaijian Zhang**, Margitta Seeck, José Del R Millán. *Annual International Conference of the IEEE Engineering in Medicine and Biology Society*. 2012.

“Connectivity mapping of the human ECoG during a motor task with a time-varying dynamic bayesian network”. **Huaijian Zhang**, Heather L Benz, Anastasios Bezerianos, Soumyadipta Acharya, Nathan E Crone, Anil Maybhate, Xiaoxiang Zheng, Nitish V Thakor. *Annual International Conference of the IEEE Engineering in Medicine and Biology Society*. 2010.

“Neural ensemble decoding of rat's motor cortex by Kalman filter and optimal linear estimation”. **Huaijian Zhang**, Jianhua Dai, Shaomin Zhang, Qingbo Wang, Qian Li, Xiaochun Liu, Yaoyao Hao, Yi Yu, Kai Jiang, Jun Liu, Fan Zhu, Weidong Chen. *International Congress on Image and Signal Processing*. 2009.